Lappeenranta
University of Technology

Joonas Talvitie

DEVELOPMENT OF MEASUREMENT SYSTEMS IN SCIENTIFIC RESEARCH: CASE STUDY

Thesis for the degree of Doctor of Science (Technology) to be presented with due permission for public examination and criticism in the Auditorium 1383 at Lappeenranta University of Technology, Lappeenranta, Finland, on the 27th of August, 2015, at noon.

Acta Universitatis
Lappeenrantaensis 652

Supervisor Professor Pertti Silventoinen
Electrical Engineering
LUT School of Energy Systems
Lappeenranta University of Technology
Finland

Reviewers Professor Raimo Sepponen
Electrical Engineering and Automation
Aalto University
Finland

Major Tapio Saarelainen
Army Academy
Finnish Defence Forces
Finland

Opponents Professor Raimo Sepponen
Electrical Engineering and Automation
Aalto University
Finland

ISBN 978-952-265-830-2
ISBN 978-952-265-831-9 (PDF)
ISSN-L 1456-4491
ISSN 1456-4491

Lappeenrannan teknillinen yliopisto
Yliopistopaino 2015

Abstract

Joonas Talvitie

Development of Measurement Systems in Scientific Research: Case Study

Acta Universitatis Lappeenrantaensis 652

Dissertation, Lappeenranta University of Technology
56 p.
Lappeenranta 2015
ISBN 978-952-265-830-2, ISBN 978-952-265-831-9 (PDF), ISSN-L 1456-4491, ISSN 1456-4491

In recent years, technological advancements in microelectronics and sensor technologies have revolutionized the field of electrical engineering. New manufacturing techniques have enabled a higher level of integration that has combined sensors and electronics into compact and inexpensive systems. Previously, the challenge in measurements was to understand the operation of the electronics and sensors, but this has now changed. Nowadays, the challenge in measurement instrumentation lies in mastering the whole system, not just the electronics.

To address this issue, this doctoral dissertation studies whether it would be beneficial to consider a measurement system as a whole from the physical phenomena to the digital recording device, where each piece of the measurement system affects the system performance, rather than as a system consisting of small independent parts such as a sensor or an amplifier that could be designed separately. The objective of this doctoral dissertation is to describe in depth the development of the measurement system taking into account the challenges caused by the electrical and mechanical requirements and the measurement environment. The work is done as an empirical case study in two example applications that are both intended for scientific studies. The cases are a light sensitive biological sensor used in imaging and a gas electron multiplier detector for particle physics.

The study showed that in these two cases there were a number of different parts of the measurement system that interacted with each other. Without considering these interactions, the reliability of the measurement may be compromised, which may lead to wrong conclusions about the measurement. For this reason it is beneficial to conceptualize the measurement system as a whole from the physical phenomena to the digital recording device where each piece of the measurement system affects the system performance. The results work as examples of how a measurement system can be successfully constructed to support a study of sensors and electronics.

Keywords: Measurement systems, instrumentation design, development, bacteriorhodopsin, gas electron multiplier detector

Acknowledgments

The work presented in this doctoral dissertation has been carried out during the years 2012–2015 in the Laboratory of Applied Electronics, LUT School of Energy Systems, Lappeenranta University of Technology, Finland and at the European Organization for Nuclear Research (CERN), Switzerland.

I would like to express my gratitude to my supervisors Professor Pertti Silventoinen and Professor Tuure Tuuva for their comments and support during the process. I wish to thank Professor Raimo Sepponen and Major Tapio Saarelainen for reviewing the dissertation.

I want to thank my colleagues at the Laboratory of Applied Electronics and the GEM project at the European Organization for Nuclear Research. My special thanks go to Dr. Mikko Kuisma, Mr. Tommi Kärkkäinen, Dr. Lasse Lensu, Dr. Arto Sankala, and Dr. Paul Aspell for their excellent advice and support. I am also very grateful to Dr. Hanna Niemelä for her effort in editing the English language of this doctoral dissertation.

The financial support by the Research Foundation of Lappeenranta University of Technology, Ulla Tuominen Foundation, Telecommunication and Electronics Association, and LUT Doctoral School is greatly appreciated.

Further, I would like to thank my loving family for their understanding and endless support during my studies. Most importantly, I would like to express appreciation to my beautiful wife Hanna for her encouragement and patience that made this possible. Thank you.

Lappeenranta, August 5th, 2015

Joonas Talvitie

Contents

Abstract **3**

Acknowledgments **5**

List of Symbols and Abbreviations **9**

List of publications **11**

1 Introduction **13**
1.1 Scientific contributions 16
1.1.1 Author's contributions 16

2 Case 1: Measurement instrumentation for a light sensitive biological sensor **19**
2.1 Bacteriorhodopsin sensor 19
2.2 Development of the measurement system 23
2.3 Results and discussion 25

3 Case 2: Instrumentation for the GEM detector for particle physics in the LHC **31**
3.1 Introduction 31
3.2 Development of the measurement system 34
3.3 Results and discussion 37

4 Results and discussion **41**

5 Conclusions **45**
5.1 Suggestions for future work 46

References **47**

Appendices **53**

A Linearity and bandwidth of the two-stage transimpedance amplifier **55**

List of Symbols and Abbreviations

Roman letters

C_F	Feedback capacitance of the transimpedance amplifier
C_m	Capacitance of the bR membrane
$C_p(EV)$	Capacitance of the photoactive part of the bR as a function of illumination
C_p	Capacitance of the photoactive part of the bR
C_{IN}	Input capacitance of the measurement instrumentation
E_p	Photoelectromotive force
R_1	Gain setting resistance of the voltage amplifier
R_2	Gain setting resistance of the voltage amplifier
R_F	Feedback resistance of the transimpedance amplifier
R_m	Resistance of the bR membrane
R_p	Resistance of the photoactive part of the bR
R_s	Series resistance
R_{IN}	Input resistance of the measurement instrumentation
T_P	Pulse width of the laser source

Greek letters

τ_{I1}	Light-on time constant of the photocurrent response
τ_{I2}	Light-off time constant of the photocurrent response
τ_{V3}	Time constant of the photovoltage response

Acronyms

AC	Alternating current

ASIC Application Specific Integrated Circuit

BNC Bayonet Neill-Concelman

bR Bacteriorhodopsin

CERN European Organization for Nuclear Research

CMS Compact Muon Solenoid

CSC Cathode Strip Chamber

DC Direct current

DT Drift Tube

ECAL Electromagnetic Calorimeter

EMI Electromagnetic interference

FPGA Field-programmable gate array

GBT Gigabit Transceiver

GEB GEM Electronics Board

GEM Gas Electron Multiplier

HCAL Hadron Calorimeter

LHC Large Hadron Collider

LVDS Low-voltage differential signaling

PCB Printed circuit board

PM Purple Membrane

PVA Polyvinyl alcohol

RC Resistor-capacitor

RMSE Root-mean-square error

RPC Resistive Plate Chamber

SNR Signal to noise ratio

TOTEM Total cross-section, elastic scattering, and diffraction dissociation measurement

VFAT2 Second generation of a front-end ASIC for silicon and gas detectors

VFAT3 Third generation of a front-end ASIC for silicon and gas detectors

List of publications

1. Talvitie, J.P., Tukiainen, T., Lensu, L., Kärkkäinen, T.J., Silventoinen, P., and Kuisma, M. (2013), "Time-variant electrical equivalent circuit of a dry bacteriorhodopsin sensor," in *Proceedings of IEEE International Instrumentation and Measurement Technology Conference (I2MTC2013)*, pp. 1218–1221.

2. Talvitie, J.P., Tukiainen, T., Lensu, L., Kärkkäinen, T.J., Silventoinen, P., and Kuisma, M. (2015), "Validation of a Time-Variant Electrical Equivalent Circuit for a Dry Bacteriorhodopsin Sensor," in *Proceedings of IEEE International Instrumentation and Measurement Technology Conference (I2MTC2015)*, pp. 352–357.

3. Talvitie, J.P., Tukiainen, T., Lensu, L., Kärkkäinen, T.J., Silventoinen, P., and Kuisma, M. (2015), "Amplifier Errors in a Dry Bacteriorhodopsin Sensor Measurements," in *Proceedings of IEEE International Instrumentation and Measurement Technology Conference (I2MTC2015)*, pp. 1185–1188.

4. Abbaneo, D., Abbrescia, M., Abi Akl, M., Ahmed, W., Armaingaud, C., Aspell, P., Asran, Y., Bally, S., Ban, Y., Banerjee, S., Barria, P., Benussi, L., Bhopatkar, V., Bianco, S., Bos, J., Bouhali, O., Cai, J., Calabria, C., Castaneda, A., Cauwenbergh, S., Celik, A., Christiansen, J., Colafranceschi, S., Colaleo, A., Conde Garcia, A., Dabrowski, M., De Lentdecker, G., De Oliveira, R., De Robertis, G., Dildick, S., Ferry, S., Flanagan, W., Gilmore, J., Guilloux, F., Gutierrez, A., Hoepfner, K, Hohlmann, M., Kamon, T., Karchin, P. E., Khotilovich, V., Korntheuer, M., Krutelyov, S., Lenzi, Th., Loddo, F., Maerschalk, T., Magazzu, G., Maggi, M., Maghrbi, Y., Marchioro, A., Marinov, A., Mazumdar, N., Merlin, J. A., Mukhopadhyay, S., Nuzzo, S., Oliveri, E., Philipps, B., Piccolo, D., Postema, H., Radi, A., Radogna, R., Raffone, G., Ranieri, A., Rodrigues, A., Ropelewski, L., Safonov, A., Sakharov, A., Salva, S., Saviano, G., Sharma, A., Talvitie, J., Tatarinov, A., Teng, H., Turini, N., Tuuva, T., Twigger, J., Tytgat, M., van Stenis, M., Verhagen, E., Yang, Y., Zaganidis, N., and Zenoni, F. (2014), "Development of the data acquisition system for the Triple-GEM detectors for the upgrade of the CMS forward muon spectrometer," *Journal of Instrumentation*, vol. 9, no. 3, pp. C03052.

5. Aspell, P., Dabrowski, M., Conde Garcia, A., De Lentdecker, G., Marinov, A., De Oliveira, R., Talvitie, J., Tuuva, T., and Yang, Y. (2014), "Development of a GEM Electronic Board (GEB) for triple-GEM detectors," *Journal of Instrumentation*, vol. 9, no. 12, pp. C12030.

Chapter 1

Introduction

Over the past few years, technological advancements in microelectronics and sensor technologies have dramatically changed the field of electrical engineering. New manufacturing techniques have enabled a higher level of integration that has combined sensors and electronics into compact and inexpensive systems within everyone's reach. The opportunity to measure the world around you is no longer a privilege of a selected few working closely with electronics. This development has led to a rapid growth in the use of sensors and electronics and widespread utilization in applications where the use of sensors and electronics has hitherto been impossible.

Previously, the challenge in measurements was to understand the operation of the electronics and sensors, but this has changed over recent years. Nowadays, even though instrument consisting of a sensor with appropriate electronics are relatively easy to use, the challenge in measurement instrumentation lies in mastering the whole system, not just the electronics (Staiger, 2009).

Naturally, the challenges come from the electronics, but also from unknown sensor characteristics and the measurement environment. Measurement conditions such as electromagnetic interference, ambient lighting, radiation, and high magnetic fields present in the measurement environment add requirements to the measurements. In addition to the electrical system design and the measurement environment, other related fields such as mechanical design and usability have to be taken into consideration.

To study and develop new sensors and related electronics, a measurement instrumentation has to be constructed. This raises a question of whether it would be beneficial to conceptualize the measurement system as a whole, from the physical phenomena to the digital recording device, where each piece of the measurement system affects the system performance, rather than as a system consisting of small independent parts such as a sensor or an amplifier that could be designed separately. Understanding of this whole measurement chain from the physical phenomena to the digital recording device is crucial, because even if a single component can

achieve a high performance in a measurement system, other system components may degrade overall system performance. This is especially harmful if the source of degradation is not understood, or even worse, goes unnoticed, because wrong conclusion may be drawn about the measurement. An example of this problematic is the report of the OPERA experiment that erroneously measured the neutrinos to travel faster than light (Adam, T. et al., 2012).

To address this issue, this doctoral dissertation concentrates on describing the development of a measurement system and highlighting the related challenges in two example applications that are both intended for scientific studies. The example applications that are used in this study are

1. A light sensitive biological sensor used in imaging;
2. A gas electron multiplier (GEM) detector for particle physics in the Large Hadron Collider (LHC).

The objective of the doctoral dissertation is to describe the development of the measurement system, discuss the challenges caused by the electrical and mechanical requirements and the measurement environment, and propose a solution to them. A practical objective of the work is to develop measurement systems for the two cases studied. The work explains in detail the development and verification of these two measurement systems.

The study is carried out as an empirical case study with these two applications as cases; the research method is well suited for studies where the number of samples is small, as is the case here. Another strength of the method is that it is applicable to new research areas or a research area for which existing theories seem inadequate (Eisenhardt, 1989). The research method also provides examples that have a high value in scientific development (Flyvbjerg, 2006). This is especially true in the field of instrumentation and measurement, where the approach is often rather problem than methodology driven.

As a research method, case study focuses on understanding the dynamics present within a single setting (Eisenhardt, 1989). A case study can be exploratory, descriptive or explanatory in nature (Yin, 2009). This study focuses on describing in depth the development of the measurement systems but is also exploratory since it tries to acquire new insight about the characteristics present in measurement system development. Yin (2009) also notes that case studies are often used to answer the questions ”how” and ”why”. This study, however, answers the questions "what" and "how".

The two cases were chosen based on their availability for the research. In both of these cases, development of a measurement system was required to enable future research. The intended future research set the requirements for the measurement system and the researcher therefore had no control over them. Lack of control over these cases and the small number of samples support the selected research method.

Both cases are measurement systems with a number of differences in physical size, measurement environment and complexity. The first case applying a light sensitive biosensor focuses

on studying the interface between the sensor and the front end. The work provides new information and methods on sensor characteristics and how the measurement front end affects the measurements. The first application needs a relatively small measurement setup, which is common when measuring a single sensor in a laboratory environment. The data acquisition of the system can be carried out using an oscilloscope without a need for extensive data storing or analysis capabilities.

The second case, which concentrates on the development of measurement electronics for particle physics is a large-scale research project. The measurement system to be designed consists of hundreds or thousands of measurement channels. Research of this scale requires significant data storing and analysis capabilities to cope with the large number of measurement channels. Because of the scale of the research project, the study concentrates on a specific part of the measurement system. The dissertation focuses on the measurement chain from the front ends to the data processing unit.

The work provides new results on the development of measurement instrumentation in these challenging applications. The results will help instrument designers as well as engineers and physicists in the development and testing of new measurement systems. In particular, the results provide answers to the following questions about the measurement system:

1. Would it be beneficial to develop a measurement system as a whole in the selected cases?

2. What are the main characteristic that need to be taken into account in these two cases in respect of measurement system design?

   (a) How does the measurement environment affect the development of the measurement system?

   (b) How should the shielding from electromagnetic interference be taken into account during the measurement system development?

   (c) What other requirements need to be taken into account?

3. How should the measurement system be implemented in the selected cases?

Most importantly, the results of this study provide examples of how a measurement system can be successfully constructed to support studies on sensors and electronics.

1.1 Scientific contributions

The main scientific contributions of the doctoral dissertation are the following:

1. Development of a measurement system for dry bacteriorhodopsin (bR) sensors;
2. New observations of the light-dependent photoelectric response from a dry bR sensor;
3. New method for modeling the light-dependent photoelectric response from a dry bR sensor;
4. Determination of the error caused by the amplifier to the photocurrent response measurements;
5. Development of a large-size motherboard for triple GEM detectors to be used in the LHC during the high-luminosity phase.

These scientific contributions of this doctoral dissertation come from five publications presented in international conferences or journals. To demonstrate the scientific contributions in more detail, an overview of the publications is presented in Table 1.1. The table summarizes the objectives of the cases and the individual publications along with the research questions, methods, and main results of each publication.

1.1.1 Author's contributions

The author is the primary author in Publications 1–3 and 5. The author is responsible for the theory and implementation of the measurement system in these publications. The data taking, analysis, and results were also mostly provided by the author. In Publication 4, the author was one of the coauthors of the publication. The author contributed to this publication by planning the part of the measurement system that the publication describes. The part of the measurement system planned in Publication 4 by the author is implemented and verified in Publication 5.

Table 1.1: Summary of the publications and the cases of the doctoral dissertation.

Objective of the case	Study the development of a measurement system for a biological sensor.			Study the development of a part of a measurement system for particle physics.	
	Publication 1	**Publication 2**	**Publication 3**	**Publication 4**	**Publication 5**
Title	Time-variant electrical equivalent circuit of a dry bacteriorhodopsin sensor	Validation of a Time-Variant Electrical Equivalent Circuit for a Dry Bacteriorhodopsin Sensor	Amplifier Errors in a Dry Bacteriorhodopsin Sensor Measurements	Development of the data acquisition system for the Triple-GEM detectors for the upgrade of the CMS forward muon spectrometer	Development of a GEM Electronic Board (GEB) for triple-GEM detectors
Objective	Solve how the intensity-dependent behavior of the bR can be taken into account in sensor modeling	Test whether the proposed method for modeling photocurrent responses of a dry bR sensor is functional if the light intensity is varied	Illustrate and determine the effect of the transimpedance amplifier on the photocurrent measurements	Introduce the application and propose a data acquisiton system for the CMS forward muon spectrometer	Find a method for connecting and powering 24 front-end chips on a triple-GEM detector
Research question	How can the intensity-dependent behavior of the bR be modeled and simulated?	Is the proposed model functional even if the light intensity is varied?	How does the limited rise time of the transimpedance amplifier distort the photocurrent measurements?	What kind of a data acquisition system is required to read out triple-GEM detectors?	How can high-speed signaling and grounding of 24 front ends be carried out without exposing the system to electromagnetic interference?
Method	Literature study and electrical measurements	Electrical measurements	Electrical simulation	Literature study	Electrical measurements
Main result	Method for modeling photocurrent responses of a dry bR sensor at a given light intensity	Validation of the proposed model even if the intensity of the light source is varied.	Estimation of the amplitude and time constant errors caused by the limited rise time of a transimpedance amplifier	Proposition of a data acquisition system to be developed for a triple-GEM detector	Large-size printed circuit board for connecting and powering 24 front end chips

Chapter 2

Case 1: Measurement instrumentation for a light sensitive biological sensor

The first case chosen for study focuses on a light sensitive protein called bacteriorhodopsin (bR). This case is a small research project that requires development of a measurement system to study the photoelectric response from the bR. This chapter introduces previous studies on bR and explains the need for further study. The development and verification of the measurement system are also discussed in detail.

The work presented in this chapter is related to Publications **1** through **3**. A literature study on the dry bR sensors along with the proposed method for modeling the light intensity dependent behavior of the bR is reported in Publication **1**. Publication **2**, again, focuses on validating the proposed model at 13 different light intensities. Finally, Publication **3** discusses errors in the photocurrent measurements that are caused by the limited rise time transimpedance amplifier.

2.1 Bacteriorhodopsin sensor

Bacteriorhodopsin is a photosensitive protein that functions as a light-driven proton pump. This protein has been under intensive research because it has been considered an important biomolecule for biochemical and technology-oriented studies (Hampp, 2000). The popularity of bR as a research target can be explained by its several favorable characteristics: an ability to function and survive under extreme environmental stress (Trissl, 1990; Silfsten et al., 1996; Xu et al., 2003; Walczak et al., 2008), a high quantum efficiency (0.65) (Tittor and Oesterhelt, 1990), and a storage life of years (Vàrò and Keszthelyi, 1983). So far,

various technical applications in optoelectronics and biosensing have been proposed, such as a bio-photoreceiver (Xu et al., 2004), an imaging sensor (Miyasaka and Koyama, 1993; Lensu, 2002; Takamatsu et al., 2005, 2011; Wang et al., 2008), an optoelectronic logic gate (Prasad and Roy, 2012), and a protein-based optical memory (Hampp, 2000; Stuart et al., 2002).

The bR has been studied in both wet and dry states. Studying wet bR samples has been more common although dry bR sensors have been more popular in technical applications because of their suitability for integration into semiconductor devices (Lensu, 2002). In technical applications, the dried bR is often used as a thin or thick film sensor. The film is considered thin if the coating thickness is less than 5 µm, and thick if it is exactly or more than 5 µm. Thin films containing only one layer of bR are more sophisticated and easier to model because the interactions between the different bR layers do not have to be taken into account. An advantage of the thick films is the easier preparation of the sensors. Both the thin and thick films can be used to study the optical and electrical properties of the bR (Lensu, 2002).

The sensors used in this study are thick dry bR films, Figure 2.1. The sensors were prepared by mixing a water solution of purple membrane (PM) fragments with polyvinyl alcohol (PVA). The substance was spread on a conductive SnO_2-coated glass, where the conductive coating formed an electrode. During the polymer drying process, no active means was used to orient the PM patches. The second electrode was prepared by sputtering a thin layer of gold on the dried bR-PVA film. A more detailed description of the sensor preparation procedure can be found in (Lensu, 2002).

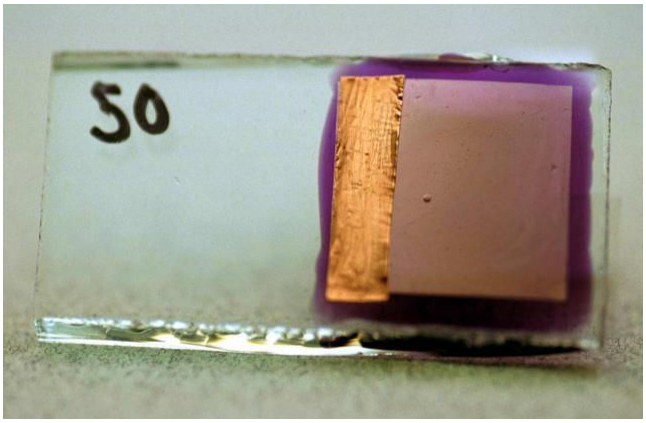

Figure 2.1: Dry bacteriorhodopsin sensor produced by sandwiching a bR-PVA solution between a conductive glass and a thin layer of gold (Tukiainen, 2008).

Upon excitation of light to the dry bR, the bR generates a photoelectric response. The photoelectric response can be measured using for example a voltage or transimpedance amplifier. Depending on whether a voltage or transimpedance amplifier is used, the response can be measured as a photovoltage or a photocurrent. Both of these responses have a characteristic shape, see Figure 2.2.

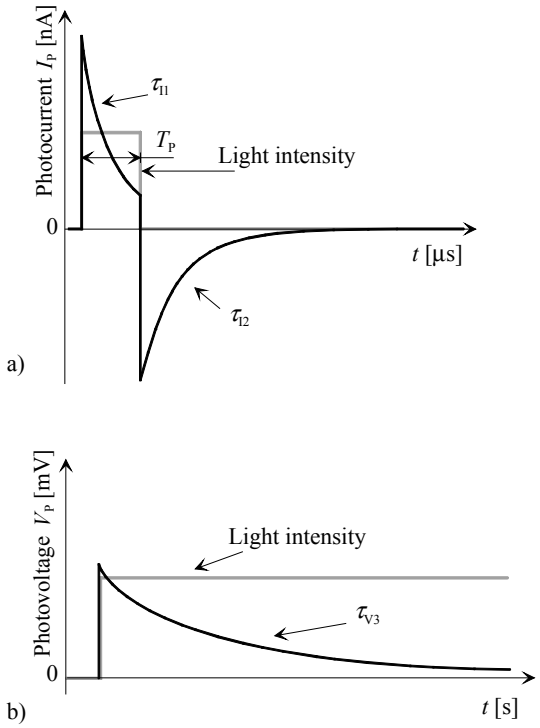

Figure 2.2: Photocurrent pulse response represented by two time constants; τ_{I1} when the light is on, and τ_{I2} when the light is off (a). The photovoltage step response showing a third time constant τ_{V3} (b) (Note different time scales in the two parts of the figure.) (Talvitie et al., 2013).

Common to the both photoelectric responses is a fast rise time, after which the amplitude starts slowly to decay back to the initial state. The difference between the photovoltage and photocurrent response is the decay time. For the photocurrent responses, the decay time is submilliseconds. The decay of the photovoltage response, on the other hand, may take seconds or even minutes. The decay time of the photovoltage response depends on the input impedance of the voltage amplifier used in the measurements (Tukiainen et al., 2014).

Challenges with the dry bR sensors come from the fact that their photoelectric functionality is still partly unknown. Understanding the functionality of the bR has been important in explaining its properties and especially to evaluate its suitability for technical applications. The functionality can be studied by a number of different methods such as polynomial fitting (Hong and Mauzerall, 1974; Trissl, 1990) or estimation of induced charges (Keszthelyi and Ormos, 1980). One approach is to electrically model the behavior of the dry bR sensor and the analog front end connected to it. An advantage of the electrical modeling compared with other methods is that it can be applied to the sensor and electronics design regardless of whether the analog electronics is integrated into the sensor directly in the silicon or whether a separate integrated circuit is used for the signal processing.

A number of different electrical equivalent circuits for bR sensors have been proposed in the literature (Hong and Mauzerall, 1974; Trissl, 1990; Vàrò and Keszthelyi, 1983). Common to all these models is that the photoelectromotive force E_p is connected to the measurement instrumentation through a capacitance C_p. The bR membrane consisting of a membrane resistance R_m and a membrane capacitance C_m is generally accepted to be modeled in parallel with the measurement instrumentation, as presented by Hong (1999). An electrical equivalent circuit presented by Hong (1999) is shown in Fig. 2.3.

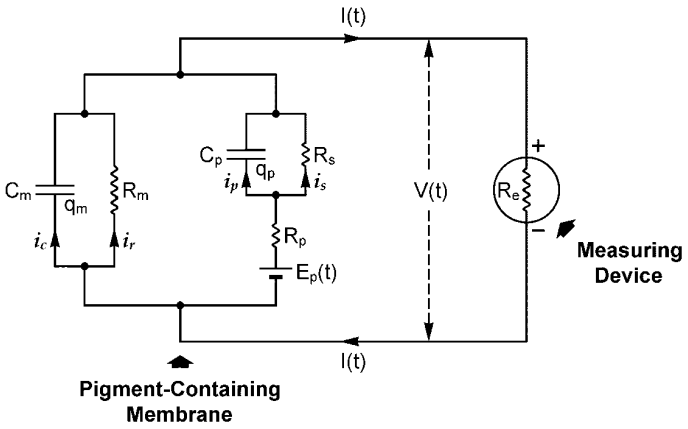

Figure 2.3: Electrical equivalent circuit of bacteriorhodopsin introduced by Hong (reproduced from (Hong, 1999)).

In previous studies (Walczak et al., 2008; Wang et al., 2006; Miyazaki et al., 2013) it has been reported that the illumination changes the photocurrent responses measured from the bR sensor. However, not the model presented by Hong (1999) or any other model can be used to calculate the component values for simulating the changes in photocurrent responses caused by the illumination of the sensor. The problem with the electrical equivalent circuits presented previously is the complexity of the models. Because of this complexity, it is impossible to calculate the components for the electrical equivalent circuit from measurements alone without simplifying the models. For example, Hong (1999) simplified the model by making a crude approximation $C_p \approx C_m$ and $R_s \approx R_m$.

To address this shortcoming, a measurement system for measuring the photoelectric responses along with the method for modeling the photoelectric responses is needed. To simplify and take into account the light-dependent behavior of the bR, this study proposes that the capacitor C_p is expressed as a function of illumination $C_p(EV)$. Also the resistance R_s, shown in Figure 2.3, represents the resistance encountered by the direct current (DC) photocurrent (Hong, 1999). Thus, its effect can be neglected when measuring fast responses. This reduces the electrical equivalent circuit at high frequencies into a model shown in Figure 2.4.

To further simplify the electrical equivalent circuit, the dry bR sensor was decided to be instrumented using a transimpedance amplifier. The advantage of the transimpedance amplifier is the ideally zero input impedance that shorts the bR membrane. The actual input impedance of the transimpedance amplifier is not zero, and also the sensor wiring and contacts add re-

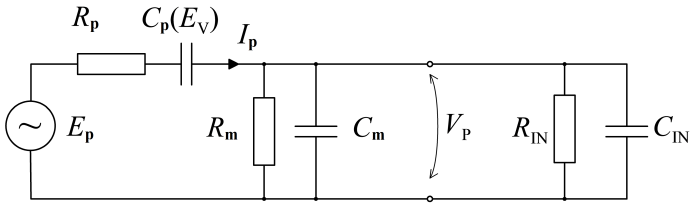

Figure 2.4: Proposed electrical equivalent circuit. The components R_m and C_m model the membrane impedance, and C_p and R_p model the photoactive part of the bR sensor. C_{IN} and R_{IN} model the input impedance of the measurement instrumentation. The light-dependent behavior is modeled by the capacitance $C_p(EV)$ (Talvitie et al., 2013).

sistance to the photocurrent path, but their effect can be neglected as the resistance is only a fraction of R_m, which is in parallel with the input. Therefore, the measurement using the transimpedance amplifier can be assumed as a short-circuit. The membrane resistance R_m has been reported to be over 10 MΩ (Walczak et al., 2008; Wang et al., 2006). This reduces the electrical equivalent circuit into a first-order resistor-capacitor (RC) circuit with a time constant $\tau_I = R_p C_p(Ev)$.

2.2 Development of the measurement system

Verification of the proposed model required the development of a system to measure the photocurrent I_p using a transimpedance amplifier. The measurement system consists of a dry bR sensor, an amplifier, and an oscilloscope. The transimpedance amplifier used in this study is a two-stage amplifier. The advantage of a two-stage amplifier is that the required gain can be shared with both stages of the amplifier, which enables higher bandwidth compared to a single stage amplifier. The reduced gain of the first amplifier stage also makes the transimpedance amplifier less sensitive to the parasitic capacitance in the feedback loop. This parasitic capacitance in the feedback loop arises from the resistor parasitics and the parasitics introduced by the printed circuit board (PCB) layout. The drawback of the two-stage amplifier design is the degraded noise performance (Graeme, 1996).

The first stage of the amplifier consists of a basic transimpedance amplifier with a transimpedance gain of 14 000, Figure 2.5. The second stage of the amplifier consists of a voltage amplifier with a voltage gain of 111. The amplifier achieved a bandwidth of 640 kHz with a total gain of 123.8 dB. More information about the linearity can be found in Appendix A. The output of the amplifier was connected to an oscilloscope using a Bayonet Neill-Concelman (BNC) cable.

For the light excitation of the sensor, a Cavitar CAVILUX Smart laser diode was selected as the light source. The peak wavelength of the laser is 690 nm, the pulse width T_p is 10 µs, and the pulse rise time is 26 ns. The power of the laser is 400 W. The peak wavelength of the laser is not ideal as the peak absorption of the wild-type bR is around 568 nm, which means

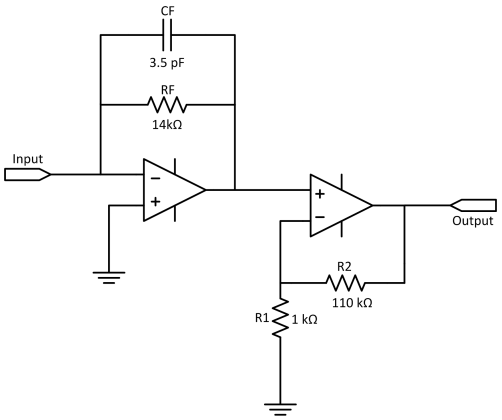

Figure 2.5: Circuit of a two-stage transimpedance amplifier used in this study. The two-stage design enables an higher bandwidth at the expense of the noise performance.

that the excitation of light with 690 nm will result in lower amplitudes of the photoelectric responses from the bR. The maximum pulse width of the selected light source is also short enough so that the resistance R_s of the DC photocurrent can be neglected.

In addition to the components of the measurement system, the optical, mechanical, and electrical requirements have to be defined for the measurement system. These comprise

1. Continuation of the conductive casing to shield against electromagnetic interference (EMI);
2. Isolation from the mains to remove coupling of the mains;
3. Option to monitor the intensity of the illumination;
4. Minimization of optical reflections.

To meet these requirements, the measurement instrumentation and the bR sensor were decided to be placed inside a shielded enclosure to minimize the electromagnetic interference from the light source and other surrounding electronics, Figure 2.6. A path for the illumination was provided by drilling an opening to the enclosure. The constant conductive shielding was ensured by placing a piece of conductive glass and gluing it to the enclosure with conductive epoxy. This way, the illumination could penetrate the enclosure without compromising the shielding from the EMI.

The possible optical reflections were minimized by placing the bR sensor close to the opening and painting the inside of the enclosure with matt black. The opportunity to monitor the intensity of the illumination was achieved by placing a photodiode after the bR sensor. Thus, the photodiode can measure the shape of the light pulse going through the bR sensor. The photodiode can also be used as a trigger in the measurement. The measurement system

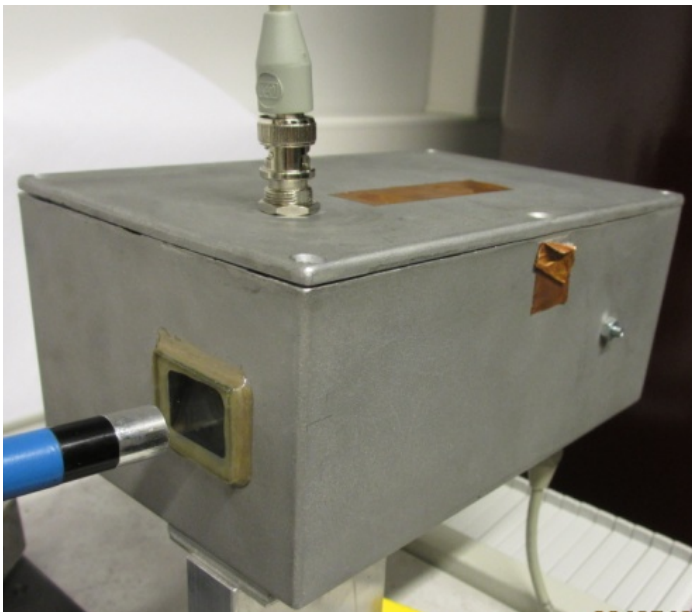

Figure 2.6: Developed measurement system for the photocurrent measurements on a dry bR sensor. The figure shows the optical fiber for laser on the left, the BNC cable from the amplifier on the top, and the BNC from the photodiode on the bottom of the enclosure (Talvitie et al., 2015b).

excluding the light source was decided to be battery powered to isolate it from the mains. This was done to prevent the conductive electromagnetic emissions from adding noise to the measurement system. The batteries were also placed inside the shielded enclosure.

2.3 Results and discussion

The developed measurement system and the proposed electrical equivalent circuit were verified by testing the system to measure a photocurrent response. The measurements were taken without any ambient illumination to prevent its potential effect on the measurement. The measurements were made at a room temperature of 25 °C.

Data acquisition of the measurements was performed with an Agilent DSO81204A 12 GHz oscilloscope and an Agilent E2697A 500 MHz 1 MΩ high impedance adapter. The oscilloscope was set to an alternating current (AC) coupling to remove the DC offset, and averaging of ten consecutive response measurements was used to reduce the noise. This approach improved the signal-to-noise ratio (SNR) without affecting the dynamics of the photocurrent response. The AC coupling has no effect on the photocurrent measurement because it introduces a high-pass filter that has a cut-off frequency of 7 Hz, whereas the measured pho-

tocurrent has time constants of less than 25 µs. Additionally, the transimpedance amplifier functions as a buffer between the bR sensor and the oscilloscope. For this reason, the series capacitor introduced by the AC coupling does not load the bR sensor.

From each measurement, 1E+6 data points (with a sampling frequency of 5 GSa/s) were stored to represent the fast changes and enable further processing of the data. An example of measured and normalized photocurrent responses is presented in Figure 2.7.

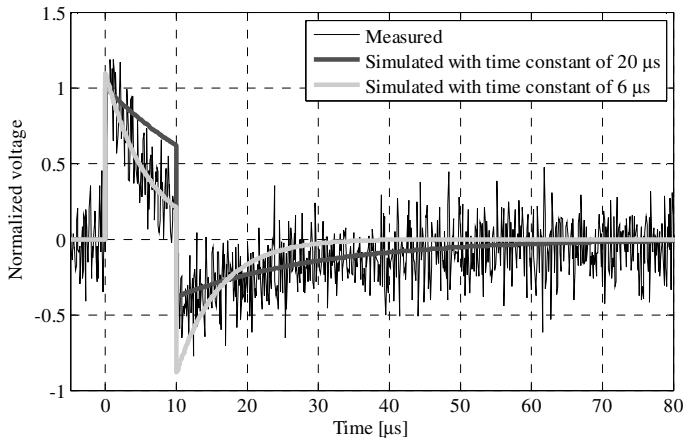

Figure 2.7: Measured and normalized photocurrent responses from the dry bR sensor with the simulated responses from the proposed model (Talvitie et al., 2013)

.

It can be seen from Figure 2.7 that the time constant of the photocurrent response changes depending on whether the light is switched on or off. The time constant in τ_{I1} is around 6 µs and the time constant τ_{I2} is around 20 µs. Thus, the light-off time constant is over three times as large as the light-on time constant. However, it has been reported by Wang et al. (2006) to be approximately two times longer. This difference between the time constants might be caused by the bR sensor, which was a thick film in our case and a thin film in the case of Wang et al. (2006). Figure 2.7 also shows that the simulated responses match the measured signal. This confirms that the proposed model with the intensity-dependent capacitor models the photocurrent response from the dry bR sensor with a high accuracy.

A closer examination of Figure 2.7 shows that the rise time of the response is not zero as it would be in an ideal case. The nonzero rise time is mainly due to the limited bandwidth of the transimpedance amplifier. This limitation affects the interpretation of the amplitudes of the photocurrent responses and may also alter the measurement results. Therefore, the error caused by the limited rise time of the transimpedance amplifier was estimated by simulations. The simulation setup is shown in Figure 2.8.

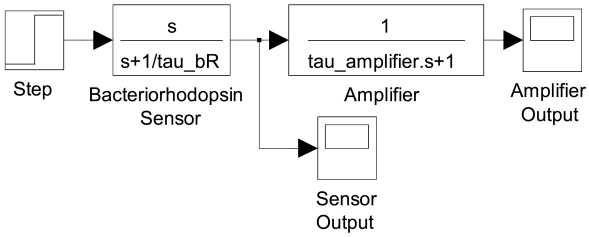

Figure 2.8: Model used to simulate the error caused by the limited rise time of the transimpedance amplifier on the photocurrent measurements (Talvitie et al., 2015a).

The simulations showed that the limited rise time of the transimpedance amplifier distorts both the peak amplitudes and time constants of the measured response. This distortion causes the measured amplitudes to appear smaller than they actually are. The simulations also show that the smallest measured amplitude has the largest relative error. The measured amplitude was 74.9% of the actual one. The largest relative error is due to the fact that the time constant corresponding to that amplitude was the shortest. The shorter the time constants get, the more the limited rise time of the amplifier affects the peak amplitudes. The longest measured time constant was with the measured amplitude of 235.2 nA. In this case, the measured amplitude was 94% of the actual amplitude.

Correspondingly, the limited rise time causes the measured time constants to be longer than they actually are. In the case of the time constants, the largest relative error is with the shortest measured time constant similarly as with the amplitude error. The measured time constant is 13.3% larger than the actual time constant. The largest measured time constant is only 1.5% larger than the actual one. By using the results from the simulations, the amount of error in both the amplitude and time constant can be estimated.

To study the photocurrent response of the dry bR sensor further, photocurrent measurements on a dry bR sensor were carried out at 13 different light intensities. The first photocurrent measurement was performed at the full intensity of the light source. After that, the light intensity was reduced by 6.25 percentage points before each measurement until only 25% of the full intensity was in use. Two examples of the measured photocurrent responses at the highest and lowest intensities are shown in Figures 2.9a and 2.9b.

The measured photocurrent responses clearly show a low SNR especially at the lower intensities. To cope with the low SNR and to extract the amplitude and time constants from the measurements, the signals were preprocessed applying a total variation denoising method. The method was selected to enable the nonlinear least-squares fitting of the two models with two exponential components to the responses without excessive manual tuning of the initial model parameters and constraints for the fitting process. The root-mean-square error (RMSE) values in the figure legends show a good correspondence between the models and the data.

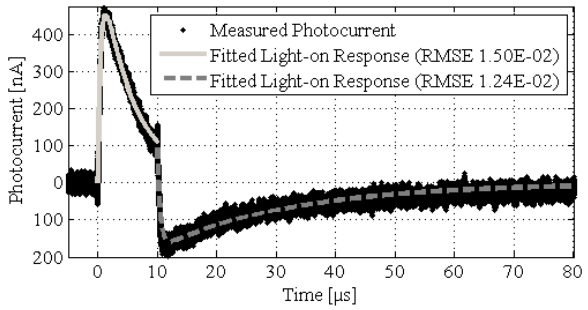

(a)

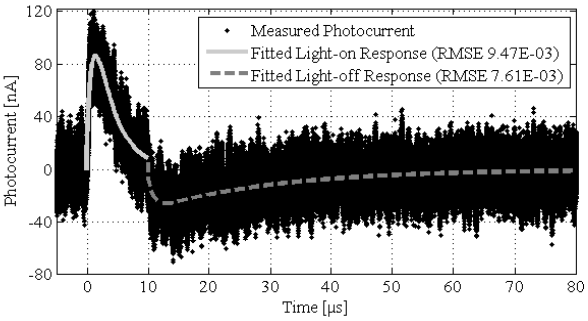

(b)

Figure 2.9: (a) Photocurrent response measured with a 100% light intensity and the transimpedance amplifier, the fitted model for the light-on component (solid line), and the model for the light-off component (dashed line). (b) Photocurrent response measured with a 25% light intensity and the transimpedance amplifier, the fitted model for the light-on component (solid line), and the model for the light-off component (dashed line) (Talvitie et al., 2015b).

Based on the measurements and with the help of the fitted exponential models, the peak amplitudes of the photocurrent responses are extracted, see Figure 2.10. On average, the peak amplitude of the light-on part is approximately three times as high as that of the light-off part. It should be noted that the measurement was influenced by the limited light-on time of the laser system (pulse width), which is why the light-on part of the response does not decay back to the initial level, as can be seen in Figures 2.9a and 2.9b. This limitation affects the interpretation of the light-off amplitudes. As explained before, the amplitudes are also affected by the rise time of the amplifier. Based on the simulations on the effect of the limited rise time of the transimpedance amplifier, the peak amplitudes without the effect of the limited rise time were estimated and added to Figure 2.10.

The estimated peak amplitudes show that the actual amplitudes are 7.5%–33% larger than the measured ones. Despite this, the linear behavior of the peak amplitudes when the intensity is changed remains the same. Based on these results, we may conclude that both the light-on and light-off peak amplitudes of the photocurrent responses increase linearly with the light intensity. This is the case even if the error caused by the linearity of the amplifier is taken into account.

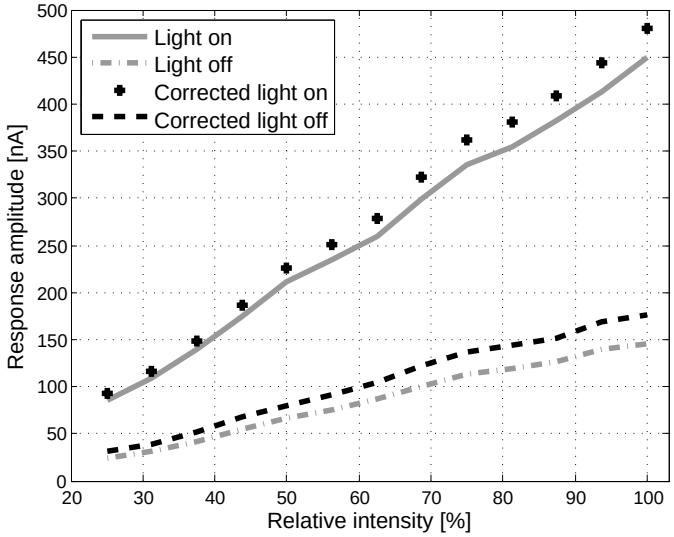

Figure 2.10: Dependence of the photocurrent response amplitude on light intensity (Talvitie et al., 2015b).

In addition to the peak amplitude measurement, the time constants in both the light-on and light-off cases were extracted from the photocurrent measurements applying the total variation denoising method. The measured time constants along with the ones corrected by using the simulations on the limited rise time of the amplifier are shown in Figure 2.11.

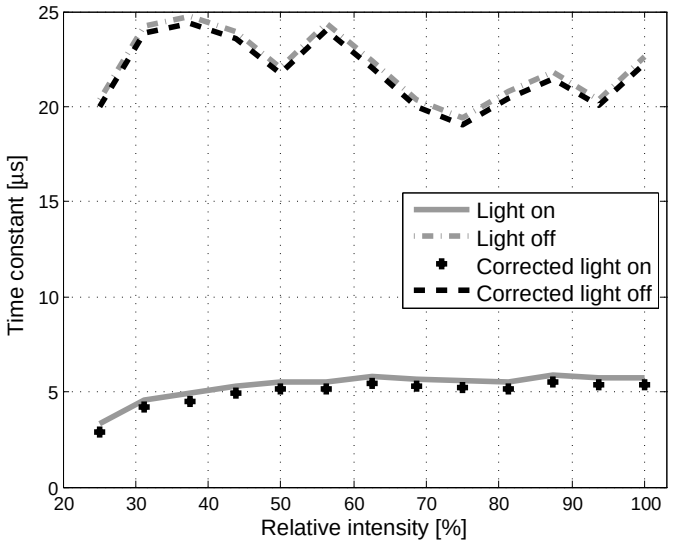

Figure 2.11: Dependence of the photocurrent response amplitude on light intensity (Talvitie et al., 2015b).

Figure 2.11 shows that the time constants both in the light-on and light-off cases are independent of the light intensity, at least when taking into account the limited SNR of the measurements and the accuracy of the model fits. Because the light-on and light-off time constants remain approximately constant even if the light intensity is varied, we may conclude that the proposed model with the light-dependent capacitor can be used to model the photocurrent response of the dry bR sensor regardless of the light intensity used.

It should be noted that the errors shown in Figures 2.10 and 2.11 were estimated using the assumption that the rise time of the light source and the bR sensor are ideal. Of course, this is not the case in reality. Therefore, the estimated errors have to be considered as the maximum error. In fact, the error is actually smaller as a result of the nonzero rise time of the light source and the bR sensor.

The results presented here can be used when analyzing and modeling photocurrent measurements from a dry bR sensor. The proposed model makes it possible to take into account the light-intensity-dependent behavior of the photosensitive biological sensor. An advantage of the proposed method is that it does not require extensive knowledge of biochemistry. Further, the developed measurement system acts as an example for others designing similar measurement systems for biological sensors.

In addition, the case shows how the measurement system is developed as a whole taking into account the sensor, the electronics, mechanics, and the measurement environment. This is important when designing and evaluating the reliability of measurements. For example, in our case, the study on the sensor showed that the photocurrent responses of the dry bR sensor were dependent on the light intensity. Furthermore, the measurement environment may include ambient lighting along with the laser, the light of which can bounce inside the enclosure if no actions are taken to minimize these effects. These reflections could increase the light intensity experienced by the bR sensor. Moreover, this increased light intensity would also change the photocurrent response because of the light dependent behavior of the bR. In this study, these effects were taken into account by designing the measurement system as a whole. This included placing the sensor closer to the opening, painting the inside of the enclosure matt black, and making the measurement without ambient light present during the measurements.

Further, the study on the effects of the limited rise time of the amplifier was shown to distort the measurements. This effect was simulated to understand how it affects the measurement. An absence of careful design and understanding of each of these issues may lead to inaccurate measurements. If these issues go unnoticed, inaccurate measurements may lead to wrong conclusions about the behavior of the dry bR sensors.

Chapter 3

Case 2: Instrumentation for the GEM detector for particle physics in the LHC

The second case chosen for study focuses on the development of a motherboard for Gas Electron Multiplier (GEM) detectors and the readout electronics for particle physics in the Large Hadron Collider (LHC). The case is a large and a complex research project that incorporates multiple input channels and an extensive data acquisition system. This chapter introduces the application and explains the need for further study. In addition to this, also the development and verification of the measurement system are explained in detail.

The work presented in this chapter is related to Publications **4** and **5**. Publication **4** introduces an application that applies GEM detectors to enhance the muon tracking and triggering capabilities in the Compact Muon Solenoid Experiment (CMS). Publication **4** also proposes a full data acquisition system needed to reach this target. Publication **5** focuses on a single part of the data acquisition system described in Publication **4**, the GEM Electronic Board. Finally, the development and initial test on the GEM Electronic Board are explained in detail in Publication **5**.

3.1 Introduction

The world's largest and most powerful particle accelerator, the LHC has been operational since 2008. Since that time, the beam energy delivered by the LHC has been increased from 3.5 TeV to 8 TeV. By 2018, the LHC will be operated at 14 TeV, which will increase the particle rate up to several tens of kHz/cm^2 and also increase the integrated charge faced by

the particle detectors. Currently in the Compact Muon Solenoid Experiment (CMS), Cathode Strip Chambers (CSC) are the only muon detectors used in the high-η region (η) > 1.5) because of the harsh environmental conditions, see Figure 3.1. The CSC detectors provide tracking functions with a limited redundancy.

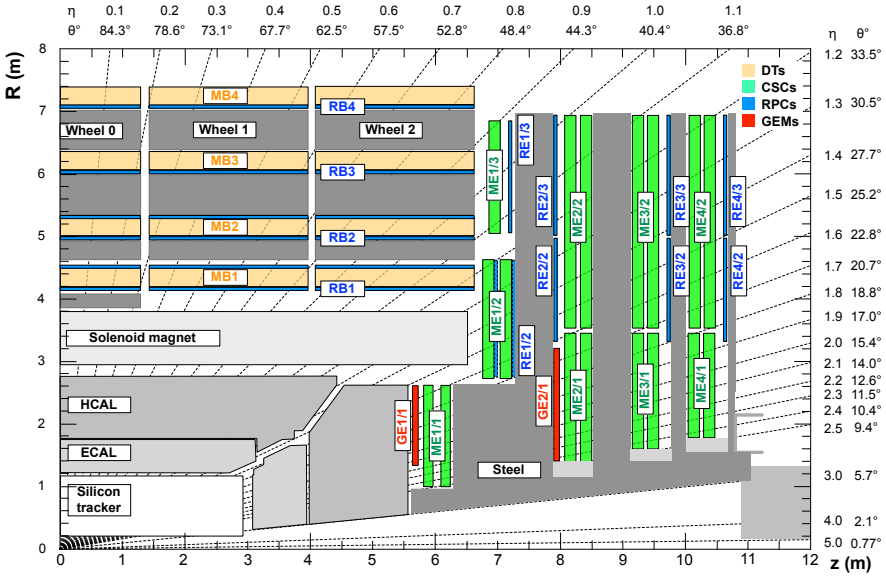

Figure 3.1: Transverse section of one quadrant of the CMS detector showing the proposed locations for the GEM detectors at the Muon stations GE1/1 and GE2/1 along with the η regions. The figure also shows locations of different detectors in CMS such as Silicon Tracker, Hadron Calorimeter (HCAL), Electromagnetic Calorimeter (ECAL), and the muon detectors such as Resistive Plate Chambers (RPC) and Drift Tubes (DT) (Abbaneo et al., 2014).

To enhance the muon tracking and triggering capabilities in the high-η region of $1.5 < \eta < 2.2$, the CMS GEM collaboration (Abbaneo et al., 2013) has proposed to use GEM detectors (Sauli, 1997) as part of its muon system upgrade in the Muon stations GE1/1 and GE2/1. The proposed GEM detectors feature excellent spacial (~100 μm) and time (~5 ns) resolutions. They have also been proven to be able to withstand particle rates up to 10 MHz/cm^2. Further, the use of the GEM detector technology in the CMS allows combination of muon triggering and tracking capabilities in a single detector. This makes it possible to design a compact system to fit the limited space available on the CMS site (Abbaneo et al., 2013).

The GEM detector is a microstrip gas detector. Charged particles passing through the GEM detector release electrons which are collected by the readout strips at the bottom of the detector. The GEM detector's active element is a thin, self-supporting composite mesh, which is made by passivating a thin insulating polymer foil, metalized on each side, with photoresist and exposing it to light. After curing, the metal is patterned on both sides by wet etching. This metal then serves as a self-alignment mask for the etching of the insulator in the open channels. The production method of the mesh is similar to photolithographic methods used to produce multilayer printed circuit boards. By placing the mesh into a suitable gas volume

with readout strips at the bottom of the gas volume parallel to the mesh, a GEM detector is produced. The GEM can be built to a multistage gas electron multiplier by placing several composite meshes within the same gas volume and biasing each mesh applying suitable voltages. Advantage of this multistage design is that the overall gain of the detector can be increased by adding more stages (Sauli, 1997). The GEM detectors in this doctoral dissertation are triple-GEM detectors that have three composite meshes in the same gas volume.

The readout from the GEM detectors is performed by using readout strips. The readout strips are located at the bottom of a thick PCB called GEM Readout Board, which is seen in Figure 3.2. The readout strips are divided into 24 sections, each of which contains 128 strips. The readout of these 128 channels is carried out through a 130 pin connector placed on top of the GEM Readout Board.

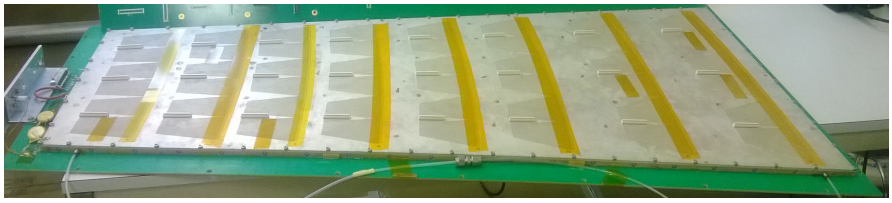

Figure 3.2: One-metre-long GEM Readout Board with 24 130 pin output connectors for reading out the strips of the GEM detectors.

To use these GEM detectors, a readout system is required. A complete electronics system is currently under design for the purpose. The proposed electronics system for the GEM detectors consists of two regions: the "on-detector" region and the "off-detector" region, presented in Figure 3.3.

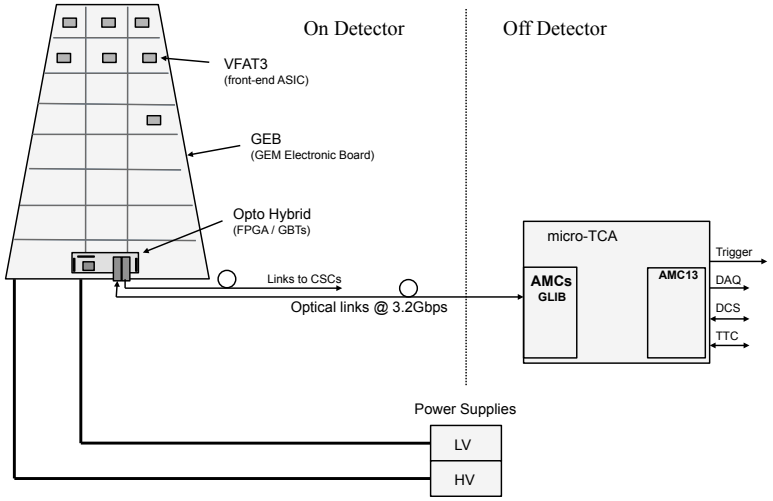

Figure 3.3: Electronics and data acquisition system architecture proposed for the CMS GE1/1 subdetector (Abbaneo et al., 2014).

The electronic components of the "on-detector" region have to be resistant to radiation. The electronics of the "off-detector" region are located in the counting room, where standard electronic components can be used. The electronics in these two regions are connected to each other using radiation hard optical links.

The proposed on-detector part of the system is optimized for use with the GEM detectors. This system comprises a front-end readout application specific integrated circuit (ASIC) for reading out the analog signal from the GEM detectors and sending them to an field-programmable gate array (FPGA) board called an optohybrid. The front-end ASIC called VFAT3 reads out 128 analog channels from the GEM detector and sends out a trigger when a particle is detected. Along with the generation of the trigger, the front-end ASIC provides a tracking function to identify the channels that were hit. Correspondingly, the optohybrid communicates with the 24 front-end ASICs and combines the triggering and tracking information received from the front ends. This information is then sent to the "off-detector" electronics using the radiation hard optical links. What is currently missing from the measurement system is the method for powering and connecting the ASICs to the optohybrid.

Challenges of this measurement system arise from the mechanical and electrical requirements. The mechanical requirements come from the predefined area in which the GEM detectors with the necessary readout electronics and cooling have to fit. The length of the trapezoid area available for the electronics and the cooling in the Muon station GE1/1 is 1003 mm. The width of the trapezoid area (with a height of 20 mm) is 345 mm at the wider end and 146 mm at the narrower end. The width of the GEM detector itself is 457 mm at the wider end and 285 mm at the narrower end, but in this extended area, the height available above the detector is only 1.8 mm. Previously in the total cross-section, elastic scattering, and diffraction dissociation measurement (TOTEM) experiment (The TOTEM Collaboration et al., 2008) in a similar system, the connection from the front ends to the optohybrid was provided by flat cables. Owing to the tight mechanical constraints on the CMS site, this is not an option.

Correspondingly, the electrical requirements arise from the fact that the system is designed to pick up low-level signals that are generated by cosmic particles. For this reason, an adequate noise performance of the system is one of the main concerns from the design point of view. The noise in the measurements can be increased by a number of different mechanisms; for instance, it can be induced by electromagnetic interference that radiates from high-speed signals in the close proximity. It can also couple into the measurement from the power supply.

To solve these problems, a new method for connecting the front ends to the optohybrid has to be provided.

3.2 Development of the measurement system

Based on the requirements for the method for connecting the front ends to the optohybrid, three main objectives can be delineated:

- to provide stable powering and ground for 24 VFAT3 front-end chips;
- to connect the 24 VFAT3 front ends to the gigabit transceivers (GBT) of the Optohybrid using high-speed digital signals;
- to shield the GEM detector from electromagnetic interference.

To meet these three main objectives, the design process was started by considering the electromagnetic shielding of the GEM detector. The strips on the GEM detectors are relatively long (from 9 cm up to 20 cm), which makes them sensitive to picking up the external electromagnetic noise generated by other electronic systems nearby. Thus, the shielding of the GEM detector requires a continuous shield that can cover the whole detector. A continuous shielding was achieved by designing a single large PCB called GEM Electronic Board (GEB) that can cover the whole over one-meter-long GEM detector. The GEM Electronic Board or the GEB is a large-size PCB that is placed on top of the GEM detector. Even though the GEB is placed on top of the GEM detector, it is a separate board. This allows the GEB board and all of the electronics on it to be replaced without opening and possibly contaminating the GEM detector. An advantage of this large continuous PCB is also that it enables the routing of 24 VFAT3 front ends to the optohybrid without a need for additional connectors or cables.

The GEM Electronic Board was designed as a multilayer PCB with six layers. The six layers have two middle layers that are used to distribute the power and ground. Another two inner layers are used to route all 288 differential pairs and 144 single-ended signals from the 24 VFAT2 front ends to the optohybrid. The top and bottom layers of the PCB are continuous ground planes. The ground planes are stitched together by vias to surround the signal lines using ground. This way, the signal lines are shielded from external electromagnetic interference, but more importantly, this prevents the noise from radiating from high-speed signals to the sensitive strips on the GEM detectors.

The VFAT3 chips are mounted on PCBs called VFAT3 hybrids. The VFAT3 hybrids have a connector to connect the analog input signals from a GEM detector to the VFAT3 chip, and a second connector to transfer the digital signals to the GEB; see Figure 3.4.

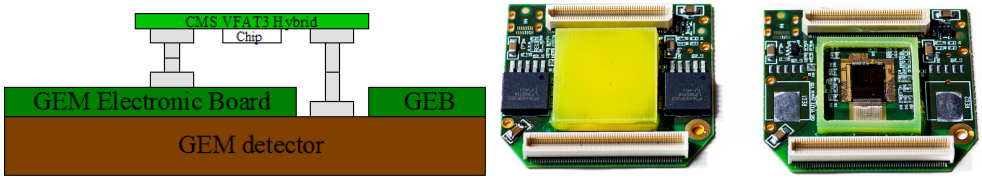

(a) (b)

Figure 3.4: (a) Mounting of the VFAT hybrids on the GEM detector and on the GEB. (b) CMS VFAT2 hybrids used with the prototype as the VFAT3 chips are still under development. Figure shows the VFAT2 hybrids with and without the protective covers that are used to provide mechanical protection (Aspell et al., 2014).

Since the GEB is placed on top of the GEM detector, these two connectors have to be of different height. This height difference also defines the thickness of the GEM Electronic Board. In our case, the height difference of these connectors was chosen to be 1 mm, which is the standard thickness in PCB manufacturing and meets our requirements for the maximum height of 1.8 mm at the edges of the detector.

In addition to the shielding and dimensions, the signal distribution of the GEB had to be designed. Signal distribution to the VFAT3 hybrids is carried out by using three separate clock and trigger lines, which each provide the clock and the trigger for a single column of eight VFAT2 hybrids; see Figure 3.5. Other differential lines were individual for each VFAT3 hybrid. Thus, they were routed directly from each VFAT3 hybrid to the optohybrid. Because of the high frequency of 320 MHz where the VFAT3 chips operate and the length of over 1 m, the differential high-speed signals required phase matching. Phase matching was performed for each whole row on the GEB that contained three VFAT3 hybrids instead of a single hybrid. This eases the determination of the delay from each VFAT3 hybrid to the optohybrid in the software development later on.

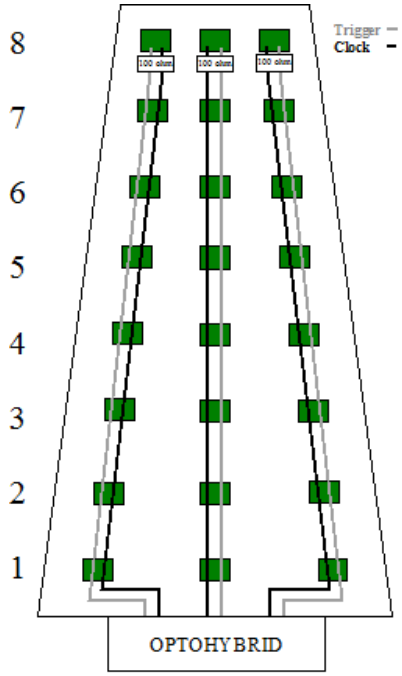

Figure 3.5: GEB clock and trigger signal distribution for 24 VFAT3 hybrids (Aspell et al., 2014).

An advantage of the clock and trigger buses is that they need a smaller number of differential pairs compared to individual clock and trigger lines. This is important since the routing density on the narrow end of the PCB is rather high. A high routing density would force the differential lines closer to each other that might increase the crosstalk between differential pairs.

3.3 Results and discussion

The primary objective of the proposed GEB board was to provide power and connect 24 front ends to the FPGA without compromising the noise performance of the system. Besides the primary objective, the first prototype was also used to study the signal integrity on the over one-meter-long signals, to find out whether the PCB has enough space for the routing of 24 front ends to the FPGA and how the proposed design affects the noise performance of the system. Another subtarget was to test the PCB's suitability for large-scale manufacturing.

The feasibility of the proposed GEB board was verified by manufacturing a few prototype PCBs, Figure 3.6. In the first manufacturing run of the proposed PCB, manufacturing problems were encountered. The finished PCBs suffered from short-circuits that were caused by laminating deviations, which were difficult to control because of the large size of the PCB. For the next manufacturing run, these problems were solved by adjusting the manufacturing process.

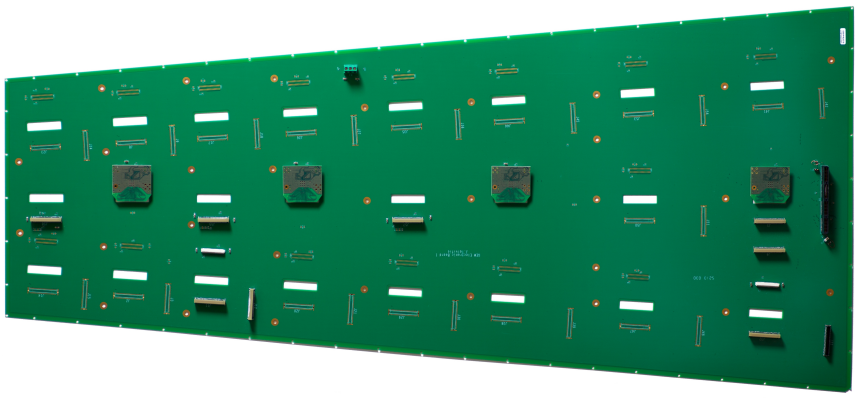

Figure 3.6: Manufactured one-meter-long GEM Electronic Board with four CMS VFAT2 hybrids mounted on it (Aspell et al., 2014).

The final system that is to be installed to the CMS in 2018 will use a custom-made front-end ASIC called VFAT3. Currently, the VFAT3 chip is still under development, which is why the initial version of the GEB was manufactured without impedance control to be operated with already available VFAT2 front-end chips that run with 40 MHz low-voltage differential signaling (LVDS) signals (Aspell et al., 2008). For this reason, the initial GEB version was used to test the signal integrity at 40 MHz on the longest over one-meter-long differential pair, not the higher operating frequency of the VFAT3, which is 320 MHz.

The LVDS test signal feed-through the PCB was generated using a signal generator. At the other end, the signal was terminated differentially with a 100 Ω resistor. The input signal from the signal generator and the output signal over the 100 Ω resistor were recorded using a differential probe and an oscilloscope. The measured signals are shown in Figure 3.7.

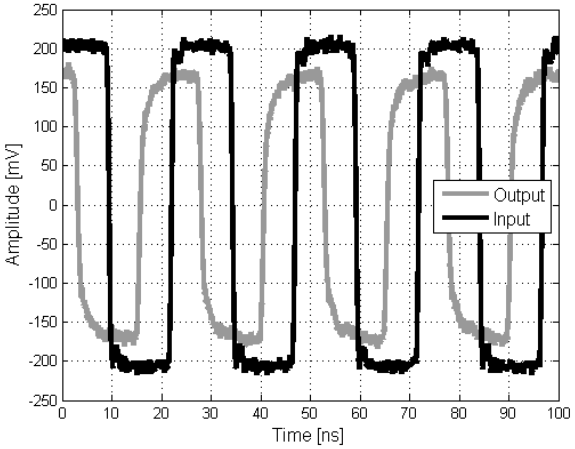

Figure 3.7: Signals measured coming in and out of the GEB board (Aspell et al., 2014).

Figure 3.7 shows that at the frequency of 40 MHz, the signal from the end of the clock line has a slightly lower amplitude. This is because the differential PCB traces have a DC resistance around 11 Ω, each of which reduces the amplitude seen over the 100 Ω terminating resistor. It can be also seen that the highest frequencies at the output signals are attenuated. Nonetheless, the signal is sufficient to enable reliable communication between the VFAT2 front end and the optohybrid board. The delay between the input and output signals is due to the propagation delay over the meter long PCB traces.

The initial version GEB-V1 has an option to read out six VFAT2 front ends out of the 24 VFAT2 front ends using the first version of the optohybrid. The rest of the VFAT2 hybrids could be read out using a different readout system called TURBO, which has been developed for the TOTEM experiment (The TOTEM Collaboration et al., 2008). The use of these two readout systems on the same PCB makes it possible to test the functionality and performance of the proposed GEM Electronic Board with VFAT2 hybrids but also enables the use of the well-known TURBO readout system as a reference for initial tests. The proposed GEB design was tested with the VFAT2 front ends and the optohybrid and found to be functional.

The initial noise performance was tested by reading out multiple VFAT2 front ends simultaneously and monitoring the noise levels on the measured responses from the front ends. No notable increase in the noise levels was detected that could be due to the electromagnetic interference generated by the readout system. Nevertheless, further study is needed in the future to verify the functionality for the next-generation VFAT3 front ends that are still under development. The major difference between these two front ends is the higher operating frequency of the VFAT3 front ends, which is 320 MHz. The operation at 320 MHz might increase the electromagnetic interference generated by the differential signals that can be then picked up by the GEM detector. Another concern could be the signal integrity on the over one-meter-long differential signals at 320 MHz. This could be a challenge because of the thin traces of the differential pairs and the long stub lengths that are defined by the application.

The results of the case two show how the development of the measurement system for the GEM detectors is carried out as a whole taking into account electrical requirements such as powering, signal integrity, and shielding of the differential pairs, but also a number of other issues. These issues include the mechanical requirements, for instance the space available for the electronics and the measurement environment that have to be taken into consideration in order to design a system that can survive in the presence of radiation and high magnetic fields.

Chapter 4

Results and discussion

The purpose of this work was to study whether it would it be beneficial to consider a measurement system as a whole from the physical phenomena to the digital recording device, where each piece of the measurement system affects the system performance, instead of a system consisting of small independent parts such as a sensor or an amplifier that could be designed separately. The practical objective of this doctoral dissertation was to develop measurement systems for a light sensitive biosensor used in imaging and for a GEM detector for studies in particle physics. The study was carried out as an empirical case study. The cases were selected based on a need for development of a measurement system for future research.

The research questions answered in this doctoral dissertation are:

1. Would it be beneficial to develop a measurement system as a whole in the selected cases?
2. What are the main characteristic that need to be taken into account in these two cases in respect of measurement system design?
   (a) How does the measurement environment affects the development of the measurement system?
   (b) How should the shielding from electromagnetic interference be taken into account during the measurement system development?
   (c) What other requirements need to be taken into account?
3. How should the measurement system be implemented in the selected cases?

The study showed that in the measurement system for the dry bR sensor, the electrical interactions between different parts of the system can be designed by considering the interactions of two parts of the system at a time. To give an example: the interface between a sensor and an

amplifier calls for planning because of the sensor characteristics and the limited bandwidth of the amplifier. Further, the connection from the amplifier and the oscilloscope has to be taken into account to prevent signal distortions caused by the loading of the oscilloscope. However, the interactions between the sensor and the oscilloscope can be considered minimal because the amplifier functions as a buffer between the two.

In the case of the measurement system for GEM detectors, more effort had to be spent on studying the electrical interactions between different parts of the system. For example, the interactions between the detector and the motherboard have to be understood along with the mechanical constraints to design protection from the electromagnetic interference. Without proper design, the EMI could induce noise to the detector. The same effect is also present in Case 1, but the consequences were easier to handle. This is because the system in case one is simpler and more compact, which makes the aggressor and the victim circuits smaller, thereby reducing the sensitivity to EMI and making the shielding more trivial.

Furthermore, the measurement environment can affect the measurements in both of the selected cases. In photocurrent measurements on a dry bR sensor, the measurement can be affected by the ambient lighting present in the measurement environment and also by reflections of the laser beam. These can increase the illumination faced by the bR sensor, which may affect the photocurrent responses because of the observed intensity dependent behavior of the dry bR sensor. Correspondingly, the measurement environment where the GEM detectors are located suffers from radiation and high magnetic fields. For this reason, the effect of the measurement environment on the measurement system should be understood in both of the cases.

Implementation of the measurement system for the bR sensor and the GEM detectors was described in detail in Sections 2.2 and 3.2. Photocurrent measurements on the dry bR sensor have produced new information about the light dependent behavior of the dry bR sensor and its modeling. Moreover, the developed large-size PCB has been successfully used to power and connect front-end ASICs to the FPGA. Thus, the objectives of the development and implementation of the measurement system can be considered to have been met.

Protecting the measurement from the electromagnetic interference was quite different for the two cases. In Case 1, the protection was achieved by simply placing the battery-powered electronics inside a metal enclosure. A path for the illumination was obtained by drilling an opening to the enclosure. The opening was covered by gluing a piece of conductive glass with conductive epoxy to retain the shielding capabilities of the metal enclosure.

Achieving this with the second case of the study was more complicated. Because of the large size of the GEM detector shielding, using an enclosure is not feasible. To protect the GEM detector against electromagnetic interference, the GEM detector was covered with a large-size PCB to function as a shield on top of the GEM detector. The PCB also provides powering and a means of connecting the front-end ASICs to the FPGA. In this method, the challenge comes from the tight mechanical constraints of the measurement environment and also from the need to manufacture an over one-meter-long PCB that would be large enough to cover the whole GEM detector. Despite these challenges, the large-size PCB was success-

fully manufactured and found to provide necessary protection against the electromagnetic interference.

Because of the many issues that have to be considered when designing these measurement systems, we may conclude that in these cases it would be beneficial to approach the development of a measurement system as a whole starting from the physical phenomena and continuing to the digital recording device. In addition to the electrical design and the measurement environment, for example, the mechanics has a significant impact on the measurement system design. This approach is especially useful when working with the GEM detector, which is a rather complex and large measurement system, but it is also beneficial with the smaller measurement system for the dry bR sensor, as explained above.

In addition, the study provides the following contributions:

Case 1: Measurement instrumentation for a light sensitive biological sensor

1. Development of a measurement system for dry bR sensors;
2. Confirmation of the light-intensity-dependent behavior of the dry bR sensor;
3. Development of an electrical equivalent circuit that takes into account the light-intensity-dependent behavior of the dry bR sensor;
4. Determination of how the rise time of the transimpedance amplifier affects the amplitudes and time constants measured from the photocurrent responses of the bR.

Case 2: Instrumentation for the GEM detector for particle physics in the LHC

1. A compact method was developed for powering, connecting 24 front-end chips to the concentrating FPGA, and providing a continuous electromagnetic shield over the GEM detector;
2. Manufacturability of over one-meter-long six-layer PCBs was tested and found to be feasible;
3. Signal integrity of over one-meter-long differential signals was tested at 40 MHz and found to be sufficient;
4. Functionality with the existing VFAT2 front ends was verified.

Furthermore, the two measurement systems developed work as examples of a measurement system needed for scientific studies. These results help instrument designers as well as engineers and physicist working on developing new sensors and electronics.

Chapter 5

Conclusions

Technological advances in both microelectronics and sensor technologies have dramatically changed the field of electrical engineering. These advancements have combined sensors and electronics into compact and inexpensive systems, which has led to the rapid growth of sensors and electronics that are relatively easy to use even without extensive knowledge of electrical engineering. Therefore, the challenge in measurements has shifted from mastering the electronics to understanding the whole system, not only the electronics. Understanding of the whole system is highly important, because even if a single component in a system can achieve high performance, other system components may degrade the overall system performance.

To study and develop new sensors and the related electronics, a measurement instrumentation has to be constructed. This doctoral dissertation studies whether it is beneficial to conceptualize a measurement system as a whole from the physical phenomena to the digital recording device, where each piece of the measurement system affects the system performance, instead of as a system consisting of small independent parts such as a sensor or an amplifier that could be designed separately. The development of a measurement system was studied empirically in two cases: a light sensitive biosensor used in imaging and a GEM detector for particle physics.

The study showed that in these two cases there were a number of different parts of the measurement system that interacted with each other. Without considering these interactions, the reliability of the measurement may be compromised, which may lead to wrong conclusions about the measurement. This is especially harmful if the source of the degradation is not understood, or even worse, goes unnoticed. To take these interactions into account, it is beneficial to design the measurement system as a whole, including not only the electronics but also other aspects such as mechanics and measurement environment.

In addition to the main results, the study also described in depth the development of the measurement system for both of the cases. This description can be used as an example how to construct a viable measurement system to support studies on sensors and electronics. Further,

the study also provides new information on number of points related to the measurement system design for a light sensitive biological sensor and a particle detector.

5.1 Suggestions for future work

Despite the answers given by the doctoral dissertation, there are still issues to be resolved in both of the cases. In the first case, the measurements on dry bR sensors were carried out by using the same sensor all the time. Thus, although the measurement results can be taken as examples, they cannot be generalized. One reason for this is the manual preparation procedure of the dry films, which may cause the sensor characteristics to vary between individual films (Lensu, 2002). To address this shortcoming, the measurements using the 13 different light intensity levels should be repeated for similar sensors. This would enhance knowledge about the repeatability of the amplitude and time constants of the measurement.

Another place for improvement is the rise time of the transimpedance, even though the error caused by the limited rise time of the transimpedance amplifier was estimated by simulations. The error caused by the rise time could be mitigated by increasing the bandwidth of the amplifier. This could be achieved by using more advanced amplifier topologies, as described in (Ciofi et al., 2007; Massarotto et al., 2006).

The designed GEM electronic board for the GEM detectors in the second case was tested for the manufacturability, functionality with the current front-end designs, and signal integrity at the frequency of 40 MHz. Although these results are promising, there are still questions to be answered. For example, the designed GEM Electronic Board was not tested in the actual measurement environment, which has radiation and high magnetic fields. However, the proposed PCB does not have any magnetic components nor any integrated circuits that could be vulnerable to radiation or high magnetic fields.

One of the unsolved issues is the manufacturability of the long PCBs in larger quantities, up to 200 pieces. A possible problem with the manufacturing is for example the need for calibration during the manufacturing process. If repeated calibration is needed, it will increase the manufacturing time and possibly the manufacturing costs. Another concern is the functionality of the next-generation VFAT3 front ends that are currently under development. The VFAT3 front ends operate at 320 MHz, which will increase the need for decoupling between the power and ground planes. This might be a problem especially when all 24 front ends operate simultaneously. Insufficient decoupling will increase the power supply noise that can couple to the front ends.

Further, the signal integrity over the 1 m differential pairs has still to be tested at 320 MHz. Possible reflections and amplitude drop may ruin the signals in the long differential pairs making them unavailable for providing a clock to the front-end chips. If this is the case, an alternative is to use an LVDS buffer in the middle of the clock line, which would help the signal integrity if a suitable buffer were found that could withstand the radiation level present in the measurement environment.

References

Abbaneo, D., Abbrescia, M., Akl, M.A., Ahmed, W., Armaingaud, C., Aspell, P., Assran, Y., Bally, S., Ban, Y., Banerjee, S., Barria, P., Benussi, L., Bhopatkar, V., Bianco, S., Bos, J., Bouhali, O., Cai, J., Calabria, C., Castaneda, A., Cauwenbergh, S., Celik, A., Christiansen, J., Colafranceschi, S., Colaleo, A., Garcia, A.C., Dabrowski, M., Lentdecker, G.D., Oliveira, R.D., Robertis, G.D., Dildick, S., Ferry, S., Flanagan, W., Gilmore, J., Guilloux, F., Gutierrez, A., Hoepfner, K., Hohlmann, M., Kamon, T., Karchin, P.E., Khotilovich, V., Korntheuer, M., Krutelyov, S., Lenzi, T., Loddo, F., Maerschalk, T., Magazzù, G., Maggi, M., Maghrbi, Y., Marchioro, A., Marinov, A., Mazumdar, N., Merlin, J.A., Mukhopadhyay, S., Nuzzo, S., Oliveri, E., Philipps, B., Piccolo, D., Postema, H., Radi, A., Radogna, R., Raffone, G., Ranieri, A., Rodrigues, A., Ropelewski, L., Safonov, A., Sakharov, A., Salva, S., Saviano, G., Sharma, A., Talvitie, J., Tatarinov, A., Teng, H., Turini, N., Tuuva, T., Twigger, J., Tytgat, M., van Stenis, M., Verhagen, E., Yang, Y., Zaganidis, N., and Zenoni, F. (2014), "Development of the data acquisition system for the triple-gem detectors for the upgrade of the cms forward muon spectrometer," *Journal of Instrumentation*, vol. 9, no. 03, p. C03052, URL `http://stacks.iop.org/1748-0221/9/i=03/a=C03052`.

Abbaneo, D., Armagnaud, C., David, E., De Oliveira, R., Ferry, S., Franconi, L., Fruboes, T., Gnanvo, K., Mehta, K., Oliveri, E., Raffone, G., Ropelewski, L., Sharma, A., Smilkjovic, N., Staib, M., Tupputi, S., Turini, N., Verhagen, E., Villa, M., Yang, Y., Zientek, M., Saviano, G., Tytgat, M., Benussi, L., Mohapatra, A., De Lentdecker, G., Formenti, F., Hohlmann, M., Karchin, P., Maggi, M., Marchioro, A., Moulik, T., Ban, Y., Cai, J., Zaganidis, N., Aspell, P., Magazzu, G., Gutierrez, A., Rodrigues, A., Christiansen, J., Bally, S., Berzano, U., Chatelain, J., De Robertis, G., Conde Garcia, A., Teng, H., Loddo, F., Colafranceschi, S., Nuzzo, S., Abbrescia, M., Colaleo, A., Bianco, S., Bunkowski, K., Bos, J., Postema, H., Marinov, A., Piccolo, D., Maerschalk, T., Duarte Pinto, S., Nemallapudi, M., and Merlin, J. (2013), "GEM based detector for future upgrade of the CMS forward muon system," *Nucl. Instrum. Methods Phys. Res., A*, vol. 718, pp. 383–386. 4 p.

Adam, T. et al. (2012), "Measurement of the neutrino velocity with the OPERA detector in the CNGS beam," *JHEP*, vol. 1210, p. 093.

Aspell, P., Anelli, G., Chalmet, P., Kaplon, J., Kloukinas, K., Mugnier, H., and Snoeys, W. (2008), "VFAT2: A front-end "system on chip" providing fast trigger information and dizitized data storage for the charge sensitive readout of multi-channel silicon and gas particle detectors," in *Proc. IEEE Nuclear Science Symposium (NSS'08)*, URL `http://stacks.iop.org/1748-0221/5/i=11/a=C11022`.

Aspell, P., Dabrowski, M., Garcia, A.C., Lentdecker, G.D., Marinov, A., Oliveira, R.D., Talvitie, J., Tuuva, T., and Yang, Y. (2014), "Development of a gem electronic board (geb) for triple-gem detectors," *Journal of Instrumentation*, vol. 9, no. 12, p. C12030, URL http://stacks.iop.org/1748-0221/9/i=12/a=C12030.

Ciofi, C., Crupi, F., Pace, C., Scandurra, G., and Patane, M. (2007), "A new circuit topology for the realization of very low-noise wide-bandwidth transimpedance amplifier," *IEEE Transactions on Instrumentation and Measurement*, vol. 56, no. 5, pp. 1626–1631.

Eisenhardt, K.M. (1989), "Building theories from case study research," *The Academy of Management Review*, vol. 14, no. 4, pp. pp. 532–550, URL http://www.jstor.org/stable/258557.

Flyvbjerg, B. (2006), "Five misunderstandings about case-study research," *Qualitative Inquiry*, vol. 12, no. 2, pp. 219–245, URL http://qix.sagepub.com/content/12/2/219.abstract.

Graeme, J. (1996), *Photodiode Amplifiers: OP AMP Solutions*, McGraw-Hill, Inc., New York, NY, USA, 1 edn.

Hampp, N. (2000), "Bacteriorhodopsin as a photochromic retinal protein for optical memories," *Chemical Reviews*, vol. 100, no. 5, pp. 1755–1776, URL http://dx.doi.org/10.1021/cr980072x, pMID: 11777419.

Hong, F. (1999), "Interfacial photochemistry of retinal proteins," *Progress in Surface Science*, vol. 62, no. 1, pp. 1–237, URL http://www.ingentaconnect.com/content/els/00796816/1999/00000062/00000001/art00014.

Hong, F. and Mauzerall, l.D. (1974), "Interfacial photoreactions and chemical capacitance in lipid bilayers," in *Proc. Natl. Acad. Sci. USA*, pp. 1564–1568.

Keszthelyi, L. and Ormos, P. (1980), "Electric signals associated with the photocycle of bacteriorhodopsin," *{FEBS} Letters*, vol. 109, no. 2, pp. 189 – 193, URL http://www.sciencedirect.com/science/article/pii/0014579380810830.

Lensu, L. (2002), *Photoelectric Properities of Bacteriorhodopsin Films For Photosensing And Information Processing*, Ph.D. thesis, Lappeenranta University of Technology, Lappeenranta, Finland.

Massarotto, M., Garcia, A., and Lopez-Martin, A. (2006), "Two-stage differential charge and transresistance amplifiers," in *Proceedings of the IEEE International Instrumentation and Measurement Technology Conference (I2MTC2006)*, pp. 1920–1925.

Miyasaka, T. and Koyama, K. (1993), "Image sensing and processing by a bacteriorhodopsin-based artificial photoreceptor," *Applied Optics*, vol. 32, pp. 6371–6379.

Miyazaki, S., Matsumoto, M., Brier, S., Higaki, T., Yamada, T., Okamoto, T., Ueno, H., Toyabe, S., and Muneyuki, E. (2013), "Properties of the electrogenic activity of bacteriorhodopsin," *European Biophysics Journal*, vol. 42, no. 4, pp. 257–265, URL http://dx.doi.org/10.1007/s00249-012-0870-0.

Prasad, M. and Roy, S. (2012), "Optoelectronic logic gates based on photovoltaic response of bacteriorhodopsin polymer composite thin films," *IEEE Transactions on NanoBioscience*, vol. 11, no. 4, pp. 410–420.

Sauli, F. (1997), "GEM: A new concept for electron amplification in gas detectors," *Nuclear Instruments and Methods in Physics Research Section A: Accelerators, Spectrometers, Detectors and Associated Equipment*, vol. 386, no. 2-3, pp. 531–534, URL http://www.sciencedirect.com/science/article/pii/S0168900296011722.

Silfsten, P., Parkkinen, S., Luostarinen, J., Khodonov, A., Jääskeläinen, T., and Parkkinen, J. (1996), "Color-sensitive biosensors for imaging," in *Proceedings of the 13th International Conference on Pattern Recognition*, vol. 3, pp. 331–335 vol.3.

Staiger, R. (2009), "Push the button — or does the art of measurement still exist?" URL http://www.fig.net/pub/monthly_articles/june_2009/june_2009_staiger.pdf, this paper has been prepared and presented as a keynote presentation in Plenary Session 3 — GNSS, Geosciences and Surveying at the FIG Working Week 2009 in Eilat, Israel, 7 May 2009.

Stuart, J.A., Marcy, D.L., Wise, K.J., and Birge, R.R. (2002), "Volumetric optical memory based on bacteriorhodopsin," *Synthetic Metals*, vol. 127, no. 1-3, pp. 3 – 15, URL http://www.sciencedirect.com/science/article/pii/S0379677901005860, novel organic material and technological advances for photonics.

Takamatsu, S., Hoshino, K., Matsumoto, K., Miyasaka, T., and Shimoyama, I. (2005), "Biomolecular image sensor of bacteriorhodopsin patterned by electrodeposition," in *Proceedings of IEEE International Conference on Micro Electro Mechanical Systems (MEMS2005)*, pp. 847–850.

Takamatsu, S., Hoshino, K., Matsumoto, K., Miyasaka, T., and Shimoyama, I. (2011), "The photo charge of a bacteriorhodopsin electrochemical cells measured by a charge amplifier," *IEICE Electronics Express*, vol. 8, no. 7, pp. 505–511.

Talvitie, J., Tukiainen, T., Lensu, L., Kärkkäinen, T., Silventoinen, P., and Kuisma, M. (2013), "Time-variant electrical equivalent circuit of a dry bacteriorhodopsin sensor," in *Proceedings of IEEE International Instrumentation and Measurement Technology Conference (I2MTC2013)*, pp. 1218–1221.

Talvitie, J., Tukiainen, T., Lensu, L., Kärkkäinen, T., Silventoinen, P., and Kuisma, M. (2015a), "Amplifier errors in dry bacteriorhodopsin sensor measurements," in *Proceedings of IEEE International Instrumentation and Measurement Technology Conference (I2MTC2015)*, pp. 1185–1188.

Talvitie, J., Tukiainen, T., Lensu, L., Kärkkäinen, T., Silventoinen, P., and Kuisma, M. (2015b), "Validation of a time-variant electrical equivalent circuit for a dry bacteriorhodopsin sensor," in *Proceedings of IEEE International Instrumentation and Measurement Technology Conference (I2MTC2015)*, pp. 352–357.

The TOTEM Collaboration, Anelli, G., Antchev, G., Aspell, P., Avati, V., Bagliesi, M.G., Berardi, V., Berretti, M., Boccone, V., Bottigli, U., Bozzo, M., Brücken, E., Buzzo, A.,

Cafagna, F., Calicchio, M., Capurro, F., Catanesi, M.G., Catastini, P.L., Cecchi, R., Cerchi, S., Cereseto, R., Ciocci, M.A., Cuneo, S., Và, C.D., David, E., Deile, M., Dimovasili, E., Doubrava, M., Eggert, K., Eremin, V., Ferro, F., Foussat, A., Galuška, M., Garcia, F., Gherarducci, F., Giani, S., Greco, V., Hasi, J., Haug, F., Heino, J., Hilden, T., Jarron, P., Joram, C., Kalliopuska, J., Kaplon, J., Kašpar, J., Kundrát, V., Kurvinen, K., Lacroix, J.M., Lami, S., Latino, G., Lauhakangas, R., Lippmaa, E., LokajÃček, M., Vetere, M.L., Rodriguez, F.L., Macina, D., MacrÃ, M., Magazzu, C., Magazzù, G., Magri, A., Maire, G., Manco, A., Meucci, M., Minutoli, S., Morelli, A., Musico, P., Negri, M., Niewiadomski, H., Noschis, E., Notarnicola, G., Oliveri, E., Oljemark, F., Orava, R., Oriunno, M., Perrot, A.L., Österberg, K., Paoletti, R., Pedreschi, E., Petäjäjärvi, J., Pollovio, P., Quinto, M., Radermacher, E., Radicioni, E., Rangod, S., Ravotti, F., Rella, G., Robutti, E., Ropelewski, L., Ruggiero, G., Rummel, A., Saarikko, H., Sanguinetti, G., Santroni, A., Scribano, A., Sette, G., Snoeys, W., Spinella, F., Squillacioti, P., Ster, A., Taylor, C., Tazzioli, A., Torazza, D., Trovato, A., Trummal, A., Turini, N., Vacek, V., Remortel, N.V., Vinš, V., Watts, S., Whitmore, J., and Wu, J. (2008), "The TOTEM experiment at the CERN large hadron collider," *Journal of Instrumentation*, vol. 3, no. 08, p. S08007, URL http://stacks.iop.org/1748-0221/3/i=08/a=S08007.

Tittor, J. and Oesterhelt, D. (1990), "The quantum yield of bacteriorhodopsin," *{FEBS} Letters*, vol. 263, no. 2, pp. 269 – 273, URL http://www.sciencedirect.com/science/article/pii/001457939081390A.

Trissl, H. (1990), "Photoelectric measurements of purple membranes," *Photochemistry and photobiology*, vol. 51, no. 6, pp. 793–818.

Tukiainen, T. (2008), *Photoelectric Measurements and Modeling of Bacteriorhodopsin*, Master's thesis, Lappeenranta University of Technology, Lappeenranta, Finland.

Tukiainen, T., Talvitie, J., Kuisma, M., Silventoinen, P., and Lensu, L. (2014), "Loading effects on the photoelectric response of dry bacteriorhodopsin sensors," in *Proceedings of the IEEE International Instrumentation and Measurement Technology Conference (I2MTC2014)*, pp. 761–765.

Vàrò, G. and Keszthelyi, L. (1983), "Photoelectric signals from dried oriented purple membranes of halobacterium halobium," *Biophysical Journal*, vol. 43, no. 1, pp. 47 – 51, URL http://www.sciencedirect.com/science/article/pii/S0006349583843227.

Walczak, K., Cheam, D., Lueking, D., Bergstrom, P., and Friedrich, C. (2008), "Electronic characteristics of bacteriorhodopsin," in *2008 IEEE Conference on Nanotechnology (NANO '08)*, pp. 553–556.

Wang, W.W., Knopf, G.K., and Bassi, A.S. (2006), "Photoelectric properties of a detector based on dried bacteriorhodopsin film," *Biosensors and Bioelectronics*, vol. 21, no. 7, pp. 1309 – 1319, URL http://www.sciencedirect.com/science/article/pii/S0956566305001818.

Wang, W.W., Knopf, G., and Bassi, A. (2008), "Bioelectronic imaging array based on bacteriorhodopsin film," *IEEE Transactions on NanoBioscience*, vol. 7, no. 4, pp. 249–256.

Xu, J., Bhattacharya, P., and Vàrò, G. (2004), "Monolithically integrated bacteriorhodopsin/semiconductor opto-electronic integrated circuit for a bio-photoreceiver," *Biosensors and Bioelectronics*, vol. 19, no. 8, pp. 885 – 892, URL http://www.sciencedirect.com/science/article/pii/S0956566303002975.

Xu, J., Stickrath, A., Bhattacharya, P., Nees, J., Vàrò, G., Hillebrecht, J., Ren, L., and Birge, R. (2003), "Direct measurement of the photoelectric response time of bacteriorhodopsin via electro-optic sampling," *Biophysical Journal*, vol. 85, no. 2, pp. 1128 – 1134, URL http://www.sciencedirect.com/science/article/pii/S0006349503745494.

Yin, R.K. (2009), *Case Study Research: Design and Methods*, SAGE Publications, Thousand Oaks, CA, USA, 4 edn.

Appendices

Appendix A

Linearity and bandwidth of the two-stage transimpedance amplifier

The photocurrent measurements on a dry bR sensor were made at multiple light intensities. These changes also affect the input amplitudes of the transimpedance amplifier. If the amplifier used in the measurements is not linear at the given amplitudes, the photocurrent measurements from the bR sensor will be distorted. If not understood, this distortion could be considered a feature of the bR sensor.

Because the two-stage transimpedance amplifier used in this doctoral dissertation was custom made, the linearity of the amplifier had to be determined. The linearity measurement was performed by applying a 1 MΩ resistor with a tolerance of one percent. One end of the resistor was connected to a signal generator and the other end to the amplifier. From the signal generator, a voltage ramp with an amplitude of 4.5 V and a duty cycle of 50% at the frequency of 40 mHz was fed through the resistor and the amplifier. The voltage over the resistor was measured by an Agilent DSOX2024A oscilloscope. The linearity error caused by the amplifier was measured in the range from 20 nA to 500 nA. This range covers all the amplitude values measured in this study. The measurements were performed at a room temperature of 25 °C, which corresponds to the temperature of the measurements on the dry bR sensors. The error calculated from the measurements is shown in Figure A.1.

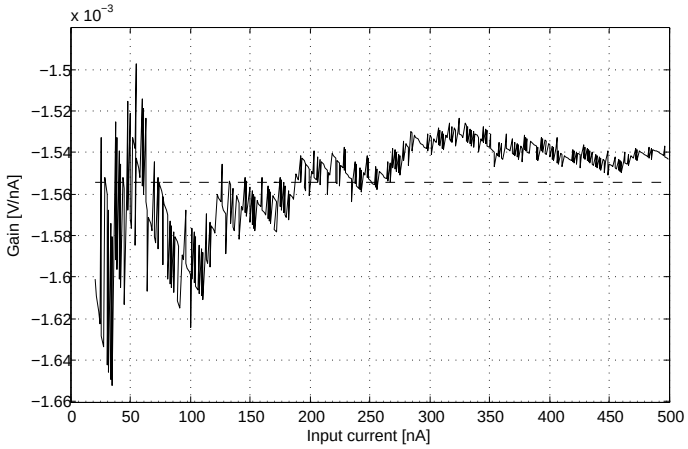

Figure A.1: Linearity error of the amplifier within the range from 20 nA to 500 nA.

Based on the measurements, the amplifier was determined to introduce a maximum error between + 6.3% and - 3.7% to the measurements within the whole measurement range. It should be noted that the measurement is also affected by the uncertainty of the oscilloscope, the tolerance of the 1 MΩ resistor, and the accuracy of the signal generator. Despite the uncertainty of the oscilloscope and the signal generator and the tolerance of the resistor, the error caused by the linearity of the amplifier is still rather small compared with the changes in the peak amplitudes of the photocurrent measurements when the light intensity is varied.

Publication 1

Talvitie, J.P., Tukiainen, T., Lensu, L., Kärkkäinen, T.J., Silventoinen, P., and Kuisma,

"Time-variant electrical equivalent circuit of a dry bacteriorhodopsin sensor"

in *Proceedings of the IEEE International Instrumentation and Measurement Technology Conference, I2MTC2013*.

Copyright © 2013, IEEE. Reprinted, with permission of IEEE.

Time-Variant Electrical Equivalent Circuit of a Dry Bacteriorhodopsin Sensor

Joonas P. Talvitie*, Teemu Tukiainen', Lasse Lensu', Tommi J. Kärkkäinen*, Pertti Silventoinen*, Mikko Kuisma*
*Department of Electrical Engineering
'Machine Vision and Pattern Recognition Laboratory, Department of Mathematics and Physics
Lappeenranta University of Technology
Lappeenranta, Finland

***Abstract*— Modeling the photoelectric response of dry bacteriorhodopsin (bR) sensors has commonly been carried out by following the theory of linear time-invariant systems. However, it has been reported that the time constants of the photovoltage responses of such sensors vary depending on whether the sensor is measured when the incident light is switched on or off. In this paper, we propose an electrical equivalent circuit for dry bR sensors. Unlike the models presented in the literature, the proposed circuit also considers the illumination on the bR sensor. The model is experimentally verified by photocurrent measurements. Further, a new result concerning the photocurrent dependence on the illumination of dry bR sensors is introduced.**

I. INTRODUCTION

Bacteriorhodopsin (bR) is a photosensitive protein found in the archaean Halobacterium salinarum [1]. The native function of bR as a light-driven proton pump with a reversible photocycle is to participate in the energy-balancing mechanism of the archaean: it produces a proton gradient across the cellular membrane allowing ATP synthases to function. This protein has been under intensive research because it has been seen as an important biomolecule for biochemical and technology-oriented studies [2]. The popularity of bR as a research target is explained by its several advantages: a high quantum efficiency (0.65) [3], an ability to function and survive under extreme environmental stress [4]–[7], and a storage life of years [8]. Owing to its advantageous properties, various technical applications in optoelectronics and biosensing have been proposed: an imaging sensor [9]–[12], a protein-based memory [2], [13], and a bio-photoreceiver [14].

The photoelectric functionality of bR has been important in explaining its properties and especially to evaluate its suitability for technical application. The photoelectric properties have been modeled by using an electrical equivalent circuit [15], [23], exponential fitting [4], and estimation of induced charges [16]. The modeling has been based on the presumption that the system is a linear time-invariant system. However, it has been reported in the literature [7], [17], [23] and in our previous studies [18] that the time constants of the photoelectric response vary in dry bR sensors depending on whether the light is switched on or off.

In this paper, we propose a new electrical equivalent circuit for dry bR sensors. Unlike the models presented in the literature, the proposed circuit also considers the illumination on the bR sensor. This first-order model has a capacitor, the value of which varies as a function of illumination. The proposed model is experimentally verified by photocurrent measurements. In addition, a new result concerning the photocurrent dependence on the illumination of a dry bR sensor is presented.

II. ELECTRICAL EQUIVALENT CIRCUIT

Different electrical equivalent circuits for bR sensors have been proposed in the literature [4], [15], [18], [19]. Common to all these models is that the photoelectromotive force E_P is connected to the measurement instrumentation through a series capacitance C_P. The bR membrane consisting of a membrane resistance R_M and a membrane capacitance C_M is generally accepted to be modeled in parallel with the measurement instrumentation, as presented by Hong [20]. However, not the model shown in Fig. 1, nor any of the reported equivalent circuits can be used to calculate component values for simulating the changes in photocurrent responses caused by the illumination of the sensor. This is despite the fact that this change in the response has been reported in the literature [7], [17], [23] and in our previous studies [18].

The model presented in Fig. 1 has two independent reactive components, thus representing a second-order system. Basically, R_P and C_P form one time constant, and C_M and R_M another one together with the input impedance of the instrumentation. The related time constants presented in the paper are illustrated in Fig. 2, where both the photocurrent I_P and the photovoltage V_P from the output of the sensor are shown.

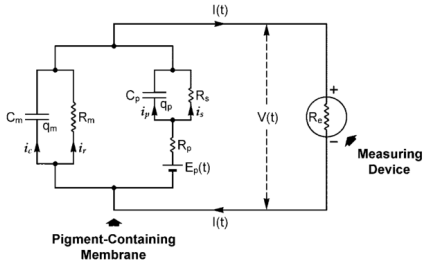

Figure 1. Electrical equivalent circuit of bacteriorhodopsin introduced by Hong (reproduced from [20])

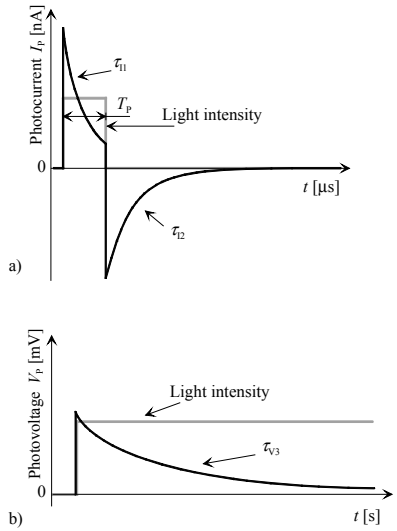

Figure 2. Photocurrent pulse response represented by two time constants, τ_{I1} when the light is on and τ_{I2} when the light is off (a). The photovoltage step response showing a third time constant τ_{V3} (b)

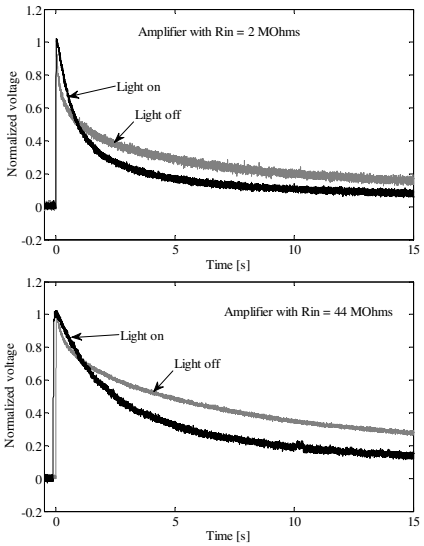

Figure 3. Normalized photovoltage step response when the light is switched on and off. The measured photovoltage decays faster when the light is switched on compared with a case when the light is switched off (reproduced from the authors' previous work [18])

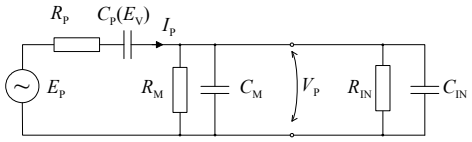

Figure 4. Proposed electrical equivalent circuit . The components R_M and C_M model the membrane impedance, andC_P and R_P model the photoactive part of the bR sensor. R_{IN} and C_{IN} model the input impedance of the measurement instrumentation. The light-dependent behavior is modeled by the capacitance $C_P(E_V)$.

Recently, Wang et al. [17], Walczak [7], and Miyazaki et al. [23] have reported that the bR capacitance varies depending on the illumination of the bR sensor. It was also found in a previous measurement [18] that the time constant varies and cannot be modeled with a linear time-invariant (LTI) model. An example of this kind of a light-dependent response is shown in Fig. 3, where a photovoltage measurement result is shown to define the time constant τ_{V3} (see Fig. 2b). In the experiments, the step response was measured both when the light was switched on and when it was switched off. Two different instrumentation amplifiers with two different input resistances of 2 MΩ and 44 MΩ were used also to test the effect of the input resistance on the response.

Fig. 3 shows that the photovoltage time constant τ_{V3} varies: it approximately doubles when the light is switched off compared with the case when the light is switched on. The effect of illumination was also similar to what was reported by Wang et al. [17]. In their study, the time constant became approximately two times longer. It is also clear that the step response does not follow a typical first- or second-order exponential function since the steepness of the voltage decay varies. This change along with the changes in the time constant τ_{V3} caused by the illumination dependence of the bR sensor complicate the determination of the component values for the model shown in Fig. 1.

To solve this problem in modeling the electrical behavior of the bR sensor during the illumination, a new approach is needed. One solution is to express the capacitor as a function of illumination $C_P(E_V)$ as proposed in the electrical equivalent circuit presented in Fig. 4.

The proposed circuit has four unknown sensor parameters. The effect of the membrane R_M and C_M can be eliminated by using the photocurrent measurement. A transimpedance amplifier with the input resistance R_{IN} of ideally zero connected to the electrical equivalent in Fig. 4 short-circuits R_M and C_M. This reduces the electrical equivalent circuit to a first-order circuit, with a time constant $\tau_I = R_P C_P(E_V)$.

III. EXPERIMENTS

Measurements and Matlab simulations were used to verify the proposed model. The hypothesis of an illumination-varying capacitance $C_P(E_V)$ was tested by measuring the photocurrent and estimating the light-on time constant τ_{I1} and the light-off time constant τ_{I2}. The test setup consisted of a light source, a

dry bR sensor, amplifiers, and an oscilloscope. Light excitation of the sensor was carried out by using a Cavitar CAVILUX Smart laser diode as the light source. The peak wavelength of the laser was 690 nm, the pulse width T_p was 10 µs, and the pulse rise time was 26 ns. The power of the laser was 400 W.

The sensors used in the experiments were dry bR thick films. The sensors were prepared by mixing a water solution of purple membrane (PM) fragments with polyvinyl alcohol (PVA). The substance was spread on conductive SnO2-coated glass, where the conductive coating formed an electrode. During the polymer drying process, no active means was used to orient the PM patches. The second electrode was prepared by sputtering a thin layer of gold on the dried bR-PVA film. A more detailed description of the procedure can be found in [10] and [22].

In the laboratory experiments, the photocurrent was measured by using a transimpedance amplifier designed in [21]. The measurement instrumentation and the bR sensor were placed inside a shielded enclosure, which had a transparent and conductive window for the illumination. Further, the inside of the shielded enclosure was painted black to prevent optical reflections. The power supply of the measurement instrumentation consisted of batteries placed inside the enclosure. The output signals of the amplifiers were connected to an oscilloscope through BNC connectors. This was done to reduce the effects of electromagnetic interference on the measurement. Data acquisition of the measurements was performed with an Agilent DSO81204A 12 GHz oscilloscope. The measurements were made at a room temperature of 25 ºC and without any ambient illumination to prevent its potential effect on the measurement.

IV. RESULTS

The photocurrent was measured using a transimpedance amplifier with the oscilloscope set to average 20 consecutive measurements to reduce noise. The measured and normalized photocurrent with the corresponding simulations is shown in Fig. 5.

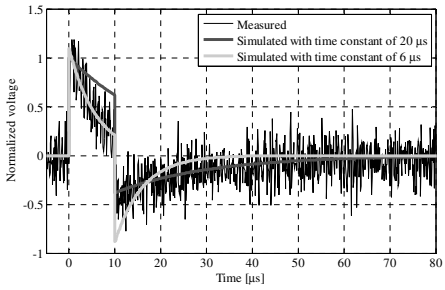

Figure 5. Photocurrent response with two different time constants τ_{l1} = 6 µs and τ_{l2} = 20 µs, measured by a transimpedance amplifier and 10 µs laser pulse excitation. Simulations with the corresponding time constants are shown overlaid on the measured response.

The change in the light-on and light-off time constants τ_{l1} and τ_{l2} can be clearly seen in Fig. 5. τ_{l1} is 6 µs and τ_{l2} is 20 µs, so in this case, with the given light intensity and parameters, the time constant is over three times as long when the light is switched off compared with the light-on condition. The simulated time constants match the measured response. Based on this result, it can be confirmed that the photocurrent response can be modeled as a first-order RC circuit with a capacitor $C_P(E_V)$, the value of which varies as a function of illumination.

The test was carried out only at two operating points, one when the light was completely off and one at a given intensity level. Therefore, a set of tests with different light intensity levels is needed to further study the phenomenon and the linearity of the model. Our test does not explain whether the capacitance causes the change in the time constant, because the resistance may also affect the time constant. Most probably, both of these components vary under the illumination, but this is out of the scope of this paper. By applying the proposed model, however, the electrical properties and the change in the time constant can be modeled at the given operating point.

V. CONCLUSION

In this paper, a new electrical equivalent circuit for dry bR sensors was introduced. The proposed model has a first-order RC circuit with a light-dependent capacitor $C_P(E_V)$ for modeling the illumination on the bR sensor. The effect of illumination on the photocurrent of the dry bR sensor was demonstrated in both cases when the illumination was introduced on the bR sensor and when it was switched off from the sensor. The measurement confirmed that the illumination changes the time constants of a dry bR sensor. Therefore, such sensors cannot be modeled as time-invariant systems. The change in the time constants, in the case of photocurrent, was shown to be approximately three times as long for the case of switching off the illumination compared with switching on.

ACKNOWLEDGMENTS

The authors wish to thank Prof. Jussi Parkkinen and Dr. Sinikka Parkkinen from the University of Eastern Finland / Monash University Sumway Campus for their work on the development of the bR sensors.

REFERENCES

[1] D. Oesterhelt and W. Stoeckenius, “Rhodopsin-like protein from the purple membrane of halobacterium halobium,” *Nature new biology*, 233(39):149–152,1971

[2] N. Hampp, “Bacteriorhodopsin as a photochromic retinal protein for optical memories,” *Chemical Reviews*, 100(5):1755–1776, 2000.

[3] J. Tittor and D. Oesterhelt, “The quantum yield of bacteriorhodopsin,” *FEBS Letters*, 263(2), 269–273, 1990.

[4] H-W. Trissl, “Photoelectric Measurements of Purple Membranes,” *Photochemistry and Photobiology*, 51(6):793–818, 1990.

[5] P. Silfsten, S. Parkkinen, J. Luostarinen, A Khodonov, T. Jääskeläinen, and J. Parkkinen, “Color-sensitive biosensors for imaging,” In *Proceedings of ICRP '96*, 3:331–335, 1996.

[6] J. Xu, A. B. Stickrath, P.Bhattacharya, J. Nees, G. Vàrò, J. R. Hillebrecht, L. Ren, and R. R. Birge, "Direct measurement of the photoelectric response time of bacteriorhodopsin via electro-optic sampling," *Biophysical Journal*, 85(2):1128–1134, 2003.

[7] K. A. Walczak, "Electronic Characteristics of Bacteriorhodopsin," in *the 8th IEEE Conference on Nanotechnology*, pp. 553–556, 2008.

[8] G. Váró, L. Keszthelyi, "Photoelectric signals from dried oriented purple membrane of halobacterium halobium," *Biophysical Journal*, 43:47–51, 1983.

[9] T. Miyasaka and K. Koyama, "Image sensing and processing by a bacteriorhodopsin-based artificial photoreceptor," *Applied Optics* 32(31):6371–6379, 1993.

[10] L. Lensu, *Photoelectric Properities of Bacteriorhodopsin Films For Photosensing And Information Processing*, PhD thesis, Lappeenranta University of Technology, 2002.

[11] S. Takamatsu, K.i Hoshino, K.i Matsumoto, T. Miyasaka, and I. Shimiyama, "Biomolecular image sensor of bacteriorhodopsin patterned by electrodeposition," in *the 18th IEEE International Conference on Micro Electro Mechanical Systems*, pages 847– 850, 2005.

[12] S. Takamatsu, "The photo charge of a bacterioRhodopsin electrochemical cells measured by a charge amplifier," *IEICE Electronics Express*, 8(7):505–511, 2011.

[13] R.R. Birge, N.B. Gillespie, E.W. Izaguirre, A. Kusnetzow, A.F. Lawrence, D. Singh, Q. Wang Song, E. Schmidt, J.A. Stuart, S. Seetharaman and K.J. Wise, "Biomolecular electronics: protein-based associative processors and volumetric memories," *Journal of Physical Chemistry B*, 103(49):10746–10766, 1999.

[14] J. Xu, P. Bhattacharya, G. Vàrò, "Monolithically integrated bacteriorhodopsin/semiconductor opto-electronic integrated circuit for a bio-photoreceiver," *Biosensors and Bioelectronics* 19:885–892, 2004

[15] F. Hong and D. Mauzerall, "Interfacial photoreactions and chemical capacitance in lipid bilayers," in *Proc. Nat, Acad. Sci. USA*, 71(4):1564–1568, 1974.

[16] L. Keszthelyi and P. Ormos, "Electric signals associated with the photocycle of bacteriorhodopsin," *FEBS Letters*, 109(2):189–193, 1980.

[17] W. W. Wang, G. K. Knoft, and A. S. Bassi, "Photoelectric properties of a detector based on dried bacteriorhodopsin film," *Biosensors and Bioelectronics*, 21:1309–1319, 2006.

[18] J. Talvitie, "Electrical Equivalent Circuit for Dry Bacteriorhodopsin Sensor," M. Sc. Thesis, Lappeenranta University of Technology, 2011.

[19] L. Keszthelyi G. Váró, "Photoelectric signals from dried oriented purple membrane of halobacterium halobium," *Biophysical Journal*, 43:47–51, 1983.

[20] F. T. Hong, "Interfacial photochemistry of retinal proteins,"*Progress in Surface Science*, 62:1–237, 1999.

[21] J. Talvitie. "Designing an implementation of transimpedance amplifier for buffering a bacteriorhodopsin-sensor," B. Sc. Thesis, in Finnish, http://urn.fi/URN:NBN:fi-fe201009222500, Lappeenranta University of Technology, 2010.

[22] T. Tukiainen, "Photoelectric measurements and modeling of bacteriorhodopsin," M. Sc. Thesis, Lappeenranta University of Technology, 2008.

[23] S. Miyazaki, M. Matsumoto, S. B. Brier, T. Higaki, T. Yamada, T. Okamoto, H. Ueno, S. Toyabe and E. Muneyuki, "Properties of the electrogenic activity of bacteriorhodopsin," *European Biophysics Journal,* published online http://dx.doi.org/10.1007/s00249-012-0870-0, 2012.

Publication 2

Talvitie, J.P., Tukiainen, T., Lensu, L., Kärkkäinen, T.J., Silventoinen, P., and Kuisma,

"Validation of a Time-Variant Electrical Equivalent Circuit for a Dry Bacteriorhodopsin Sensor"

in *Proceedings of the IEEE International Instrumentation and Measurement Technology Conference, I2MTC2015*.

Copyright © 2015, IEEE. Reprinted, with permission of IEEE.

This full text paper was peer-reviewed at the direction of IEEE Instrumentation and Measurement Society prior to the acceptance and publication.

Validation of a Time-Variant Electrical Equivalent Circuit for a Dry Bacteriorhodopsin Sensor

Joonas P. Talvitie*, Teemu Tukiainen', Lasse Lensu', Tommi J. Kärkkäinen*, Pertti Silventoinen*, Mikko Kuisma*
*Department of Electrical Engineering
'Machine Vision and Pattern Recognition Laboratory, Department of Mathematics and Physics
Lappeenranta University of Technology
Lappeenranta, Finland

***Abstract*—The photoelectric response of dry bacteriorhodopsin sensors varies depending on whether the incident light is on or off. To model this behavior, we have proposed an electrical equivalent circuit that has a capacitor that varies with the light intensity. In this paper, the proposed model is experimentally validated and found to be appropriate even when the light intensity is changed. The results also confirm that the amplitude of the measured photocurrent changes linearly with the light intensity. The results can be used to correctly analyze and model photocurrent measurements taking the time-variant behavior of the photosensitive biological sensor into account. This knowledge will be useful in sensing systems that utilize photosensitive biological sensors.**

***Index Terms*—Current measurement, Bioelectric phenomena, Biological system modeling, Modeling, Time-varying circuits.**

I. Introduction

BACTERIORHODOPSIN (bR) is a photosensitive protein found in the archaean, Halobacterium salinarum [1]. The natural function of bR as a light-driven proton pump with a reversible photocycle is to participate in the energy-balancing mechanism of the archaean. bR generates a proton gradient across the cellular membrane allowing adenosine triphosphate (ATP) synthases to function and produce ATP from adenosine diphosphate (ADP). This protein has been under intensive research because it has been seen as an important biomolecule for biochemical and technology-oriented studies [2]. The popularity of bR as a research target can be explained by several favorable characteristics: a high quantum efficiency (0.65) [3], an ability to function and survive under extreme environmental stress [4]–[7], and a storage life of years [8]. Owing to its advantageous properties, various technical applications in optoelectronics and biosensing have been proposed, such as an imaging sensor [9]–[12], a protein-based memory [2], [13], and a bio-photoreceiver [14].

Understanding of the photoelectric functionality of bR has been important in explaining its properties and evaluating its suitability for technical application. The photoelectric properties have been modeled, for instance, by using an electrical equivalent circuit [15], [16], exponential fitting [4], and estimation of induced charges [17]. This early modeling was based on the presumption that the system is a linear time-invariant system. However, it has been reported in the literature [7], [18], [16] and in our previous studies [19], [20] that the time constants of the photoelectric response vary in dry bR sensors depending on whether the sensors are under the effect of incident light or not.

In this paper, we focus on validating an electrical equivalent circuit we proposed in [20] for dry bR sensors when the intensity of the incident light is varied. Unlike earlier models, the proposed model considers also the illumination on the bR sensor. This first-order model has a capacitor, the value of which varies as a function of the illumination. The proposed model is experimentally verified by photocurrent measurements at 13 different light intensities. Based on the photocurrent measurements, it is also found that the amplitude of the photocurrent changes linearly with the light intensity. The results can be used to correctly analyze and model photocurrent measurements taking the time-variant behavior of the photosensitive biological sensor into account. This can be especially useful in sensing systems utilizing photosensitive biological sensors. Such systems have been studied by e.g. Giakos et al. [21].

II. Electrical Equivalent Circuit

Different electrical equivalent circuits for bR sensors have been proposed in the literature [4], [15], [19], [22]. Common to all these models is that the photoelectromotive force E_P is connected to the measurement instrumentation through a series capacitance C_P. It is generally accepted that the bR membrane consisting of a membrane resistance R_M and a membrane capacitance C_M is modeled in parallel with the measurement instrumentation, as presented by Hong [23]. However, neither the model shown in Fig. 1, nor any of the reported equivalent circuits can be used to calculate the component values for simulating the changes in photocurrent responses caused by illumination of the sensor. This is despite the fact that this change in the response has been reported in the literature [7], [17], [16] and in our previous studies [19], [20].

The model presented in Fig. 1 has two independent reactive components, thus representing a second-order system. Basically, R_P and C_P form one time constant, and C_M and R_M another one together with the input impedance of the instrumentation. The related time constants presented in the paper are illustrated in Fig. 2, which shows both the photocurrent I_P and the photovoltage V_P from the output of the

978-1-4799-6144-6/15/$31.00 ©2015 IEEE

sensor. The photocurrent response has two time constants in the range of microseconds. The photovoltage, on the other hand, has a time constant in the range of seconds. Exact values of the three time constants vary depending on the input impedance of the instrumentation and wavelength of the light source [24].

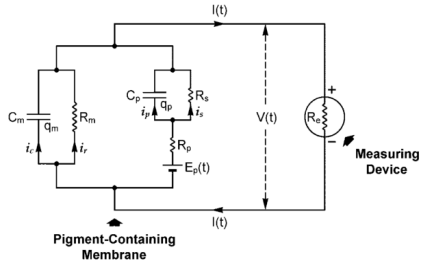

Fig. 1. Electrical equivalent circuit of bacteriorhodopsin introduced by Hong (reproduced from [23])

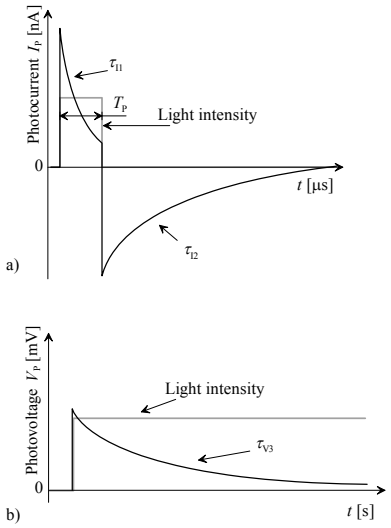

Fig. 2. Illustration of photocurrent pulse response represented by two time constants, τ_{I1} when the light is on and τ_{I2} when the light is off (a). The photovoltage step response showing a third time constant τ_{V3} (b). (Note different time scales in the two parts of the figure.)

Recently, Wang et al. [18], Walczak [7], and Miyazaki et al. [16] have reported that the bR capacitance varies depending on the illumination of the bR sensor. Our previous measurements [19] found that the time constant varies and that it cannot be modeled by a linear time-invariant (LTI) model.

Research on the time-variant nature of the response was continued in [20]. The results showed that the photovoltage time constant related to the decay varies: it approximately doubled when the light was switched off compared with the case when the light was switched on. The effect of illumination was similar to that reported by Wang et al. [18]. In their study, the time constant became approximately two times longer. It is obvious that the step response does not follow a typical exponential model because the steepness of the voltage decay varies. This change along with changes in the time constant τ_{V3} caused by the illumination dependence of the bR sensor complicate the determination of the component values for the model shown in Fig. 1.

To solve this problem in modeling the electrical behavior of the bR sensor during illumination, a new approach was needed. Our solution [20] was to express the capacitor as a function of illumination $C_P(E_V)$ as proposed in the electrical equivalent circuit presented in Fig. 3.

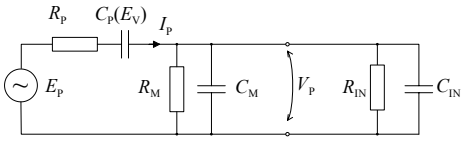

Fig. 3. Electrical equivalent circuit of a bR sensor authors proposed in [20]. The components R_M and C_M model the membrane impedance, and C_P and R_P model the photoactive part of the bR sensor. R_{IN} and C_{IN} model the input impedance of the measurement instrumentation. The light-dependent behavior is modeled by the capacitance $C_P(E_V)$. The model is reduced to a first order system when a transimpedance amplifier with a R_{IN} of zero ohms is connected to the sensor.

The circuit has four unknown sensor parameters R_P, C_P, R_M and C_M. Resistance R_S, shown in Fig. 1, represents the resistance encountered by the DC photocurrent [23]. Its effect on the measured high frequency photocurrent response can therefore be neglected, and hence it is not shown in Fig. 3. The effect of the membrane R_M and C_M can be eliminated by using the photocurrent measurement. A transimpedance amplifier with an input resistance R_{IN} of ideally zero connected to the electrical equivalent circuit short-circuits R_M and C_M. This reduces the electrical equivalent circuit to a first-order circuit with a time constant $\tau_1 = R_P C_P(E_V)$. Capacitor $C_P(E_V)$ changes its value depending on the illumination, which causes different time constants for the decays related to the light-on (τ_{I1}) and light-off (τ_{I2}) cases. It should be noted that the electromotive force E_P is generated by the illumination E_V but they are not the same.

III. Experiments

Our previous publication [20] presented the change in two time constants τ_{I1} and τ_{I2} when the light was turned on and off at a selected intensity along with the proposed model. However, the previous results could not verify that the proposed model would be appropriate at different light intensities. To address this shortcoming and in order to validate the model and confirm our initial results, a set of new measurements were performed at different light intensities. The measurements were carried out by varying the intensity of the light source from 100 % to 25 % in steps of 6.25 percentage points.

The test setup consisted of a light source, a dry bR sensor, an amplifier, and an oscilloscope. Light excitation of the sensor was carried out using a Cavitar CAVILUX Smart laser diode as the light source. The peak wavelength of the laser was 690 nm, the maximum pulse width T_p was 10 µs, and the pulse rise time was 26 ns. The power of the laser was 400 W.

The sensors used in the experiments were dry bR thick films. The sensors were prepared by mixing a water solution of purple membrane (PM) fragments with polyvinyl alcohol (PVA). The substance was manually spread on conductive SnO2-coated glass, where the conductive coating formed an electrode. During the polymer drying process, no active means was used to orient the PM patches. The second electrode was prepared by sputtering a thin layer of gold on the dried bR-PVA film. A more detailed description of the procedure and the film characteristics can be found in [10] and [25].

In the laboratory experiments, the photocurrent was measured using a transimpedance amplifier designed in [26]. The measurement instrumentation and the bR sensor were placed inside a shielded enclosure, which had a transparent and conductive window for the illumination, Fig 4. Further, the inside of the shielded enclosure was painted black to prevent optical reflections. The power supply of the measurement instrumentation consisted of batteries placed inside the enclosure. The output signals of the amplifiers were connected to an oscilloscope through BNC connectors. This was done to reduce the effects of electromagnetic interference on the measurement. Data acquisition of the measurements was performed with an Agilent DSO81204A 12 GHz oscilloscope and Agilent E2697A 500 MHz 1MΩ high impedance adapter. The oscilloscope was set to an AC coupling to remove the DC offset and averaging of ten consecutive response measurements was used to reduce the noise. This approach improved the signal-to-noise ratio (SNR) without affecting the dynamics of the photocurrent response.

The AC-coupling has no effect on the photocurrent measurement because it introduces a high-pass filter that has a cut-off frequency of 7 Hz, whereas the measured photocurrent has time constants of less than 25 µs. Additionally, the transimpedance amplifier functions as a buffer between the bR sensor and the oscilloscope so the series capacitor introduced by the AC-coupling does not load the bR sensor.

From each measurement, 1E+6 data points (with a sampling frequency of 5 GSa/s) were stored to represent the fast changes and enable further processing of the data. The measurements were made at a room temperature of 25 ºC and without any ambient illumination to prevent its potential effect on the measurement.

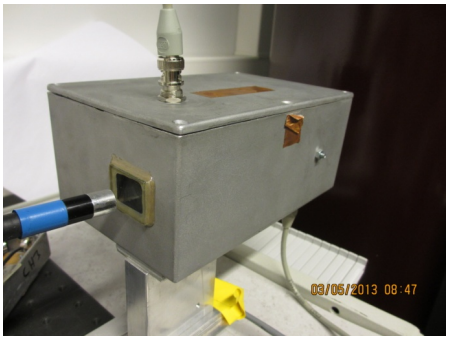

Fig. 4. Test setup used during the measurements. The figure shows the light source on the left, the metal enclosure and the BNC cables to the oscilloscope.

An algorithm was selected to define time constants from the stored data. The standard approach to modeling phenomena related to physico-chemical reactions, including photoelectric responses, is to decompose a response into a set of exponential components [23, 27]. The decomposition can be performed by a nonlinear fitting of a number of exponentials and by estimating the relevant parameters. When successful, a response *r* can be expressed in the general case as follows:

$$r(t) = A_0 + \sum_{i=1}^{n} A_i \exp(-t/\tau_i) \quad (1)$$

Despite the straightforward nature of the standard approach, it involves certain important requirements. For example, the time resolution/bandwidth of the measurement equipment and the SNR of the response must be high enough to resolve the components in the signal [27]. In view of the wide frequency bandwidth of the measured responses and the low SNR, in the case under study, it was necessary to pre-process the responses. To remedy the problem with the wide-band noise and to keep the dynamics of the actual response, a method based on total variation denoising [28] was applied instead of standard digital filtering. The applied method preserves the components of the response with high rise times much better than the standard methods.

To perform the actual decomposition, a nonlinear least-squares fitting with the trust region method was used. The fitting was performed in two stages: the first fit just for the light-on and the second for the light-off part of the response. The two-stage fitting was done to avoid using an unnecessarily high number of exponentials to represent the response (the discontinuity in the response was due to the limited maximum pulse width of the light source) and to avoid manual tuning of the constraints of the optimization. Two exponentials are needed for each stage due to the rise and decay parts of the response. Therefore, the model to fit to the unbiased response part *j* was as follows:

$$\hat{r}_j(t) = A_{j,1} \exp(-t/\tau_{j,1}) + A_{j,2} \exp(-t/\tau_{j,2}) \quad (2)$$

where *j* is an index specifying either the light-on or light-off part of the response.

IV. Results and Discussion

The photocurrent was measured using a transimpedance amplifier with the oscilloscope set to average ten consecutive response measurements to reduce noise. In the experiment, 13 different intensity levels for the light excitation were used. Two examples of the measured photocurrent responses with the corresponding exponential models are shown in Figs. 5 and 6.

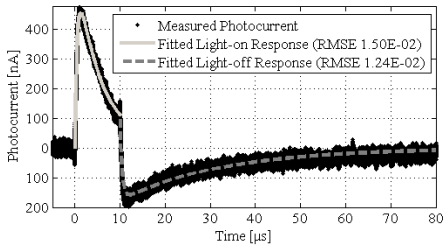

Fig. 5. Photocurrent response measured with 100 % light intensity and the transimpedance amplifier, the fitted model for the light-on component (solid line) and the model for the light-off component (dashed line).

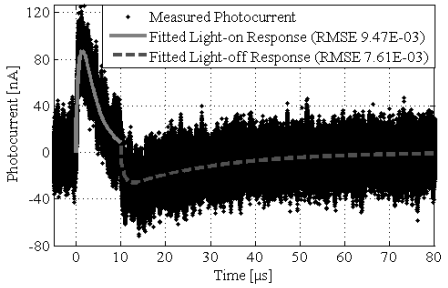

Fig. 6. Photocurrent response measured with 25 % light intensity and the transimpedance amplifier, the fitted model for the light-on component (solid line) and the model for the light-off component (dashed line).

The photocurrent responses clearly show a low SNR and the need for signal pre-processing. The total variation denoising method was applied to enable the nonlinear least-squares fitting of the two models with two exponential components to the responses without excessive manual tuning of the initial model parameters and the constraints for the fitting process. The MSE values in the figure legends show a good correspondence between the models and the data.

The fitted exponential models for the different measurements with varying light intensities were used in characterization of the photocurrent response. The first characteristic is the peak amplitude, which is shown in Fig. 7.

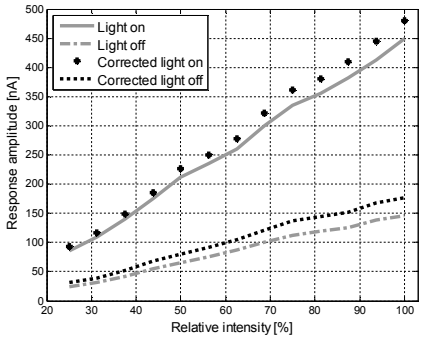

Fig. 7. Photocurrent response amplitude dependence on light intensity.

The peak amplitude of the light-on part is approximately three times as high as that of the light-off part. It should be noted that because of the limited light-on time of the laser system, the light-on part of the response does not decay back to the initial level, as can be seen in Figs. 5 and 6. This limitation affects the interpretation of the amplitudes.

The peak amplitude measurement is affected by the limited the rise time of the transimpedance amplifier. It can be seen from Figs. 5 and 6 that the rising edge of the measured current is not vertical which will affect especially the interpretation of the peak amplitudes but it will also have an effect to the time constant measurement. The effect of the limited rise time of the amplifier was investigated in [29]. Based on the simulations done in [29], it was estimated what the peak amplitude would be without the effect of limited rise time. These estimated values for the peak amplitudes were added to the Fig. 7 for comparison.

On the other hand, the actual non-zero input impedance of the transimpedance amplifier and sensor wiring and contacts have negligible impact to the amplitude measurement. The effect of the input impedance and wiring etc. can be neglected when simplifying the electrical equivalent circuit because the resistance is only a fraction of the R_M which is in parallel with the input. Therefore, the measurement using the transimpedance amplifier can be assumed as a short-circuit. The membrane resistance R_M has been reported to be over 10 MΩ, [7], [18].

Fig. 8 shows a comparison between the time constants τ_{l1} and τ_{l2} relative to the photocurrent of the responses. Overall, the decay time is approximately 5 µs for the light-on part and 22 µs for the light-off part. The decay of the responses is 3.5-6 times faster for the light-on part than for the light-off case. Time constants between the light-on and light-off responses were reported by Wang et al. [18] to be approximately two times longer. The differences in the measurements may be caused by the bR sensor, which was a thin film in the case of Wang et al. and a thick film in our case.

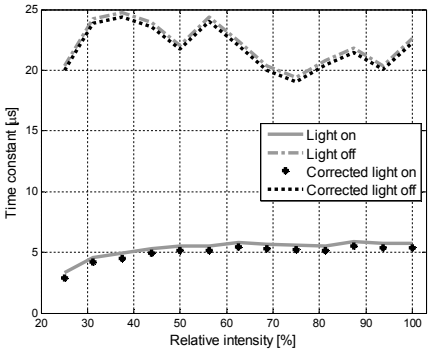

Fig. 8. Comparison of the modeled time constants of the photocurrent response.

As mentioned the limited rise time of the amplifier affects the measured time constants. For this reason the estimated time constants without the effect of the rise time limitation were added to the Fig. 8 for comparison.

In our previous study [20], it could not be verified whether the equivalent circuit model would be appropriate at different light intensities. The test was carried out only in two operating points; one when the light was completely off and one at a given intensity level.

Based on the results of this study, it can now be confirmed that the response peak amplitude changes linearly with light intensity. This is true even if the error caused by the amplifier is taken into account. The errors shown in Figs. 7 and 8 were estimated using the assumption that the rise time of the light source and the bR sensor are ideal. This is not the case in reality. Therefore the estimated errors are to be considered as the maximum error. In fact the error is actually smaller due to the non-zero rise time of the light source and the bR sensor. In addition, the time constants are independent of the light intensity, at least when taking into account the limited SNR of the measurements and the accuracy of the model fits.

When considering the results of this work, it should be noted that our test does not explain whether the capacitance causes the change in the time constant, because the resistance may also affect the time constant. Most probably, both of these components vary under the illumination, but this is out of the scope of this paper.

Based on this work and our previous publication [20], it can be concluded that the proposed model can be used to model the time-variant photocurrent response measured from dry bR sensors when light is switched on and off even if light intensity is varied. Owing to the manual preparation procedure of the dry films, the sensor characteristics may vary between individual films [30]. This variation affects the exact component values, but not the appropriateness of the proposed model.

The results presented here can be used when designing measurement setups and, more importantly, when analyzing and modeling measurement results. The results enable the time-variant behavior of the photosensitive biological sensor to be taken into account. An advantage of this method is that it does not require extensive knowledge of biochemistry. The proposed electrical equivalent circuit could be especially useful in sensing systems that utilize photosensitive biological sensors.

V. Conclusion

In this paper, an electrical equivalent circuit for dry bR sensors was experimentally validated by performing photocurrent measurements at 13 different light intensities. The measured data were processed taking a total variation approach to reduce the noise, preserve the dynamics of the responses, and enable the robust nonlinear fitting of the exponential models required to estimate the amplitudes and time constants of the signal components.

The results confirm that the proposed model is appropriate also for cases with varying light intensity. The response peak amplitudes were found to depend linearly on the intensity. A new observation was that both the switch-on and switch-off time constants remain approximately constant even when the light intensity is varied. The results can be used to correctly analyze and model photocurrent measurements taking the time-variant behavior of the photosensitive biological sensor into account. This knowledge could be especially useful in sensing systems that utilize photosensitive biological sensors.

Acknowledgment

The authors wish to thank Prof. Jussi Parkkinen and Dr. Sinikka Parkkinen from the University of Eastern Finland for their work on the development of the bR sensors.

References

[1] D. Oesterhelt and W. Stoeckenius, “Rhodopsin-like protein from the purple membrane of halobacterium halobium,” *Nature new biology*, 233(39):149–152,1971

[2] N. Hampp, “Bacteriorhodopsin as a photochromic retinal protein for optical memories,” *Chemical Reviews*, 100(5):1755–1776, 2000.

[3] J. Tittor and D. Oesterhelt, “The quantum yield of bacteriorhodopsin,” *FEBS Letters*, 263(2), 269–273, 1990.

[4] H-W. Trissl, “Photoelectric Measurements of Purple Membranes,” *Photochemistry and Photobiology*, 51(6):793–818, 1990.

[5] P. Silfsten, S. Parkkinen, J. Luostarinen, A Khodonov, T. Jääskeläinen, and J. Parkkinen, “Color-sensitive biosensors for imaging,” In *Proceedings of ICRP '96*, 3:331–335, 1996.

[6] J. Xu, A. B. Stickrath, P.Bhattacharya, J. Nees, G. Vàrò, J. R. Hillebrecht, L. Ren, and R. R. Birge, “Direct measurement of the photoelectric response time of bacteriorhodopsin via electro-optic sampling,” *Biophysical Journal*, 85(2):1128–1134, 2003.

[7] K. A. Walczak, “Electronic Characteristics of Bacteriorhodopsin,” in *the 8th IEEE Conference on Nanotechnology*, pp. 553–556, 2008.

[8] G. Váró and L. Keszthelyi, “Photoelectric signals from dried oriented purple membrane of halobacterium halobium,” *Biophysical Journal*, 43(1):47–51, 1983.

[9] T. Miyasaka and K. Koyama, “Image sensing and processing by a bacteriorhodopsin-based artificial photoreceptor,” *Applied Optics* 32(31):6371–6379, 1993.

[10] L. Lensu, *Photoelectric Properties of Bacteriorhodopsin Films For Photosensing And Information Processing*, PhD thesis, Lappeenranta University of Technology, 2002.

[11] S. Takamatsu, K. Hoshino, K. Matsumoto, T. Miyasaka, and I. Shimiyama, “Biomolecular image sensor of bacteriorhodopsin patterned by electrodeposition,” in *the 18th IEEE International Conference on Micro Electro Mechanical Systems*, pages 847– 850, 2005.

[12] S. Takamatsu, “The photo charge of a bacterioRhodopsin electrochemical cells measured by a charge amplifier,” *IEICE Electronics Express*, 8(7):505–511, 2011.

[13] R.R. Birge, N.B. Gillespie, E.W. Izaguirre, A. Kusnetzow, A.F. Lawrence, D. Singh, Q. Wang Song, E. Schmidt, J.A. Stuart, S. Seetharaman and K.J. Wise, “Biomolecular electronics: protein-based associative processors and volumetric memories,” *Journal of Physical Chemistry B*, 103(49):10746–10766, 1999.

[14] J. Xu, P. Bhattacharya, G. Vàrò, “Monolithically integrated bacteriorhodopsin/semiconductor opto-electronic integrated circuit for a bio-photoreceiver,” *Biosensors and Bioelectronics* 19:885–892, 2004

[15] F. Hong and D. Mauzerall, ”Interfacial photoreactions and chemical capacitance in lipid bilayers,” in *Proc. Nat, Acad. Sci. USA*, 71(4):1564–1568, 1974.

[16] S. Miyazaki, M. Matsumoto, S. B. Brier, T. Higaki, T. Yamada, T. Okamoto, H. Ueno, S. Toyabe and E. Muneyuki, “Properties of the electrogenic activity of bacteriorhodopsin,” *European Biophysics Journal,* published online http://dx.doi.org/10.1007/s00249-012-0870-0, 2012.

[17] L. Keszthelyi and P. Ormos, “Electric signals associated with the photocycle of bacteriorhodopsin,” *FEBS Letters*, 109(2):189–193, 1980.

[18] W. W. Wang, G. K. Knopf, and A. S. Bassi, “Photoelectric properties of a detector based on dried bacteriorhodopsin film,” *Biosensors and Bioelectronics*, 21:1309–1319, 2006.

[19] J. Talvitie, “Electrical Equivalent Circuit for Dry Bacteriorhodopsin Sensor,” M. Sc. Thesis, Lappeenranta University of Technology, 2011.

[20] J. Talvitie, T. Tukiainen, L. Lensu, T. J. Kärkkäinen, P. Silventoinen, M. Kuisma, ”Time-Variant Electrical Equivalent Circuit of a Dry Bacteriorhodopsin Sensor,” *in 30th the IEEE International Conference on Instrumentation and Measurement Technology*, pages 1218-1221 2013.

[21] G. C. Giakos, S. A. Paturi, K. Valluru, V. Adya, S. Sukumar, K. Ambadipubi, B. Mandadi, M. Becker, S. Athawale, P. Farajipour, S. Marotta, D. Sheffer, G. Livanos, and M. Zervakis, “Efficient Molecular Imaging Techniques Using Optically Active Molecules,” *IEEE Trans. Instrum. Meas.*,59(11):2877-2886, 2010.

[22] L. Keszthelyi and G. Váró, “Photoelectric signals from dried oriented purple membrane of halobacterium halobium,” *Biophysical Journal*, 43:47–51, 1983.

[23] F. T. Hong, “Interfacial photochemistry of retinal proteins,”*Progress in Surface Science*, 62:1–237, 1999.

[24] T. Tukiainen, J. Talvitie, M. Kuisma, P. Silventoinen, and L. Lensu. ” Loading Effects on the Photoelectric Response of Dry Bacteriorhodopsin Sensors” *in 31th the IEEE International Conference on Instrumentation and Measurement Technology*, pages 761-765, 2014.

[25] T. Tukiainen, “Photoelectric measurements and modeling of bacteriorhodopsin,” M. Sc. Thesis, Lappeenranta University of Technology, 2008.

[26] J. Talvitie. ”Designing an implementation of transimpedance amplifier for buffering a bacteriorhodopsin-sensor,” B. Sc. Thesis, in Finnish, http://urn.fi/URN:NBN:fi-fe201009222500, Lappeenranta University of Technology, 2010.

[27] A. Istratov, “Exponential analysis in physical phenomena,” *Review of Scientific Instruments*, 70:1233-1257, 1999.

[28] M. A. T. Figueiredo, J. B. Dias J. P. Oliveira and R. D. Nowak, “On total variation denoising: a new majorization-minimization algorithm and an experimental comparison with wavalet denoising,” in 2006 IEEE International Conference on Image Processing, 2633-2636, 2006.

[29] J. Talvitie, T. Tukiainen, L. Lensu, T. J. Kärkkäinen, P. Silventoinen, M. Kuisma, ”Amplifier Errors in Dry Bacteriorhodopsin Sensor Measurements,” *Accepted for publication in 32th the IEEE International Conference on Instrumentation and Measurement Technology*, 2015.

[30] L. Lensu, M. Frydrych, S. Parkkinen, T. Jaaskelainen, and J. Parkkinen, “Color-sensitive biosensors for imaging applications,” in George K. Knopf and Amarjeet S. Bassi, eds., *Smart Biosensor Technology*, CRC Press, Boca Raton, FL, USA, 2007.

Publication 3

Talvitie, J.P., Tukiainen, T., Lensu, L., Kärkkäinen, T.J., Silventoinen, P., and Kuisma,

"Amplifier Errors in a Dry Bacteriorhodopsin Sensor Measurements"

in *Proceedings of the IEEE International Instrumentation and Measurement Technology Conference, I2MTC2015*.

Copyright © 2015, IEEE. Reprinted, with permission of IEEE.

This full text paper was peer-reviewed at the direction of IEEE Instrumentation and Measurement Society prior to the acceptance and publication.

Amplifier Errors in Dry Bacteriorhodopsin Sensor Measurements

Joonas P. Talvitie*, Teemu Tukiainen', Lasse Lensu', Tommi J. Kärkkäinen*, Pertti Silventoinen*, Mikko Kuisma*
*Department of Electrical Engineering
'Machine Vision and Pattern Recognition Laboratory, Department of Mathematics and Physics
Lappeenranta University of Technology
Lappeenranta, Finland

***Abstract*—Bacteriorhodopsin is considered an important biomolecule for biochemical and technology-oriented studies. The modeling and functionality of bacteriorhodopsin sensors have been extensively studied, but the studies lack the analysis of the errors present in the measurements. Further, the impacts of these errors on photoelectric measurements are mostly unknown. In this paper, we discuss the errors caused by a transimpedance amplifier in the photocurrent measurements on a dry bacteriorhodopsin sensor. This information is especially useful when evaluating the reliability of photocurrent measurements.**

***Index Terms*— Error analysis, Operational amplifier, Current measurement, Bioelectric phenomena.**

I. Introduction

BACTERIORHODOPSIN (bR) is a photosensitive protein found in the archaean, Halobacterium salinarum [1]. The natural function of bR as a light-driven proton pump with a reversible photocycle is to participate in the energy-balancing mechanism of the archaean. The protein has been under intensive research as it has been considered an important biomolecule for biochemical and technology-oriented studies [2]. The popularity of bR as a research target can be explained by its several favorable characteristics: a high quantum efficiency (0.65) [3], an ability to function and survive under extreme environmental stress [4]–[7], and a storage life of years [8]. Owing to its advantageous properties, various technical applications in optoelectronics and biosensing have been proposed, such as an imaging sensor [9]–[12], a protein-based memory [2], [13], and a bio-photoreceiver [14].

In this paper, we examine the errors caused by the transimpedance amplifier in the photocurrent measurements on a dry bacteriorhodopsin sensor. Previously [15], we have found that the amplifier introduces errors to the photocurrent measurements. The size of the error has not been determined, even though measurement results have been used to calculate component values for electrical equivalent circuits by different research groups, [14] and [16]. The results of this paper can be used to evaluate the reliability of the photocurrent measurements. This is especially useful when the bandwidth of the measured responses is close to the bandwidth of the amplifier.

II. Definition of the Error

The main objective of the measurements on bacteriorhodopsin sensors is to understand the behavior of the biomolecule so that it can be applied to the design of new sensors. To this end, a better knowledge of the measurement instrumentation and its effects on the measurement is required. With this knowledge, it is possible to minimize or even remove some of the measurement errors. In some cases, the measurement errors cannot be removed, and they have a notable effect on the measurement. In this case, the effect of the measurement errors on the measurement can be estimated with proper understanding of the error source.

The photocurrent measurements on dry bacteriorhodopsin sensors are carried out by illuminating the dry bR sensor with a light source, in our case Cavitar CAVILUX Smart laser diode with a peak wavelength of 690 nm and a pulse width of 10 µs. The output of the bR sensor was measured by using a transimpedance amplifier and an oscilloscope [15], Fig. 1.

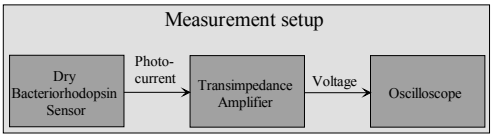

Fig 1. Overview of the measurement setups used in the photocurrent measurements on a dry bacteriorhodopsin sensor in this and our previous studies [15, 17]. The dry bacteriorhodopsin sensor is illuminated by a light source not indicated in the figure. The photocurrent from the bR sensor is amplified by a transimpedance amplifier and recorded by an oscilloscope.

The photocurrent responses from the bR sensor have fast rising edges with rise times down to a picosecond range [6, 18]. This is something that transimpedance amplifiers with large transimpedance gains cannot reach because of the limited gain-bandwidth product of the amplifiers. A large transimpedance gain is needed to amplify the small photocurrent from the bR sensors, which are in the order of tens to a few hundred nanoamperes in our measurements [15], [17]. For this reason, the measured photocurrent response is distorted by the limited rise time of the amplifier. The severity of this distortion depends on the bandwidth/rise time of the amplifier.

978-1-4799-6144-6/15/$31.00 ©2015 IEEE

The limited rise time of the amplifier introduces two types of errors, Fig. 2. The first one is the amplitude error between the peak amplitudes of the measured photocurrent and the expected photocurrent response from the bR sensor. The second one is the error between the measured and expected time constants.

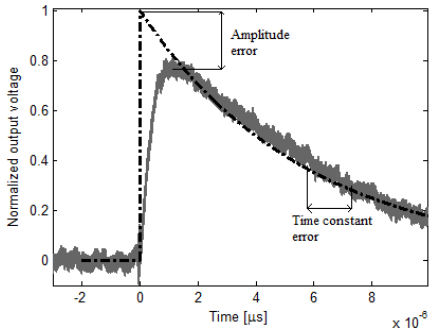

Fig 2. Errors in the photocurrent measurements caused by the limited rise time of the amplifier.

III. Effect of the Error

The effect of the error caused by the rise time limitation of the amplifier was estimated by simulations, Fig. 3. Based on our proposed model [15], [17], the sensor was modeled as a first-order high-pass filter. The time constants of the sensors used in the simulation were selected based on our previous measurements [15] to give the maximum and minimum values for the errors. The selected time constants were the shortest (3.3 µs) and the longest (24.7 µs) ones we had in our previous measurements. A step response was fed to the bR sensor to describe a stimulus caused by the light. The output of the sensor was then fed to the amplifier, which was modeled as a low-pass filter. The time constant of the filter was based on a 550 ns rise time measured from the transimpedance amplifier.

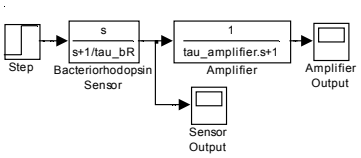

Fig 3. Simulation model used to study the error caused by the limited rise time of the amplifier.

Simulations were performed using two input signal levels to find out how the amplifier affects the amplitude measurements, Fig. 4. The simulations show that the limited rise time induces error to the measured peak amplitude. The simulations also show that the relative error in the amplitudes between the input and output of the amplifier remains unchanged even if the input signal level is varied.

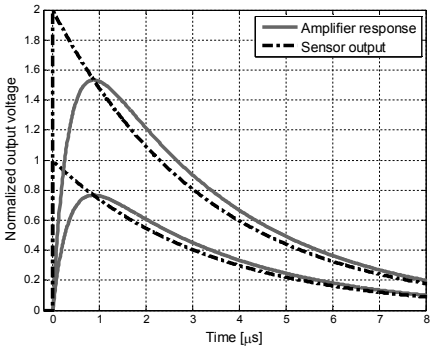

Fig 4. Simulated responses from the bR sensor and the amplifier output. The input signal is the response detected from the bR sensor with the time constant of 3.3 µs. The amplifier response is the output of the amplifier when the input signal is used as the input of the amplifier.

The simulations were also performed with two bR sensor time constants 3.3 µs and 24.7 µs at the same signal level to see how the error caused by the limited rise time of the amplifier behaves, Fig. 5. The figure shows that the amplitude error caused by the limited rise time of the amplifier decreases when the time constant of the sensor is increased.

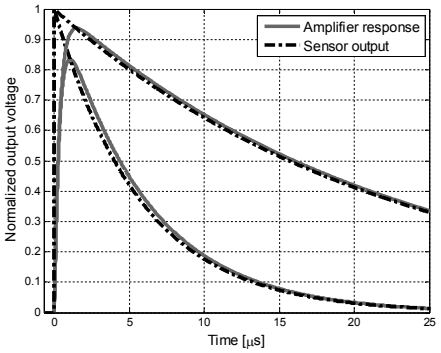

Fig 5. Simulated responses from the bR sensor and the amplifier output. The input signal is the response detected from the bR sensor with the shortest measured time constants of 3.3 µs and the longest of 24.7 µs. The amplifier response is the output of the amplifier when the input signal is used as the input of the amplifier.

The error between the measured and expected time constants was also investigated. The simulations revealed that the limited rise time of the amplifier causes the measured time constants to be longer than they actually are. The error between the measured and expected time constants decreases when the time constant of bR is changed from 3.3 µs to 24.7 µs.

It should be noted that the errors are estimated using the assumption that the rise time of the light source and the bR sensor are ideal. In reality this is not the case. So the estimated errors show the maximum error possible. In practice this error is in fact smaller than the one estimated with the simulations.

It can thus be concluded that the rise time of the amplifier does not affect the linearity of the amplitude measurement but only causes the measured amplitudes to be smaller than they would be in the case of an ideal amplifier. Even though the relative amplitude error does not change at different input levels, the different time constants of bR affect the errors in both the amplitude and the time constant. For this reason, the amplitude and time constant errors must be calculated for each time constant of bR individually.

IV. Results and Discussion

The effect of the transimpedance amplifier on the photocurrent measurements on a dry bR sensor was simulated. Based on the simulations, it was found that the limited rise time of the amplifier distorts both the amplitudes and time constants of the measured response. The limited rise time causes the measured amplitudes to be smaller than they actually are. Correspondingly, the rise time limitation causes the measured time constants to be longer than they are.

In our previous study [17], we proposed an electrical equivalent circuit for a dry bacteriorhodopsin sensor. The proposed electrical equivalent circuit was verified in [15] to be functional even at different light intensities. When analyzing the results in [15], it was found that the limited rise time of the amplifier causes an error to the amplitude and time constant measurements. Now, using the results of this paper, the error caused by the limited rise time of the amplifier can be evaluated.

Based on the simulations, the actual photocurrent amplitudes of the bR sensors were estimated for different light intensities, Table 1. The limited rise time of the amplifier caused the smallest measured amplitude to have the largest error. The measured amplitude was 74.8 % of the actual one. This was the largest error because the time constant corresponding to that amplitude was the shortest. The longest measured time constant was with the measured amplitude of 235.2 nA. In this case, the measured amplitude was only 94% of the actual amplitude.

Table 1. Measured and estimated amplitudes of light-on and light-off responses at different light intensities.

	Light-on response		Light-off response	
Relative intensity [%]	Measured amplitude [nA]	Actual amplitude [nA]	Measured amplitude [nA]	Actual amplitude [nA]
25	24.0	32.1	86.2	92.7
31.25	31.3	39.2	109.4	116.5
37.5	41.8	51.8	139.6	148.5
43.75	55.2	67.5	174.7	186.1
50	66.0	80.3	211.4	226.2
56.25	75.3	91.7	235.2	250.4
62.5	86.8	104.8	259.9	277.8
68.75	100.5	121.7	299.3	321.7
75	112.8	136.9	335.1	361.2
81.25	118.8	144.5	355.1	381.2
87.5	125.8	151.6	382.1	409.1
93.75	139.0	168.3	413.5	444.3
100	145.8	176.2	450.0	480.9

The estimated actual time constants were also calculated for the time constants presented in [15], Table 2. The table shows that the largest error is with the shortest measured time constant similarly as with the amplitude error. The measured time constant is 13.3 % larger than the actual time constant. The largest measured time constant is only 1.5 % larger than the actual one.

Table 2. Measured and estimated time constants of light-on and light-off responses at different light intensities.

	Light-on response		Light-off response	
Relative intensity [%]	Measured time constant [µs]	Actual time constant [µs]	Measured time constant [µs]	Actual time constant [µs]
25	3.31	2.92	20.34	19.98
31.25	4.60	4.22	24.20	23.85
37.5	4.91	4.53	24.74	24.39
43.75	5.33	4.96	23.95	23.60
50	5.50	5.13	22.08	21.72
56.25	5.50	5.13	24.40	24.05
62.5	5.81	5.45	22.38	22.03
68.75	5.70	5.33	20.33	19.96
75	5.61	5.24	19.39	19.03
81.25	5.55	5.18	20.81	20.45
87.5	5.90	5.52	21.83	21.47
93.75	5.73	5.35	20.39	20.03
100	5.77	5.40	22.60	22.25

Based on this work, we may conclude that the rise time of the amplifier introduces errors to the measured peak amplitudes and time constants. The effect of this error can be

estimated by simulations and taken into account when analyzing the measured photocurrent responses. Another option for decreasing the error requires the use of a transimpedance amplifier with a higher bandwidth. This could be achieved by using a more advanced amplifier topologies as described in [19–20].

V. Conclusion

In this paper, errors caused by the transimpedance amplifier in photocurrent measurements on a dry bacteriorhodopsin sensor were discussed. The limited rise time of the amplifier was found to affect the measured photocurrent responses from a dry bacteriorhodopsin sensor. The limited rise time causes errors when interpreting the peak amplitudes and the time constants from the photocurrent responses.

The effect of the rise time was estimated by simulations. The simulations showed that the limited rise time caused a relative error to the amplitude, which varied with the different time constants. On the other hand, the relative error in amplitudes was not affected by the input amplitudes. The error between the measured and estimated amplitudes and time constants increased when the measured time constants became shorter. Correspondingly, the error decreased with longer time constants.

With these results, the effect of the limited rise time was estimated for the measurements made in our previous study. The results of this paper can be used to evaluate the reliability of the photocurrent measurements. This is especially useful when the bandwidth of the measured responses is close to the bandwidth of the amplifier.

Acknowledgment

The authors wish to thank Prof. Jussi Parkkinen and Dr. Sinikka Parkkinen from the University of Eastern Finland for their work on the development of the bR sensors.

References

[1] D. Oesterhelt and W. Stoeckenius, “Rhodopsin-like protein from the purple membrane of halobacterium halobium,” *Nature new biology*, 233(39):149–152,1971

[2] N. Hampp, “Bacteriorhodopsin as a photochromic retinal protein for optical memories,” *Chemical Reviews*, 100(5):1755–1776, 2000.

[3] J. Tittor and D. Oesterhelt, “The quantum yield of bacteriorhodopsin,” *FEBS Letters*, 263(2), 269–273, 1990.

[4] H-W. Trissl, “Photoelectric Measurements of Purple Membranes,” *Photochemistry and Photobiology*, 51(6):793–818, 1990.

[5] P. Silfsten, S. Parkkinen, J. Luostarinen, A Khodonov, T. Jääskeläinen, and J. Parkkinen, “Color-sensitive biosensors for imaging,” In *Proceedings of ICRP '96*, 3:331–335, 1996.

[6] J. Xu, A. B. Stickrath, P.Bhattacharya, J. Nees, G. Vàrò, J. R. Hillebrecht, L. Ren, and R. R. Birge, “Direct measurement of the photoelectric response time of bacteriorhodopsin via electro-optic sampling,” *Biophysical Journal*, 85(2):1128–1134, 2003.

[7] K. A. Walczak, “Electronic Characteristics of Bacteriorhodopsin,” in *the 8th IEEE Conference on Nanotechnology*, pp. 553–556, 2008.

[8] G. Váró and L. Keszthelyi, “Photoelectric signals from dried oriented purple membrane of halobacterium halobium,” *Biophysical Journal*, 43(1):47–51, 1983.

[9] T. Miyasaka and K. Koyama, “Image sensing and processing by a bacteriorhodopsin-based artificial photoreceptor,” *Applied Optics* 32(31):6371–6379, 1993.

[10] L. Lensu, *Photoelectric Properties of Bacteriorhodopsin Films For Photosensing And Information Processing*, PhD thesis, Lappeenranta University of Technology, 2002.

[11] S. Takamatsu, K. Hoshino, K. Matsumoto, T. Miyasaka, and I. Shimiyama, “Biomolecular image sensor of bacteriorhodopsin patterned by electrodeposition,” in *the 18th IEEE International Conference on Micro Electro Mechanical Systems*, pages 847– 850, 2005.

[12] S. Takamatsu, “The photo charge of a bacterioRhodopsin electrochemical cells measured by a charge amplifier,” *IEICE Electronics Express*, 8(7):505–511, 2011.

[13] R.R. Birge, N.B. Gillespie, E.W. Izaguirre, A. Kusnetzow, A.F. Lawrence, D. Singh, Q. Wang Song, E. Schmidt, J.A. Stuart, S. Seetharaman and K.J. Wise, “Biomolecular electronics: protein-based associative processors and volumetric memories,” *Journal of Physical Chemistry B*, 103(49):10746–10766, 1999.

[14] J. Xu, P. Bhattacharya, G. Vàrò, “Monolithically integrated bacteriorhodopsin/semiconductor opto-electronic integrated circuit for a bio-photoreceiver,” *Biosensors and Bioelectronics* 19:885–892, 2004

[15] J. Talvitie, T. Tukiainen, L. Lensu, T. J. Kärkkäinen, P. Silventoinen, M. Kuisma, ”Validation of a Time-Variant Electrical Equivalent Circuit for a Dry Bacteriorhodopsin Sensor,” Accepted for publication in *32th the IEEE International Conference on Instrumentation and Measurement Technology, 2015.*

[16] L. Lensu, M. Frydrych, S. Parkkinen, T. Jaaskelainen, and J. Parkkinen, “Color-sensitive biosensors for imaging applications,” in George K. Knopf and Amarjeet S. Bassi, eds., *Smart Biosensor Technology*, CRC Press, Boca Raton, FL, USA, 2007.

[17] J. Talvitie, T. Tukiainen, L. Lensu, T. J. Kärkkäinen, P. Silventoinen, M. Kuisma, ”Time-Variant Electrical Equivalent Circuit of a Dry Bacteriorhodopsin Sensor,” *in 30th the IEEE International Conference on Instrumentation and Measurement Technology*, pages 1218-1221 2013.

[18] F. T. Hong, “Interfacial photochemistry of retinal proteins,”*Progress in Surface Science*, 62:1–237, 1999.

[19] C. Ciofi, F. Crupi, C. Pace, G. Scandurra, and M. Patanè, “A New Circuit Topology for the Realization of Very Low-Noise Wide-Bandwidth Transimpedance Amplifier,” *IEEE Trans. Instrum. Meas.*,56(5):1626-1631, 2007.

[20] M. Massarotto, A. Carlosena, and A. J. López-Martín, “Two-Stage Differential Charge and Transresistance Amplifiers,” *IEEE Trans. Instrum. Meas.*,57(2):309-320, 2008.

Publication 4

Abbaneo, D., Abbrescia, M., Abi Akl, M., Ahmed, W., Armaingaud, C., Aspell, P., Assran, Y., Bally, S., Ban, Y., Banerjee, S., Barria, P., Benussi, L., Bhopatkar, V., Bianco, S., Bos, J., Bouhali, O., Cai, J., Calabria, C., Castaneda, A., Cauwenbergh, S., Celik, A., Christiansen, J., Colafranceschi, S., Colaleo, A., Conde Garcia, A., Dabrowski, M., De Lentdecker, G., De Oliveira, R., De Robertis, G., Dildick, S., Ferry, S., Flanagan, W., Gilmore, J., Guilloux, F., Gutierrez, A., Hoepfner, K, Hohlmann, M., Kamon, T., Karchin, P. E., Khotilovich, V., Korntheuer, M., Krutelyov, S., Lenzi, Th., Loddo, F., Maerschalk, T., Magazzu, G., Maggi, M., Maghrbi, Y., Marchioro, A., Marinov, A., Mazumdar, N., Merlin, J. A., Mukhopadhyay, S., Nuzzo, S., Oliveri, E., Philipps, B., Piccolo, D., Postema, H., Radi, A., Radogna, R., Raffone, G., Ranieri, A., Rodrigues, A., Ropelewski, L., Safonov, A., Sakharov, A., Salva, S., Saviano, G., Sharma, A., Talvitie, J., Tatarinov, A., Teng, H., Turini, N., Tuuva, T., Twigger, J., Tytgat, M., van Stenis, M., Verhagen, E., Yang, Y., Zaganidis, N., and Zenoni, F.

"Development of the data acquisition system for the Triple-GEM detectors for the upgrade of the CMS forward muon spectrometer"

Journal of Instrumentation, vol. 9, no. 3, 2014

Copyright © 2014, IOP. Reprinted, with permission of IOP.

PUBLISHED BY IOP PUBLISHING FOR SISSA MEDIALAB

RECEIVED: *November 14, 2013*
ACCEPTED: *January 20, 2014*
PUBLISHED: *March 27, 2014*

TOPICAL WORKSHOP ON ELECTRONICS FOR PARTICLE PHYSICS 2013,
23–27 SEPTEMBER 2013,
PERUGIA, ITALY

2014 JINST 9 C03052

Development of the data acquisition system for the Triple-GEM detectors for the upgrade of the CMS forward muon spectrometer

D. Abbaneo,[a] M. Abbrescia,[b] M. Abi Akl,[c] W. Ahmed,[d] C. Armaingaud,[a] P. Aspell,[a] Y. Assran,[e] S. Bally,[a] Y. Ban,[f] S. Banerjee,[g] P. Barria,[h] L. Benussi,[i] V. Bhopatkar,[j] S. Bianco,[i] J. Bos,[a] O. Bouhali,[c] J. Cai,[f] C. Calabria,[b] A. Castaneda,[c] S. Cauwenbergh,[k] A. Celik,[l] J. Christiansen,[a] S. Colafranceschi,[a] A. Colaleo,[b] A. Conde Garcia,[a] M. Dabrowski,[a] G. De Lentdecker,[h,1] R. De Oliveira,[a] G. De Robertis,[b] S. Dildick,[k] S. Ferry,[a] W. Flanagan,[l] J. Gilmore,[l] F. Guilloux,[m] A. Gutierrez,[n] K. Hoepfner,[o] M. Hohlmann,[j] T. Kamon,[l] P.E. Karchin,[n] V. Khotilovich,[l] M. Korntheuer,[h] S. Krutelyov,[l] Th. Lenzi,[h] F. Loddo,[b] T. Maerschalk,[h] G. Magazzu,[p] M. Maggi,[b] Y. Maghrbi,[c] A. Marchioro,[a] A. Marinov,[a] N. Mazumdar,[g] J.A. Merlin,[a] S. Mukhopadhyay,[g] S. Nuzzo,[b] E. Oliveri,[a] B. Philipps,[o] D. Piccolo,[i] H. Postema,[a] A. Radi,[e] R. Radogna,[b] G. Raffone,[i] A. Ranieri,[b] A. Rodrigues,[a] L. Ropelewski,[a] A. Safonov,[l] A. Sakharov,[n] S. Salva,[k] G. Saviano,[i] A. Sharma,[a] J. Talvitie,[q] A. Tatarinov,[l] H. Teng,[f] N. Turini,[p] T. Tuuva,[q] J. Twigger,[j] M. Tytgat,[k] M. van Stenis,[a] E. Verhagen,[h] Y. Yang,[h] N. Zaganidis[k] and F. Zenoni[h]

[a] *CERN, Geneva, Switzerland*
[b] *Politecnico di Bari, Università di Bari and INFN Sezione di Bari, Bari, Italy*
[c] *Texas A&M University at Qatar, Doha, Qatar*
[d] *National Centre for Physics, Islamabad, Pakistan*
[e] *Academy of Scientific Research and Technology, ENHEP, Cairo, Egypt*

[1] Corresponding author.

© CERN 2014, published under the terms of the Creative Commons Attribution 3.0 License by IOP Publishing Ltd and Sissa Medialab srl. Any further distribution of this work must maintain attribution to the author(s) and the published article's title, journal citation and DOI.

doi:10.1088/1748-0221/9/03/C03052

[f] *Peking University,*
Beijing, China
[g] *Saha Institute for Nuclear Physics (SINP),*
Kolkata, India
[h] *Université Libre de Bruxelles,*
Brussels, Belgium
[i] *Laboratori Nazionali di Frascati – INFN,*
Frascati, Italy
[j] *Florida Institute of Technology,*
Melbourne, U.S.A.
[k] *Ghent University, Dept. of Physics and Astronomy,*
Gent, Belgium
[l] *Texas A&M University,*
College Station, U.S.A.
[m] *CEA-Saclay,*
Saclay, France
[n] *Wayne State University,*
Detroit, U.S.A.
[o] *RWTH Aachen University, III Physikalisches Institut A,*
Aachen, Germany
[p] *INFN Sezione di Pisa,*
Pisa, Italy
[q] *Lappeenranta University of Technology,*
Lappeenranta, Finland

E-mail: gdelentd@ulb.ac.be

ABSTRACT: In this contribution we will report on the progress of the design of the readout and data acquisition system being developed for triple-GEM detectors which will be installed in the forward region ($1.5 < |\eta| < 2.2$) of the CMS muon spectrometer during the 2nd long shutdown of the LHC, expected in the period 2017–2018. The system will be designed to take full advantage of current generic developments introduced for the LHC upgrades. The current design is based on the use of CERN GLIB boards hosted in micro-TCA crates for the off-detector electronics and the Versatile Link with the GBT chipset to link the front-end electronics to the GLIB boards. In this contribution we will describe the physics goals, the hardware architectures and report on the expected performance of the CMS GEM readout system, including preliminary timing resolution simulations.

KEYWORDS: Electronic detector readout concepts (gas, liquid); Data acquisition circuits

2014 JINST 9 C03052

Contents

1 Introduction 1

2 The "on-detector" electronics 3
- 2.1 The CMS triple-GEM detector 3
- 2.2 The front-end electronics 3

3 The "off-detector" electronics 5

4 Time resolution studies 5

5 Summary 6

2014 JINST 9 C03052

1 Introduction

The CMS GEM collaboration [1] is performing a feasibility study to install triple-GEM [2] detectors in the forward muon spectrometer of the CMS [3] experiment at the LHC, to enhance the muon tracking and the triggering capabilities in the region $1.5 < |\eta| < 2.2$. The triple-GEMs are Micro Pattern Gaseous Detectors (MPGD) able to sustain very high particle rates up to $10\,\mathrm{MHz/cm^2}$, featuring a spatial resolution of the order of $100\,\mu\mathrm{m}$, a time resolution of a few ns and detection efficiencies above 98%. They can be operated in a stable manner in high radiation environments at high gains, exceeding 10^4. Their performance makes the triple-GEM technology, a very good candidate to be used in the forward muon spectrometer of the CMS experiment for the LHC high luminosity phase, when one expects particle rates of several $\mathrm{kHz/cm^2}$. The CMS GEM collaboration aims for the installation during the second LHC long shutdown (2017–2018) of an entire ring of triple-GEMs, referred to as GE1/1, in the first endcap station of the CMS forward muon spectrometer, as shown in figure 1. The triple-GEM system will re-establish the redundancy of the muon spectrometer which in the region $1.5 < |\eta| < 2.2$ is only equipped with Cathode Strip Chambers (CSC). The installation of triple-GEM detectors in the second endcap stations (labeled GE2/1) could be done during the third LHC long shutdown scheduled beyond 2020 and will not be discussed further in this note.

To control and read-out this new CMS sub-detector we propose the electronics system shown in figure 2. The architecture is composed of two regions: the "on-detector" region and the "off-detector" region, the latter being located in the counting room. All electronics located "on-detector" typically require custom made electronics components which have to be resistant to the radiation. The "off-detector" electronics can be designed using relatively inexpensive and available "off the shelf" components. The communication between the two regions will be done via optical fibers which also require to be resistant to radiation.

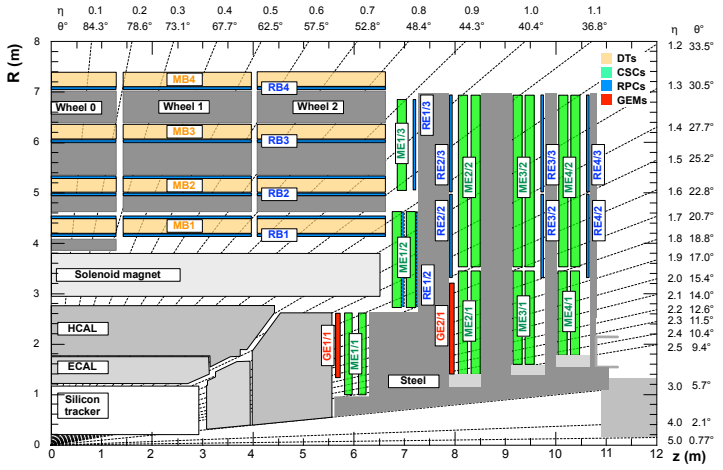

Figure 1. Transverse section of one quadrant of the CMS detector showing the present muon system and the proposed locations for the triple-GEM detectors.

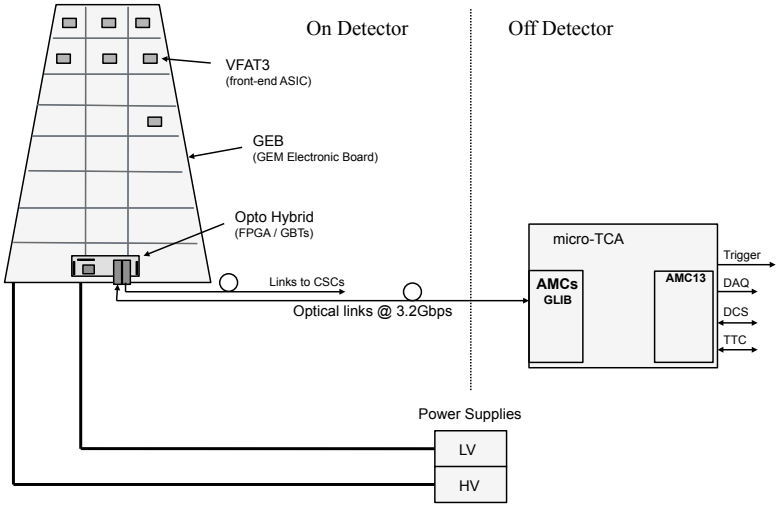

Figure 2. Electronics and data acquisition system architecture proposed for the CMS GE1/1 sub-detector.

The proposed architecture for the readout system is very similar to other LHC experiment upgrades and hence common needs exist between sub-detector systems. Common areas are typically the power regulation and the optic data transmission link. At CERN, generic developments, such as the Gigabit Transceiver (GBT) [4], the Versatile Link [5] and DC/DC converters [6] projects have

2014 JINST 9 C03052

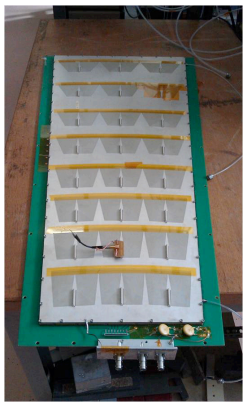

Figure 3. Latest version of the CMS GE1/1 triple-GEM prototypes.

been put in place since several years already to satisfy the "on-detector" common needs. In addition the Gigabit Link Interface Board (GLIB) project [7] addresses common off-detector needs. The CMS GEM electronics system intends to make full use of these generic developments as far as possible, in order to minimize duplication effort and to ensure that design resources within the project are focused on the project specific designs needed.

2 The "on-detector" electronics

In this section we will first review the design of the CMS triple-GEM detector, in particular its readout properties, and then examine the requirements as well as the design specifications of the front-end electronics

2.1 The CMS triple-GEM detector

The latest version of the CMS GE1/1 prototypes is shown in figure 3. The triple-GEMs have a trapezoidal-shaped active area of $990 \times (220\text{–}455)\,\mathrm{mm}^2$ with a 3/1/2/1 mm drift/transfer-1/transfer-2/induction gap configuration. The side of the detector seen in figure 3 is the readout board. Its inner side contains a pattern of readout strips oriented radially along the long side of the detector. The strip pattern is segmented in 8×3 partitions in $\eta - \phi$, with a strip pitch varying from 0.6 mm at the short end (at high η in CMS) to 1.2 mm at the wide end (at low η in CMS). The strips are connected through metalized vias to the outer side of the board where 128-channel connectors are soldered for the signal transfer to the front-end electronics.

2.2 The front-end electronics

The functional requirements on the readout system (and therefore on its front-end ASIC) are to provide both triggering and tracking information. These are similar basic requirements to that needed for the TOTEM experiment [8] that uses the VFAT2 [9] chip to read-out both silicon and GEM detectors. Consequently the VFAT2 architecture is the baseline for the new front-end ASIC,

2014 JINST 9 C03052

the VFAT3, being currently developed for the CMS triple-GEM system. The features of the new ASIC are listed below:

- Operation at high particle rate using large GEM detectors;
- Provide trigger data at 40 MHz as well as precise tracking data upon Level-1 Accept (L1A) signal;
- Large detector capacitance 20–60 pF;
- Relatively long signal charge collection $\sim$ 80 ns;
- Programmable shaping time: 25, 50, 100, 250, 500 ns;
- Interface required: slvds elinks to GBT at 320 Mbps;
- Level-1 latency up to 20 μs;
- Integrated calibration, bias and monitoring functions.

Similarly to VFAT2 it will have 128 channels of preamplifier, shaper and comparator. The shaping time and gain will be programmable in order to optimize the signal charge collection from the GEM detector whilst maintaining excellent timing resolution ($\sim$4.5 ns rms for VFAT2). A longer shaping time will result in improved signal to noise ratio when used with GEM detectors due to reduced ballistic deficit. However increased shaping times come at the cost of degrading time-resolution due to increased time-walk. As discussed in section 4, we are studying techniques to compensate for time walk and restore the original time resolution.

Both trigger and tracking data are sent to the off-detector electronics located in the CMS service cavern via the new Versatile Link. The Versatile Link is bi-directional and operates at a rate of 4.8 Gbps. On-detector the GBT radiation hard chipset will transmit the data from the detector through the Versatile Link. The VFAT3 chip will embed an e-Port to be connected directly to the GBT chipset. The trigger data will be sent in parallel to the Cathode Strip Chamber (CSC) Trigger Mother Board (TMB) to be combined with the CSC data and to improve the Level-1 trigger efficiency of the CSC system.

To send the trigger data to the CSC TMB we will use existing optical fibers located along the CSC detectors inside CMS. These fibers cannot sustain the GBT protocol. Consequently an FPGA will be placed on-detector to concentrate the trigger signals from the 24 VFAT3, to perform zero-suppression and transmit the data to the CSC as well as to the micro-TCA off-detector electronics. About 400 I/Os will be required to connect the FPGA to the 24 VFAT3 chips. This FPGA will be mounted on a board called "opto-hybrid" which will host in addition the GBT chipsets as well as the optical connectors. Initially a Xilinx Virtex 6 was considered to equip the opto-hybrid board because it is the type of FPGA used on the CFEB boards located on the CMS CSC detectors. In addition radiation studies described in ref. [10] show that the FPGA Block RAMs would encounter $\sim$ 9 SEU/day at high LHC luminosities. Mitigation processes are being investigated. Given the little space ($240 \times 225\,\mathrm{mm}^2 \times 11$ mm in height) left on-detector for the opto-hybrid and to reduce the heat, a smaller FPGA like the Xilinx Artix7 is now under study.

2014 JINST 9 C03052

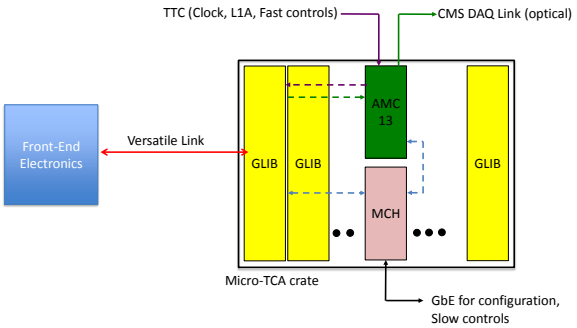

Figure 4. Layout of the "off-detector" electronics for the CMS triple-GEM system.

3 The "off-detector" electronics

The off-detector electronics provides the interfaces from the detector (and front-end electronics) to the CMS DAQ, TTC and Trigger systems. The design foreseen for the CMS GEM off- detector electronics is based on FPGAs and Multi-GBit/s links that adhere to the micro-TCA (μTCA) standard [11]. Micro-TCA is a recent standard that has been introduced for the Telecom industry and aims at high data throughput (2 Tbit/s) and high availability (the proportion of time the device is actually operating correctly compared with the planned time of operation = 99.999%). It is compact, hot swappable and has a high speed serial backplane. The μTCA is now a common standard for all the CMS upgrades and will replace the VME electronics.

The CMS GEM "off-detector" electronics, shown in figure 4, will be composed of the preferred CMS μTCA crate, the VadaTech VT892 [12], which supports 12 double-width, full-height AMC cards and two μTCA Carrier Hub (MCH) slots. The MCH1 slot houses a commercial MCH module, used for gigabit Ethernet communication and IPMI control. The MCH2 slot houses a custom AMC developed by Boston University and called AMC13 [13]. The AMC13 became the standard module within CMS to interface the μTCA crates to the CMS data acquisition system and to provide the CMS Trigger Timing and Control (TTC) signals downlink.

Each μTCA crate will house 12 GLIB AMC boards as the GEM trigger and tracking data receiver. The GLIB AMC is based on a Xilinx Virtex-6 FPGA with Multi-Gigabit Transceivers (MGT) operating at rates of up to 6.5 Gb/s. In addition the GLIB board features two high-pin count (HPC) FMC Mezzanine Card (FMC) sockets that can be used to extend the I/O connectivity of the GLIB AMC. Consequently each GLIB could accommodate up to 8 GBT high-speed data links and read-out a 10° ϕ-sector of triple-GEMs. In total 6 μTCA crates are needed to read-out the entire GE1/1 system tracking data and 2 crates for the trigger data.

4 Time resolution studies

An important parameter of the CMS GEM system is to provide a time resolution better than 8 ns to unambiguously identify the LHC bunch crossings. Measurements performed in beam tests have shown that a time resolution of the order of 5 ns is achievable with triple-GEM detectors oper-

2014 JINST 9 C03052

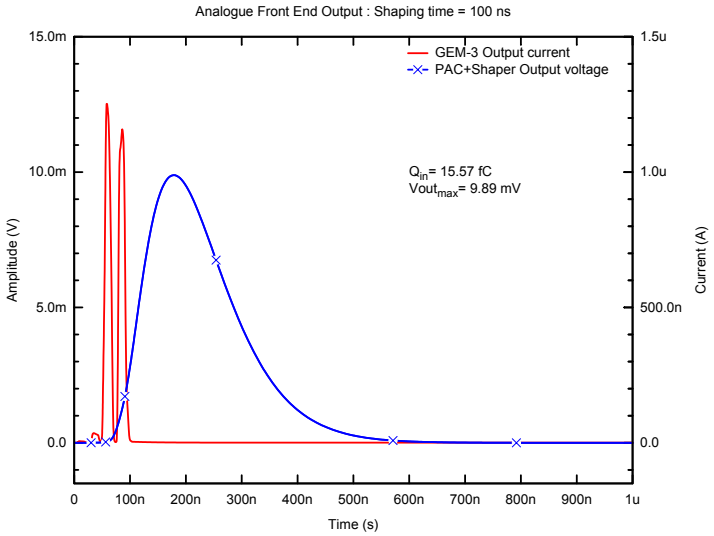

Figure 5. Example of a simulated CMS triple-GEM detector signal. The induced signal on the anodes is represented in red and the corresponding VFAT3 output in blue, with a shaping time of 100 ns.

ated with $Ar/CO_2/CF_4$ (45/15/40) gas mixture and the VFAT2 front-end electronics [14]. While the VFAT3 design is ongoing, detailed simulations of the CMS triple-GEM detector response to 1 GeV/c momentum muons have been performed. A detection cell has been simulated in 3D with the GARFIELD [15] software using electric field maps computed by the finite element (FEM) software Ansys [16]. Using the response function of the pre-amplifier of the current VFAT3 design we have studied the time resolution with two different methods that could be implemented on the front-end chip: the Time-Over-Threshold (TOT) and the Constant Fraction Discriminator (CFD).

Figure 5 shows an example of a simulated triple-GEM induced signal on the anodes (red) and the corresponding amplified and shaped signal obtained with a shaping time of 100 ns (blue). The two peaks observed in the induced signal are due to the spread of the primary ionization along the muon track in the 3 mm-long drift gap. Figure 6 shows the evolution of the time resolution as a function of the shaping time for the two methods, TOT and CFD. With both methods a time resolution better than 5 ns can be achieved for shaping times above 50 ns with the $Ar/CO_2/CF_4$ (45/15/40) gas mixture.

5 Summary

The installation of a new sub-detector in the CMS forward muon spectrometer is essential for enhancing both the muon tracking and triggering capabilities, ensuring a highly performing muon system during the LHC High Luminosity phase. Triple-GEM detectors have shown to have the requested performance to achieve these goals. In this paper we reviewed the status of the electronics system for this CMS upgrade, to be installed during the second LHC long shutdown. The

2014 JINST 9 C03052

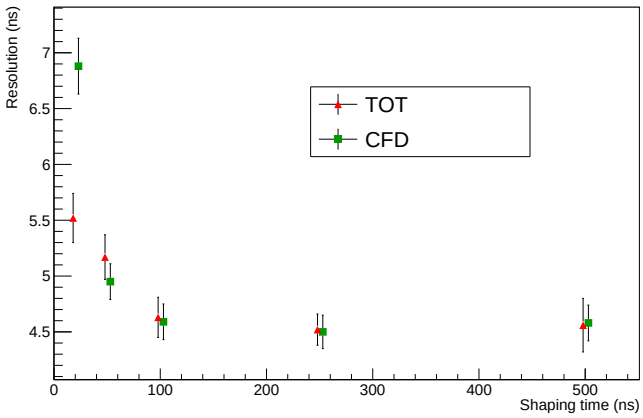

Figure 6. Time resolution as a function of the shaping time for the TOT and CFD methods.

system requires the design of a new front-end chip, the VFAT3, with similar functionalities that the TOTEM VFAT2 chip. In addition to make full use of generic projects and to minimize duplication efforts, the system will use the Versatile Link, the GBT chipset and the GLIB boards that will be hosted in the "CMS standard μTCA crate", the VadaTech VT892. The "CMS standard AMC13 board" will be used to interface the μTCA crates to the CMS data acquisition system. Nevertheless an FPGA opto-hybrid board located on the detector is necessary to transmit the GEM trigger data to the new CSC trigger boards through existing optical fibers.

Finally we present preliminary studies on the time resolution that could be achieved with the VFAT3 chip under design with two methods: the TOT and the CFD. In both cases a time resolution better than 5 ns can be achieved for shaping times above 50 ns with the $Ar/CO_2/CF_4$ (45/15/40) gas mixture.

Acknowledgments

The authors would like to acknowledge the continuous support of the CMS GEM Collaboration for this work. They also thank their colleagues from the CMS CSC group, from the CMS DAQ group and from the CERN micro-electronics group for their numerous advices. The corresponding author is supported by the Belgian FRS-FNRS.

References

[1] D. Abbaneo et al., *GEM based detector for future upgrade of the CMS forward muon system*, *Nucl. Instrum. Meth.* **A 718** (2013) 383.

[2] F. Sauli, *GEM: A new concept for electron amplification in gas detectors*, *Nucl. Instrum. Meth.* **A 386** (1997) 531.

2014 JINST 9 C03052

[3] CMS collaboration, *The CMS experiment at the CERN LHC*, 2008 *JINST* **3** S08004.

[4] P. Moreira et al., *The GBT SerDes ASIC prototype*, 2010 *JINST* **5** C11022.

[5] J. Troska et al., *Versatile transceiver developments*, 2011 *JINST* **6** C01089.

[6] F. Faccio et al., *Development of custom radiation-tolerant DCDC converter ASICs*, 2010 *JINST* **5** C11016.

[7] P. Vichoudis et al., *The Gigabit Link Interface Board (GLIB), a flexible system for the evaluation and use of GBT-based optical links*, 2010 *JINST* **5** C11007.

[8] TOTEM collaboration, G. Anelli et al., *The TOTEM experiment at the CERN Large Hadron Collider*, 2008 *JINST* **3** S08007.

[9] P. Aspell et al., *The VFAT production test platform for the TOTEM experiment*, *Nuclear Science Symposium Conference Record NSS '08*, (2008).

[10] J. Gilmore et al., *Very forward muon trigger and data acquisition electronics for CMS: Design and radiation testing*, 2013 *JINST* **8** C02040.

[11] PICMG μTCA website, http://www.picmg.org/v2internal/microTCA.htm.

[12] VT892: μTCA chassis with 12 double-width AMC slots webpage, http://www.vadatech.com/products/?show=product&product=186.

[13] E. Hazen et al., AMC13, http://www.amc13.info.

[14] D. Abbaneo et al., *Characterization of GEM Detectors for Application in the CMS Muon Detection System*, Proceedings of the *2010 IEEE Nuclear Science Symposium*, Knoxville, TN, U.S.A. (2010).

[15] R. Veenhof, *Garfield – simulation of gaseous detectors*, http://cern.ch/garfield.

[16] Ansys simulation software, http://www.ansys.com/.

2014 JINST 9 C03052

Publication 5

Aspell, P., Dabrowski, M., Conde Garcia, A., De Lentdecker, G., Marinov, A., De Oliveira, R., Talvitie, J., Tuuva, T., and Yang, Y.

"Development of a GEM Electronic Board (GEB) for triple-GEM detectors"

Journal of Instrumentation, vol. 9, no. 12, 2014

Copyright © 2014, IOP. Reprinted, with permission of IOP.

PUBLISHED BY IOP PUBLISHING FOR SISSA MEDIALAB

RECEIVED: *October 31, 2014*
ACCEPTED: *November 14, 2014*
PUBLISHED: *December 15, 2014*

TOPICAL WORKSHOP ON ELECTRONICS FOR PARTICLE PHYSICS 2014,
22–26 SEPTEMBER 2014,
AIX EN PROVENCE, FRANCE

2014 JINST 9 C12030

Development of a GEM Electronic Board (GEB) for triple-GEM detectors

P. Aspell,[a] **M. Dabrowski,**[a] **A. Conde Garcia,**[a] **G. De Lentdecker,**[b] **A. Marinov,**[b] **R. De Oliveira,**[a] **J. Talvitie,**[c,1] **T. Tuuva**[c] **and Y. Yang**[b]

[a] *CERN, Geneva, Switzerland*
[b] *Université Libre de Bruxelles, Brussels, Belgium*
[c] *Lappeenranta University of Technology, Lappeenranta, Finland*

E-mail: joonas.petteri.talvitie@cern.ch

ABSTRACT: Developed for use with triple GEM detectors, the GEM Electronic Board (GEB) forms a crucial part of the electronics readout system being developed as part of the CMS muon upgrade program. The objective of the GEB is threefold; to provide stable powering and ground for the VFAT3 front ends, to enable high-speed communication between 24 VFAT3 front ends and an optohybrid, and to shield the GEM detector from electromagnetic interference. The paper describes the concept and design of a large-size GEB in detail, highlighting the challenges in terms of design and feasibility of this deceptively difficult system component.

KEYWORDS: Electronic detector readout concepts (gas, liquid); Data acquisition circuits

[1] Corresponding author.

© CERN 2014, published under license by IOP Publishing Ltd and Sissa Medialab srl

doi:10.1088/1748-0221/9/12/C12030

Contents

1 **Introduction** 1

2 **GEM Electronic Board (GEB)** 1

3 **Proof of concept** 3

4 **Summary** 5

2014 JINST 9 C12030

1 Introduction

The CMS GEM collaboration [1] is planning to use triple GEM detectors [2] as part of its muon system upgrade in order to enhance the muon tracking and triggering capabilities in the region of $1.5 < \eta > 2.2$. A complete electronics system is currently under design for the purpose [3]. The electronics system consists of two regions: the "on-detector" region and the "off-detector" region, presented in figure 1. The electronic components of the "on-detector" region are required to be resistant to radiation. The electronics of the "off-detector" region are located in the counting room, where standard electronic components can be used. The electronics in these two regions are connected to each other using radiation hard optical links.

The on-detector part of the system is optimized for use with the GEM detectors and comprises a new front-end readout ASIC (VFAT3), a dedicated GEM Electronic Board (GEB) and an optohybrid with embedded Gigabit Transceiver (GBT) [4] chip sets. In this paper, we introduce in detail one crucial part of the readout system, the GEM Electronic Board. The main objectives of the GEB are to provide stable powering and ground for 24 VFAT3 front end chips, to connect the 24 VFAT3 front ends to the GBTs of the optohybrid using digital high-speed signals and to shield the GEM detector from electromagnetic interference. In addition, the GEB enables a compact system design needed for installation within the limited space of the Muon stations GE1/1, GE2/1 and ME0.

2 GEM Electronic Board (GEB)

The GEM chamber with all the readout electronics and cooling has to fit in the limited space of the Muon station. The height available for the electronics and cooling is at best 20 mm at the Muon station GE1/1. Because of these tight mechanical constraints, connecting each of the 24 VFAT3 to the optohybrid using flat cables is not possible. To overcome this problem, the GEM Electronic Board is proposed. The GEM Electronic Board or GEB is a large-size printed circuit board (PCB) that is placed on top of the GEM detector. Even though the GEB is placed on top of the GEM detector, it is a separate board. This allows the GEB board and all of the electronics on it to be replaced without opening and possibly contaminating the GEM detector. The GEB functions as a motherboard with three main objectives:

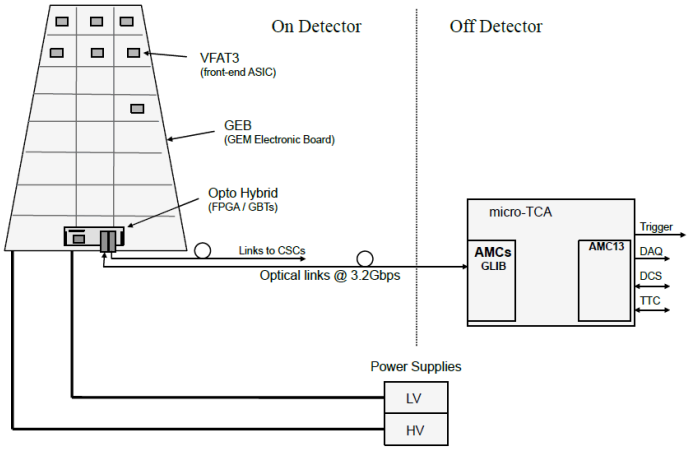

Figure 1. Electronics and data acquisition system architecture proposed in [3] for the CMS GE1/1 subdetector.

- to provide stable powering and ground for 24 VFAT3 front end chips
- to connect the 24 VFAT3 front ends to the GBTs of the optohybrid using high-speed digital signals
- to shield the GEM detector from electromagnetic interference.

The design was started by defining the mechanical dimensions of the GEB. The length of the trapezoid area available for the electronics and the cooling in the Muon station GE1/1 is 1003 mm. The width of the trapezoid area (with a height of 20 mm) is 345 mm at the wider end and 146 mm at the narrower end. The width of the GEB board can be as large as the detector itself, which is 457 mm at the wider end and 285 mm at the narrower end as long as the thickness of the GEB does not exceed 1.8 mm.

The strips on the GEM detectors are relatively long (up to 20 cm), which makes them sensitive to picking up the external electromagnetic noise generated by other electronic systems nearby. Thus, to shield the GEM detector from electromagnetic interference, the GEB was decided to be made large enough to cover the whole detector. This unusual size makes it possible to provide a continuous shield to protect the noise-sensitive strips of the GEM detector, but at the same time, it introduces the challenges of the design and manufacturing processes. Another advantage of this large continuous PCB is that it enables the routing of the 24 VFAT3 front ends to the optohybrid without a need for additional connectors or cables.

The GEB board was designed as a multilayer PCB with six layers. The number of layers was defined by the fact that it requires two layers to route all the 288 differential pairs and 144 single-ended signals from the 24 VFAT3 front ends to the optohybrid. Two layers were also used for distributing the power and the ground planes. In addition to these four inner layers, the top and bottom layers of the PCB were connected to the ground to surround the high-speed signals from

2014 JINST 9 C12030

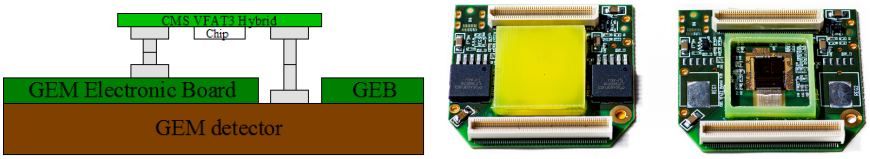

(a) (b)

Figure 2. (a) Mounting of the VFAT hybrids to the GEM detector and to the GEB. (b) The CMS VFAT2 Hybrids used with the prototype as the VFAT3 chips are still under development. Figure shows the VFAT2 Hybrids with and without the protective covers that are used to provide mechanical protection.

the VFAT3 front-ends to the optohybrid. This way, the high-speed signals are shielded from the external electromagnetic interference, but more importantly, it prevents the noise from radiating from the high-speed signals to the sensitive strips on the GEM detectors.

To make it possible to connect the VFAT3 front end chips to the GEM detector and the GEB, the VFAT3 chips are mounted on VFAT3 hybrids, which are PCBs with one connector to the GEM detector for the analog input signals and a second one for transferring digital signals to the GEB; see figure 2. The height difference of these two connectors defines the thickness of the GEM Electronic Board. In our case, the height difference of these connectors is 1 mm, which is a standard thickness in the PCB manufacturing and meets our requirements for the maximum height of 1.8 mm at the edges of the detector.

The signal distribution planned for the GEB is shown in figure 3. The signal distribution to the VFAT3 hybrids is carried out by using three separate clock and trigger lines, which each provide the clock and the trigger for a single column. A single column contains eight VFAT3 hybrids. Other differential high-speed signals are not shared with other hybrids, and thus, are routed directly from each of the hybrids to the optohybrid. Since the signals are over one metre long and operate at a frequency of 320 MHz, the differential high-speed signals require phase matching. The phase matching is provided for each whole row on the GEB that contains three VFAT3 hybrids instead of a single hybrid to ease the software and firmware development later on.

3 Proof of concept

An initial version of the GEB board was manufactured to verify its suitability for large-scale manufacturing, figure 5. The manufacturing of the GEB was successful but not without problems. The first manufacturing run suffered from short circuits. They were due to the laminating deviations that were more difficult to control because of the large size of the PCB. Nevertheless, after a rerun, this problem was solved.

The first GEB prototype was manufactured without an impedance control as it was designed to operate with VFAT2 chips that run with 40 MHz LVDS signals. A second prototype (with an impedance control) has been submitted to study the 320 Mbps operation for the VFAT3. For this reason, the initial GEB version was used to test the signal integrity at 40 MHz. The clock signal was generated by using a signal generator and fed through the PCB. At the other end, the signal

2014 JINST 9 C12030

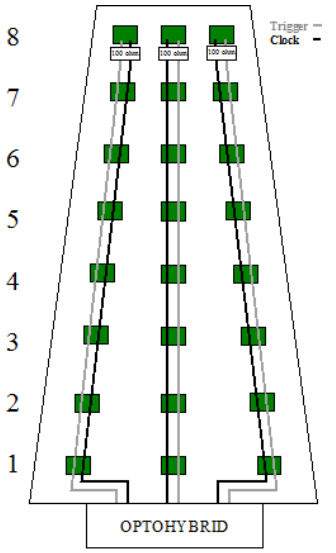

Figure 3. GEB clock and trigger signal distribution for the 24 VFAT3 hybrids.

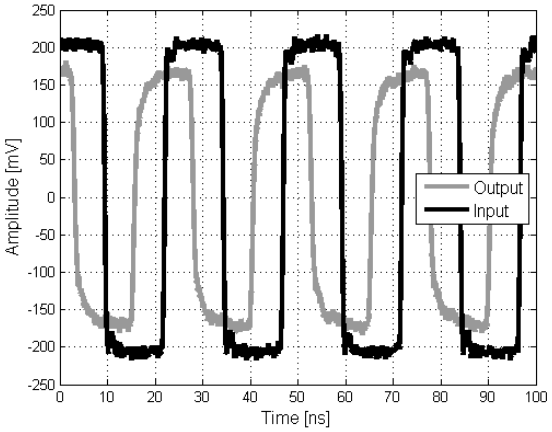

Figure 4. Signals measured coming in and out of the GEB board.

was terminated by using a 100 Ω resistor and recorded by a differential probe and an oscilloscope. The measured signals are shown in figure 4.

Figure 4 shows that at the frequency of 40 MHz, the signal from the end of the clock line has a slightly reduced amplitude. This is because the differential PCB traces have a resistance around 11 Ω, each of which reduces the amplitude seen over the 100 Ω terminating resistor. Otherwise, the signal looks good.

2014 JINST 9 C12030

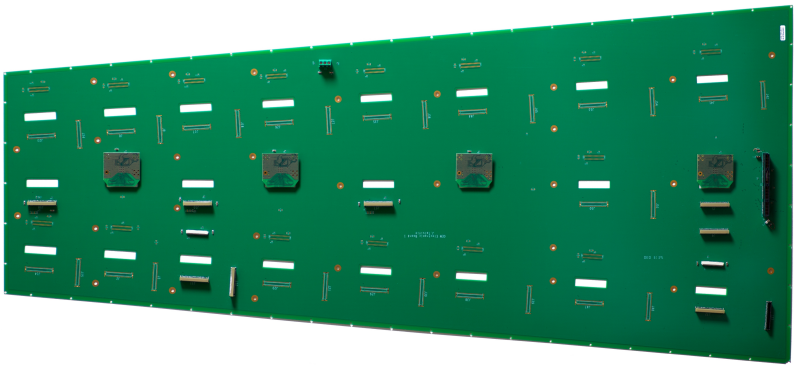

Figure 5. Manufactured large-size GEM Electronic Board with four CMS VFAT2 hybrids mounted on it.

The initial version of the GEB-V1 has the option to read out six VFAT2 front ends out of 24 VFAT2 front ends by using the first version of the optohybrid. The first prototype uses VFAT2 front end chips [5] as the VFAT3 front end chip is currently under development. The rest of the VFAT hybrids can be read out by using the TURBO readout system, which has been developed for the TOTEM experiment [6]. The use of these two readout systems makes it possible to test the functionality and performance of the proposed GEM Electronic Board with VFAT hybrids, but also enables the use of the well-known TURBO readout system as a reference for initial tests.

Using the VFAT2 hybrids, the optohybrid and the GEB the system were tested with the GEM detector and found to be functional. Even though the strips on the GEM were read out simultaneously by using different VFAT2 hybrids at 40 MHz, no notable increase in noise was detected that could be due to the electromagnetic interference generated by the readout system. The results were promising, but further study is needed especially on the electromagnetic interference when operating at 320 MHz. These tests need a second version of the readout system to be completed.

4 Summary

An initial version of the GEB board (GEBv1) has been manufactured. The objectives were to verify the manufacturing process and the electrical characterization. The GEBv1 prototype measured slightly over one metre to be compatible with the existing GEM detectors. The manufacturing with six layers was found to be feasible and cost efficient. Electrical measurements were performed to characterize the signal integrity at 40 MHz. Moreover, the functionality of the GEB board with the VFAT2 hybrids was tested. The tests showed that the system functions as intended, and the electromagnetic interference was observed not to cause problems.

Acknowledgments

The authors would like to acknowledge the continuous support of the CMS GEM Collaboration for this work. They also thank their colleagues from the CMS CSC group, from the CMS DAQ group and from the CERN microelectronics group for their advice.

2014 JINST 9 C12030

References

[1] D. Abbaneo et al., *GEM based detector for future upgrade of the CMS forward muon system*, *Nucl. Instrum. Meth.* **A 718** (2013) 383.

[2] F. Sauli et al., *GEM: new concept for electron amplification in gas detectors*, *Nucl. Instrum. Meth.* **A 386** (1997) 531.

[3] G. De Lentdecker et al., *Development of the data acquisition system for the Triple-GEM detectors for the upgrade of the CMS forward muon spectrometer*, 2014 *JINST* **9** C03052.

[4] P. Moreira et al., *The GBT SerDes ASIC prototype*, 2010 *JINST* **5** C11022.

[5] P. Aspell et al., *VFAT2: a front-end "system on chip" providing fast trigger information and digitized data storage for the charge sensitive readout of multi-channel silicon and gas particle detectors*, *IEEE Nucl. Sci. Symp.* (2008) 1095.

[6] TOTEM collaboration, G. Anelli et al., *The TOTEM experiment at the CERN Large Hadron Collider*, 2008 *JINST* **3** S08007.

2014 JINST 9 C12030

ACTA UNIVERSITATIS LAPPEENRANTAENSIS

615. UUSITALO, ANTTI. Working fluid selection and design of small-scale waste heat recovery systems based on organic rankine cycles. 2014. Diss.

616. METSO, SARI. A multimethod examination of contributors to successful on-the-job learning of vocational students. 2014. Diss.

617. SIITONEN, JANI. Advanced analysis and design methods for preparative chromatographic separation processes. 2014. Diss.

618. VIHAVAINEN, JUHANI. VVER-440 thermal hydraulics as computer code validation challenge. 2014. Diss.

619. AHONEN, PASI. Between memory and strategy: media discourse analysis of an industrial shutdown. 2014. Diss.

620. MWANGA, GASPER GODSON. Mathematical modeling and optimal control of malaria. 2014. Diss.

621. PELTOLA, PETTERI. Analysis and modelling of chemical looping combustion process with and without oxygen uncoupling. 2014. Diss.

622. NISKANEN, VILLE. Radio-frequency-based measurement methods for bearing current analysis in induction motors. 2014. Diss.

623. HYVÄRINEN, MARKO. Ultraviolet light protection and weathering properties of wood-polypropylene composites. 2014. Diss.

624. RANTANEN, NOORA. The family as a collective owner – identifying performance factors in listed companies. 2014. Diss.

625. VÄNSKÄ, MIKKO. Defining the keyhole modes – the effects on the molten pool behavior and the weld geometry in high power laser welding of stainless steels. 2014. Diss.

626. KORPELA, KARI. Value of information logistics integration in digital business ecosystem. 2014. Diss.

627. GRUDINSCHI, DANIELA. Strategic management of value networks: how to create value in cross-sector collaboration and partnerships. 2014. Diss.

628. SKLYAROVA, ANASTASIA. Hyperfine interactions in the new Fe-based superconducting structures and related magnetic phases. 2015. Diss.

629. SEMKEN, R. SCOTT. Lightweight, liquid-cooled, direct-drive generator for high–power wind turbines: motivation, concept, and performance. 2015. Diss.

630. LUOSTARINEN, LAURI. Novel virtual environment and real-time simulation based methods for improving life-cycle efficiency of non-road mobile machinery. 2015. Diss.

631. ERKKILÄ, ANNA-LEENA. Hygro-elasto-plastic behavior of planar orthotropic material. 2015. Diss.

632. KOLOSENI, DAVID. Differential evolution based classification with pool of distances and aggregation operators. 2015. Diss.

633. KARVONEN, VESA. Identification of characteristics for successful university-company partnership development. 2015. Diss.

634. KIVYIRO, PENDO. Foreign direct investment, clean development mechanism, and environmental management: a case of Sub-Saharan Africa. 2015. Diss.

635. SANKALA, ARTO. Modular double-cascade converter. 2015. Diss.

636. NIKOLAEVA, MARINA. Improving the fire retardancy of extruded/coextruded wood-plastic composites. 2015. Diss.

637. ABDEL WAHED, MAHMOUD. Geochemistry and water quality of Lake Qarun, Egypt. 2015. Diss.

638. PETROV, ILYA. Cost reduction of permanent magnet synchronous machines. 2015. Diss.

639. ZHANG, YUNFAN. Modification of photocatalyst with enhanced photocalytic activity for water treatment. 2015. Diss.

640. RATAVA, JUHO. Modelling cutting states in rough turning of 34CrNiMo6 steel. 2015. Diss.

641. MAYDANNIK, PHILIPP. Roll-to-roll atomic layer deposition process for flexible electronics applications. 2015. Diss.

642. SETH, FRANK. Empirical studies on software quality construction: Exploring human factors and organizational influences. 2015. Diss.

643. SMITH, AARON. New methods for controlling twin configurations and characterizing twin boundaries in 5M Ni-Mn-Ga for the development of applications. 2015. Diss.

644. NIKKU, MARKKU. Three-dimensional modeling of biomass fuel flow in a circulating fluidized bed furnace. 2015. Diss.

645. HENTTU, VILLE. Improving cost-efficiency and reducing environmental impacts of intermodal transportation with dry port concept – major rail transport corridor in Baltic Sea region. 2015. Diss.

646. HAN, BING. Influence of multi-phase phenomena on semibatch crystallization processes of aqueous solutions. 2015. Diss.

647. PTAK, PIOTR. Aircraft tracking and classification with VHF passive bistatic radar. 2015. Diss.

648. MAKKONEN, MARI. Cross-border transmission capacity development – Experiences from the Nordic electricity markets. 2015. Diss.

649. UUSITALO, ULLA-MAIJA. Show me your brain! Stories of interdisciplinary knowledge creation in practice. Experiences and observations from Aalto Design Factory, Finland. 2015. Diss.

650. ROOZBAHANI, HAMID. Novel control, haptic and calibration methods for teleoperated electrohydraulic servo systems. 2015. Diss.

651. SMIRNOVA, LIUDMILA. Electromagnetic and thermal design of a multilevel converter with high power density and reliability. 2015. Diss.